POLITECNICO DI TORINO

Master's Degree in Biomedical Engineering

Master's Degree Thesis

Boosting Working Memory: Adaptive Neurostimulation in Virtual Reality

Supervisor
Prof. Luca Mesin

Candidates
Gabriele D'Amato
Alice Fazio

Academic Year 2023-2024

Abstract

Neurostimulation in closed-loop represents a promising technique for enhancing human cognitive functions. This thesis aims to explore its effectiveness in boosting the working memory (WM) of healthy individuals through virtual reality. The focus is on the improvement of specific aspects of WM such as the ability to maintain and manipulate information, sustained attention, and real-time information updating. These elements are crucial for a wide range of cognitive functions, directly impacting the efficient management of mental information, a critical aspect in daily life.

Through a meticulous methodological approach, users are presented with an n-back task implemented in virtual reality with Unity, a platform that enables the development of interactive games. During the task, users' EEG signals are recorded using an 8-channel Enobio device and NIC2, software that controls the device from a computer. In the initial calibration phase, these tools operate offline. The recorded signal is then processed in Matlab, from which the most relevant features are extracted. These features, along with performance labels, are used to create a construction set for the training of an SVR. In the subsequent real-time phase, users undergo 5 testing trials with conscious and unconscious stimuli, including neurostimulation with fixed or adaptive alpha-band Binaural Beats (BB), adaptive theta-band pulsed light, visual neurofeedback with a fill bar, and adaptive BB combined with neurofeedback. Additionally, a control condition without stimuli is included. During this phase, NIC2 transfers the signal to Matlab in real-time, where it is processed to calculate the working memory level (WML) every 500 ms. Unity compares this index with personalized thresholds for the user and decides any changes to stimulation parameters to optimize performance. By recalculating subsequent WMLs, the positive or negative effect of this change is evaluated, thereby closing the loop.

Task outcomes are assessed by considering the percentage of correct responses (PC), reaction time (RT), and the inverse efficiency score (IES), a metric that synthesizes the first two. In the 2-back test, no significant differences are observed in the PC, RT, and IES parameters, possibly due to the test's simplicity, which limits errors, making it challenging to detect substantial improvements. Conversely, in the 3-back test, significant differences emerge, with notable improvements in IES under alpha-band adaptive BB, both individually and in combination with neurofeedback ($p < 0.05$). The use of adaptive BB also lead to a significant reduction in RT compared to both the control conditions ($p < 0.05$) and the traditional use of constant BB ($p < 0.05$).

Results suggest that alpha-band adaptive BB may contribute to the improvement of working memory performance in healthy subjects. Furthermore, they could prove beneficial for cognitive rehabilitation of pathological subjects, even in situations with limited conscious interactions, harnessing the power of 'unconscious brain entrainment'.

Contents

List of Tables

List of Figures

Chapter 1

Nervous System Anatomy and Electrophysiology

The study of the human brain is fundamental to the discipline of biomedical engineering because it sheds light on its memory and cognitive processing abilities. This chapter explores the complex electrophysiology and architecture of the nervous system, providing a foundational understanding that is essential for the implementation of user-adaptive neurostimulation methods intended to improve working memory that is described in the last section. The intricate structure and functions of the brain are at the center of this investigation. The brain's distinct architecture, which is made up of an enormous network of neurons and synapses, has an important effect on how well it processes and remembers information. Understanding the processes involved in memory creation and retrieval is largely dependent on this neuronal interconnections [1].

Moreover, electroencephalography (EEG) plays a crucial role in recording the electrical activity of the brain. EEG technology records and analyzes brainwave patterns in a non-invasive manner. This is especially pertinent since customized neurostimulation techniques can be developed with the help of EEG data, which offers insightful information about the electrophysiological state of the brain [2].

The physiological processes that underpin working memory are also covered in this chapter. Working memory is a dynamic process where information is temporarily stored and manipulated. It is essential to comprehend these mechanisms in order to design targeted neurostimulation protocols [3].

By means of this investigation, we establish a connection between the intricate biological functions of the brain and the inventive technical approaches

aimed at enhancing human cognitive capacities.

1.1 Nervous System Anatomy

In this section, we explore the structure of the brain, outlining its main components and its various lobi, each of which performs unique and essential functions for memory and thought processes.

1.1.1 Main Tissues of the Human Brain

There are two types of neural tissue that make up the human brain: *grey matter* and *white matter* as in Figure 1.1. These two types of tissue play vital roles in the nervous system's operation.

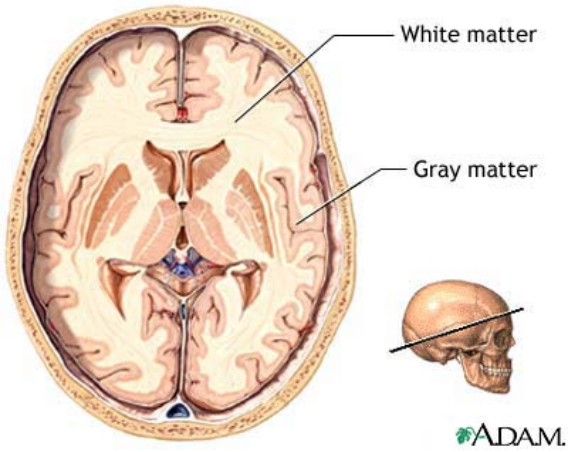

Figure 1.1. Section of a human skull where it is possible to observe the distinction between the tissues that make up the brain [4].

Unmyelinated axons, dendrites, and neuronal cell bodies make up the majority of grey matter. The brain's ability to integrate and process information depends on this structure. The cerebral cortex and a few subcortical regions, including the thalamus and basal nuclei, contain grey matter [1]. In contrast, myelinized nerve fibres found in white matter connect various brain regions to one another, enabling quick communication and effective information processing. Myelin, which envelops axons, is essential for the quick transmission of nerve impulses [5].

There is a close relationship between the white and grey matter's functions.

Coordinated and integrated processing of sensory, motor, and cognitive information is ensured by the white matter, which transmits information to various brain regions while the grey matter processes and interprets it [1].

Academic investigations into the ways in which changes in grey and white matter may impact a range of neurological and psychiatric disorders underscore the significance of these anatomical regions in preserving both mental and physical well-being. Understanding grey and white matter in-depth is essential for understanding the intricate workings of the human brain and creating specialised treatments for a range of neurological conditions [6].

1.1.2 Key Elements of the Brain

The human brain can be divided into three main parts 1.2:

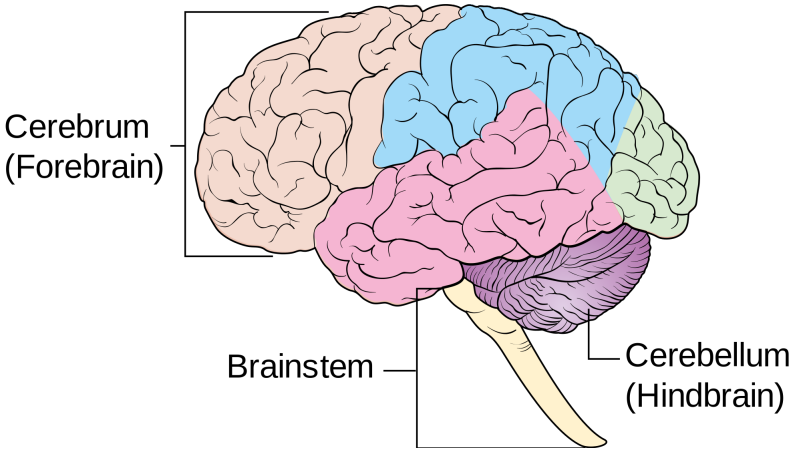

Figure 1.2. Lateral view of the cerebral hemisphere depicting the main components [7]

Cerebrum: is the largest and most superior part of the brain and performs multiple functions, including muscle movement, language and the processing of sensory information. It comprises grey matter (cerebral cortex) and white matter at its centre and is the largest part of the brain, initiating and coordinating movement and regulating temperature. Other areas of the brain enable speech, judgement, thinking and reasoning, problem solving, emotions and learning [8]. The left and right cerebral hemispheres make up the two structural halves of the brain, which are divided by the dura mater's sickle cerebri. Two thirds of the weight of the brain is made up of these hemispheres. The cerebral cortex is in charge of controlling higher order intellectual functions, integrating sensory impulses, and directing motor activity. Four regions

of the brain are referred to as lobes: the frontal, temporal, parietal, and occipital. Every one of these lobes performs distinct roles and duties:

1. *Frontal lobe* is involved in executive functions such as abstract thinking and planning; it is fundamental to working memory (WM) and is responsible for temporarily retaining information for periods of several seconds. Although distinct from long-term memory (LTM), there is considerable overlap between the frontally mediated processes involved in both. Investigations of the encoding and retrieval image in the LTM often involve the retention and manipulation of information in the WM. Conversely, information maintained in the WM may be encoded in the LTM. Moreover, working memory is often used to describe the ability to retain information in the service of a specific task or goal [9].

2. *Temporal lobe* essential for the processing of language and hearing, and it is situated in the lower part of the brain. Long-term memory is greatly influenced by this lobe, particularly through the hippocampus and other structures. It also plays a role in the perception of music and language. Among its many duties are the integration of sensory data and a major role in memory formation, both of which are critical for learning and recognition [9].

3. *Parietal lobe* essential to the processing of sensory inputs, including touch, temperature, and pain, is situated in the upper central region of the brain. It contributes to the comprehension and processing of spatial and mathematical information and is essential for body awareness, navigation, and spatial orientation [9].

4. *Occipital lobe* positioned at the rear of the brain, serves as the primary hub for processing visual information including the identification of colors, shapes, and motions, all of which are critical for navigating and interacting with one's environment [9].

Cerebellum. It is a central nervous system structure located at the base of the brain. It plays a key role in motor control, and is particularly active in coordination, precision and timing of movements, as well as motor learning. Its dysfunction is often manifested by motor signs, underscoring its importance in the regulation of voluntary movements [10]. The cerebellum is situated in the posterior cranial fossa, positioned behind the fourth ventricle, as well as the pons and the medulla oblongata. The tentorium cerebelli, an extension of the dura mater, separates the cerebellum from the brain. This strategic

location allows the cerebellum to interact effectively with other parts of the central nervous system [10]. The cerebellum also contributes to the refinement of motor movements, making them smooth and precise. It also plays a role in some cognitive functions, such as attention and language processing.

Brainstem. It is a crucial structure connecting the cerebrum of the brain to the spinal cord and cerebellum. Composed of three sections — the midbrain, pons, and medulla oblongata — it is responsible for many vital life functions, such as breathing, consciousness, blood pressure, heart rate, and sleep. The brainstem contains critical collections of white and grey matter, essential for various neural functions. This structure is also where ten of the twelve cranial nerves arise from their cranial nerve nuclei [11].

Meninges. They are crucial in safeguarding the brain and spinal cord. They are protective membranes that surround the central nervous system. They consist of three separate layers:

- The outermost layer, known as the *dura mater*, is made of resistant, dense tissue. This membrane acts as a barrier to prevent harm from mechanical sources.
- Cerebrospinal fluid can pass through the thin, transparent *arachnoid* membrane that makes up the middle layer.
- The innermost layer, the *pia mater*, adheres to the surface of the spinal cord and brain. Tiny blood vessels that supply the central nervous system are present in this membrane.

In addition to providing physical protection for the brain, the meninges aid in the movement of cerebrospinal fluid, which is necessary to keep the nervous system's homeostasis intact [1].

1.2 Brain Neurophysiology

The two main cell types that make up the central nervous system (CNS) are neurons, which are the main component of computation, and glia, which are the most abundant and have a regulatory, protective, and supportive role [12].

The neuron is a cell specialized in transmitting signals, playing a key role in the functioning of the nervous system. As can be seen in Figure 1.3, it is composed mainly of three parts: the cell body or soma, the dendrites, and the axon.

- The nucleus and various organelles necessary for cellular operations are located in the *soma* [13].

- From the cell body, the *dendrites* branch like a tree to receive messages from neighboring neurons and send them centripetally towards the cell body. The shape and signal-receiving capacity of a neuron are influenced by the dendritic tree's complexity [13].

- In contrast, the signal is transmitted by the *axon* to other cells in a centrifugal motion. Its homogeneous diameter and myelin sheath enhance the speed at which nerve impulses are sent. The terminal part of the axon is called the synaptic button, through which tiny substances known as neurotransmitters are released, which bind to receptor molecules on the receiving neuron. The chemical code is subsequently transformed by the latter into an electrical signal that can be sent through the following axon. The ability of synapses to change based on previous activity in the system is a crucial characteristic. They thus play a crucial part in memory, learning, and damage adaptation [13].

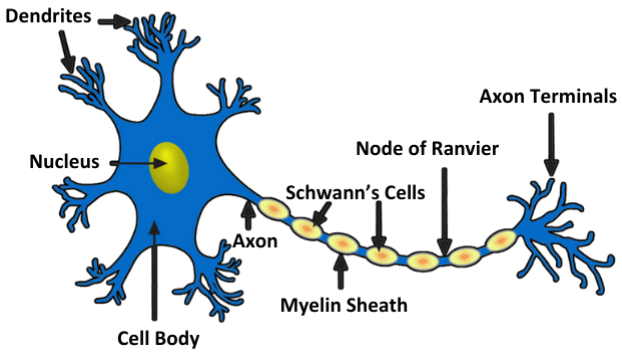

Figure 1.3. Structure of a typical neuron.

The glia are multicellular structures that carry out a wide range of vital tasks. The most prevalent are the *astrocytes*, which are long, star-shaped processes that may play a role in nutrient transfer when they come into contact with neurons. Also, some astrocytes may line the outside of blood capillaries and form the blood-brain barrier, which controls which chemicals from the blood are allowed to enter the brain. Additionally, astrocytes appear to play a significant role in controlling the potassium ion concentration surrounding

neurons, which is crucial in regulating the voltage across the neuronal membrane. They also play a role in the uptake of neurotransmitters following their release from synapses and in the synthesis of the precursor molecules that neurons convert into neurotransmitters. In order to protect neurons and facilitate the conduct of their electrical impulses, two additional types of glia are involved: *Schwann cells* and *oligodendrocytes*. The latter cover the axons in the CNS with their membrane, resulting in the formation of the myelin sheath, a specialized membrane differentiation. On the other hand, Schwann cells surround peripheral neurons, or nerves that are not part of the brain and spinal cord. Each neuron is contacted by many Schwann cells, each of which spans the distance between two nodes of Ranvier, periodic interruptions in the myelin sheath that covers the axon of a neuron. These nodes enhance the propagation of the nerve impulse by enabling it to leap from one node to the next, consequently boosting the overall velocity of signal transmission along the axon (achieving speeds exceeding 100 m/s). Finally, immune cells called *microglia* phagocytose and eliminate germs and viruses to help prevent infection and harm to the brain [12].

1.2.1 Classification of Neurons

Neurons can be classified based on both their structural characteristics and their operational functions.

Functional Classification

There are three categories of neurons based on the way nerve impulses propagate and their function.

1. Sensory or afferent neurons take part in the process of acquiring stimuli and transfer data from sensory organs to the central nervous system [14].
2. Interneurons, also known as intercalating neurons, are neurons with input and output neurons. They combine information from sensory neurons and send it to motor neurons in the central system.
3. Efferent neurons or motor neurons send out motor-like impulses to the body's peripheral organs [14].

Morphological Classification of Neurons

In terms of shape, the most representative types of neurons are described below and represented in Figure 1.4:

- The gray matter consists of *pyramidal cells*, which are surface neurons of the cortical region with a truncated pyramidal soma that gives rise to function. While the fundamental dendrites are distributed horizontally, the apical dendrite rises upward. The axon frequently pushes into deeper regions of the cortex, often entering the subcortical white matter. Electrodes to pick up the EEG signal primarily detect the electrical activity of neighboring neurons when placed to the scalp; thus, the pyramidal neurons are the primary sources [15].

- *Stellate cells* are interneurons present in the cerebral cortex. They are smaller in size (compared with pyramidal cells), polygonal in shape, and possess multiple branching dendrites with a relatively short axon.

- *Fusiform cells* are also a type of interneuron, predominantly situated in the deepest layers of the cortex, farthest from the cortical surface. These cells extend dendrites towards the cortex's surface, branching out to influence neurons located in the outermost layers of the cortex.

- The outermost layer of the cortex contains the *horizontal cells*. These are tiny, horizontally oriented fusiform cells. These axons connect with the ascending dendrites of pyramidal cells as they run parallel to the cortex's surface.

- *Martinotti cells* are found throughout the cortex at various levels. They send axons that terminate in the cortex's outermost layers.

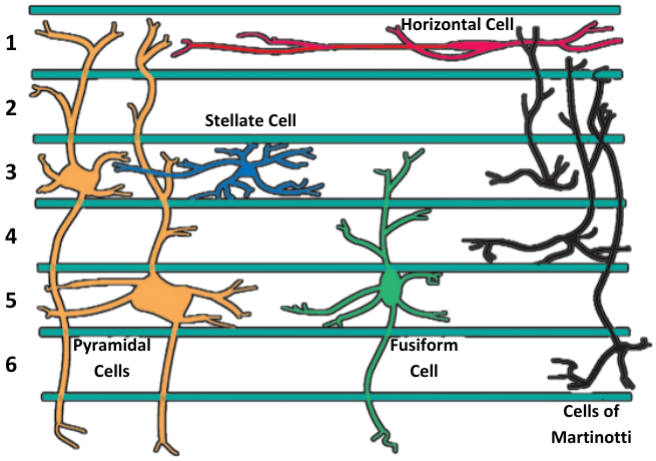

Figure 1.4. Cortical neurons. (1) corresponds to cortical surface; (6) innermost area of the cortex; (2),(3),(4),(5) intermediate zones.

1.2.2 Transmission of the Electrical Impulse

Axons in the CNS transmit information through all-or-none electrical impulses known as **action potentials**. They are very brief (1 ms) electrical event. These impulses begin at the initial segment of the cell body and are initiated by processed inputs from dendrites [13]. Larger axons' diameters result in a proportionally smaller membrane capacitance and internal electrical resistance, speeding up the depolarization of adjacent sections of the membrane. Every neuron has an electrical potential across its membrane, meaning that its inside is approximately 70 mV negative relative to its exterior. Variations in the concentration of charged ions, especially Na^+ and K^+, between the inside and exterior are what generate the potential. A unique pump called the Na^+/K^+ moves K^+ into the cell membrane and Na^+ out of that [13]. The concentrations of Na^+ and K^+ ions play a crucial role. Na^+ concentration outside the neuron is approximately 10 times higher than inside, while K^+ concentration inside is about 20 times higher than outside. The membrane is considerably impermeable to Na^+ and K^+, establishing a net negative charge inside due to large proteins and amino acids. Continuous ion pumping is required to maintain concentration differentials, and any interruption leads to the disappearance of membrane potential [12].

The key to the process is the voltage-sensitive Na^+ channel. As shown in the Figure 1.5, at a *resting state*(1), the channel is closed, so sodium and potassium ions cannot cross the membrane and the neuron's interior is negatively charged (-70 mV). Immediately after the triggering of the action potential, the neuron *depolarizes* beyond the threshold potential (-55 mV) (2), opening the sodium channel and permitting sodium ions to flow across its membrane. This process leaves the neuron positively charged and the extracellular fluid negatively charged. Following the attainment of the action potential, the neuron initiates *repolarization* (3), a process in which the potassium channels open and the sodium channels close, permitting potassium ions to permeate the membrane and overflow into the extracellular fluid. This results in a positive charge within the extracellular fluid and a negative charge inside the neuron that is beneath his resting potential. Ultimately, during the *refractory phase* (4), the potassium channels closes and the membrane potential returns to its resting condition. By exchanging three sodium ions for every two potassium ions across the plasma membrane, the sodium-potassium pump keeps the concentration gradient constant over time [16].

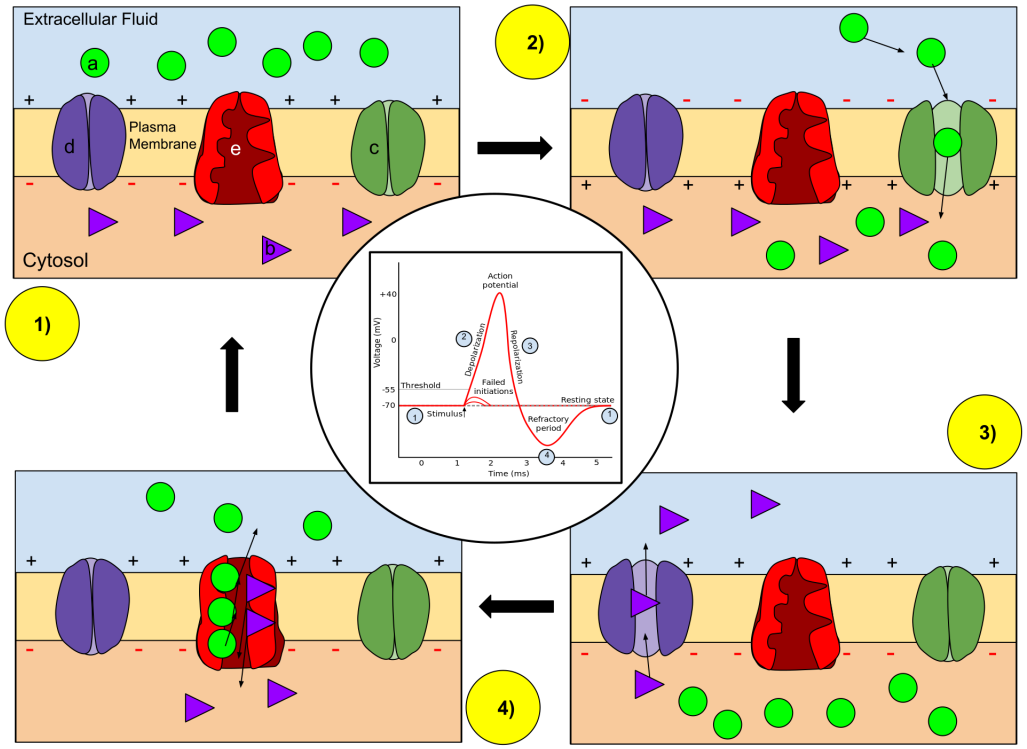

Figure 1.5. Membrane permeability of a neuron during an action potential [16]. (a) Na^+ ion. (b) K^+ ion. (c) Na^+ channel. (d) K^+ channel. (e) Na^+/K^+ pump.

1.2.3 Synapses

The location of transmission of information between two neurons is called synapse (or synaptic cleft). It consists of an tiny gap through which chemicals (*neurotransmitters*) released from the specific axon ending diffuse, transmitting information. Molecules on the other side of the gap that are introduced into the dendrite detect them. Information sent as electrical impulses must be converted into a chemical code in the presynaptic axon, and the opposite transformation must occur in the postsynaptic dendrite, where the chemical code must be converted back into an electrical code. Synapses are extremely intricate regions of neurons that can be altered based on previous activity patterns in the pre- and postsynaptic neurons [17].

The term synapse can also be used to refer to communication between cells of different types. Taking into consideration this second meaning, synapse can either stimulate or inhibit the other cell. When the action potential arrives, the target cell becomes excitatory, and when it suppresses it, it becomes

inhibitory.

The Figure 1.6 that follows illustrate the specifics of transmission at the synapse. Voltage-sensitive Ca^{2+} channels are present in the presynaptic axon in the synapse area, and they open when the action potential's wave of depolarization reaches the synapse. The concentration of Ca^{2+} ions is significantly larger outside the neuron than it is inside, so when the action potential arrives, it induces an inflow of these ions. A neurotransmitter is kept in tiny, membrane-enclosed pockets called vesicles within the presynaptic terminal. These vesicles fuse with the neuronal membrane with a rapid Ca^{2+} influx through a sequence of intermediate processes, releasing their contents into the synaptic space. Receptor molecules on the dendrites can bind to neurotransmitters on the postsynaptic membrane, initiating the opening of ion channels that bring about changes in the postsynaptic membrane potential. The specific ion channels that are open and their duration are determined by the neurotransmitter and receptor that they bind to. Postsynaptic membrane polarizations usually last between 10 and 20 milliseconds, while some might go on for several hundred ms. In comparison, an action potential's depolarization lasts for roughly 5 milliseconds [12].

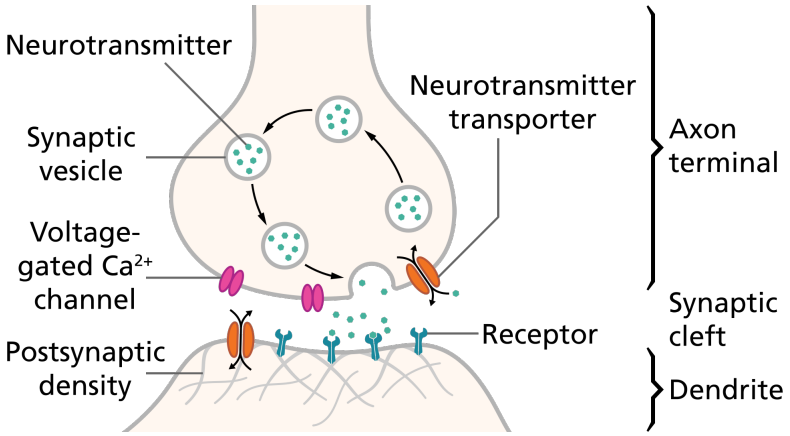

Figure 1.6. Schematic of a synapse [18]

The fact that an action potential is the result of the summation of inputs from numerous synapses that are all active at the same time is a crucial characteristic of the synaptic connections between the majority of neurons. The input from any one synapse has only a very little effect on the potential at the trigger zone in the axon hillock. To put it simply, the neuron counts the synaptic inputs that come in and generates an impulse that moves on to the next set of synapses if they ever cross the threshold. This elementary

model of a functioning neuron has undergone numerous improvements [17].

It is commonly acknowledged that synapses contribute to memory formation. Because of the signaling mechanisms of the receptors, which are triggered by neurotransmitters across the synaptic cleft, when two neurons are activated simultaneously, the link between them is reinforced. Memory is assumed to be the outcome of information being stored in two connected brain pathways. Long-term potentiation is the term used to describe this process of synapse strengthening [17].

1.3 EEG: Deciphering Brain Activity

In the field of brain investigation, several tools have played crucial roles in improving our understanding of how the brain works. The introduction of advanced imaging techniques such as functional magnetic resonance imaging (fMRI) and positron emission tomography (PET) have provided significant insights and revolutionised clinical routines [19, 20]. Electroencephalography stands out remarkably for its long-term use and significant simplicity of implementation. With its high temporal resolution, EEG remains a crucial tool in the diagnosis and monitoring of epilepsy, as well as in the real-time observation of brain activity during surgery [21]. Recently, there has been a renewed interest in the use of EEG, especially in the development of innovative applications such as adaptive neurofeedback and brain-computer interfaces [22].

1.3.1 From Origins to Clinical Practice

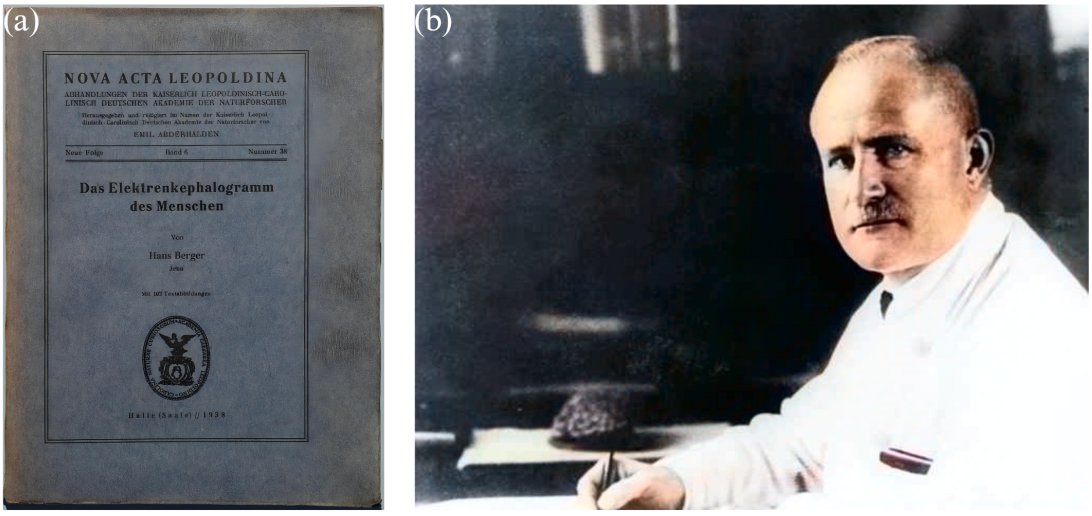

Figure 1.7. (a) The first work on electroencephalography. (b) Hans Berger

Electroencephalography originated in the last quarter of the 19th century with the discovery of electrical potentials that could be recorded from activated nerves and muscles in animals and from the cerebral cortex. In the 1920s, Hans Berger (Figure 1.7), a German neuropsychiatrist, recorded potentials from the scalp of patients with cranial defects and, later, with more sensitive equipment from intact subjects. Berger noted how the signals acquired depended strongly on the positioning of the electrodes on the scalp and the mental state of the subject acquired. At the same time, American physiologists introduced vacuum electron tube amplification and the cathode ray oscilloscope, which were interested in peripheral nerve recordings. Berger's findings were independently confirmed by Lord Adrian in England and Hallowell Davis at Harvard, USA, in the early 1930s. In the United States, initial advancements in the study of human electroencephalography were contributed by notable figures including Hallowell Davis, Herbert H. Jasper, Frederic A. Gibbs, William Lennox, and Alfred L. Loomis. Following the Harvard group's 1935 report, which linked electrographic findings with clinical observations in patients suffering from absence seizures and changes in consciousness, EEG's utility as a clinical instrument saw substantial progress. The technical aspects of the EEG and further clinical correlations were clarified by these investigators and many others. Further studies led to meetings of EEG pioneers in

Loomis' laboratory in New York (1935-1939), the formation of regional EEG societies and the American Clinical Neurophysiology Society in 1946. Over time, the EEG has been refined to become more sensitive and precise, expanding its use in various fields, from the diagnosis of neurological disorders to sleep monitoring and understanding cognitive functions such as memory and attention [23].

1.3.2 EEG Sampling Systems

In the field of biomedical engineering, EEG technology plays a crucial role in monitoring brain activity. The EEG signal is acquired through the use of electrodes, which are typically made of silver/silver chloride (Ag/AgCl). These electrodes are placed on the scalp following internationally standardised positions, the purpose of which is to ensure a uniform and replicable acquisition of brain signals. The number of electrodes used varies according to the specific requirements of the application: in standard clinical practice, 21 electrodes are used, while in more sophisticated applications, such as high-density EEG, up to 128 or 256 electrodes can be used [24].

To facilitate the placement of the electrodes, specially designed caps are often used, which allow them to be quickly identified and placed on the scalp. Electrodes can be disposable or reusable, the latter often having a cup shape that facilitates the insertion of the conductive gel. These cups also have a hole at the top, which is useful for adding the conductive gel even after the electrodes have been placed [25].

Before applying the electrodes, the skin must be carefully prepared: it must be cleaned and the surface layer of grease removed to ensure optimal contact. However, the use of conductive gel can sometimes cause short circuits between adjacent electrodes, especially when electrode density is high. To mitigate this problem, 'dry' electrodes have been developed, which improve contact with the skin without the use of gel [26].

In the analysis of EEG signals, the electrical potentials detected by individual channels are measured with respect to one or more reference electrodes, whose potential is considered to be zero Volt. Ideally, these reference electrodes should be placed infinitely far away from the signal source, a condition that is not feasible in practice. Therefore, it is common to position them as far as possible from the cortical areas of interest, to minimise any interference in the signal detected [25, 26].

These practices and considerations in the use of EEG electrodes are fundamental to ensuring the accuracy and reproducibility of the data collected,

which are essential aspects in the research and clinical application of electroencephalography.

1.3.3 International 10-20 Electrode Positioning System

The most popular standardised technique for EEG electrode insertion is the International 10-20 System. The basis of this approach, which was first presented by Jasper in 1958, is the partition of the skull into proportionate zones, which makes it easier to place electrodes in the same location among the patients. The electrodes in the 10-20 system of EEG electrode placement are positioned at particular sites on the skull. Repere points, which are measures based on anatomical landmarks, are used to determine these locations. Main locations that are used are:

- The Nasion, which is located at the root of the nose.
- The Inion, located at the base of the skull on the midline.
- Pre-ear points, which are located on the sides of the head, aligned with the ear.

The two most important distances measured are the separation between the left and right pre-auricular locations and the distance from Nasion to Inion. As a proportion (10% or 20%) of these observed distances, electrode sites are determined. Two separate components make up the 10-20 system's electrode location nomenclature:

1. The first element indicates the underlying brain region, represented by abbreviations such as:
    - Fp for the polar frontal region;
    - F for the frontal region;
    - C for the central sulcus;
    - P for the parietal region;
    - O for the occipital area;
    - T for the temporal region.
2. The second element differentiates electrodes based on their relative position to the midline of the skull:
    - The letter 'z' identifies electrodes placed on the midline.

- A number is assigned to other electrodes: even numbers for those located to the right of the midline, odd numbers for those to the left. Higher numbers indicate a position farther from the midline, while lower numbers indicate a position closer.

This nomenclature and positioning system, originally proposed by Jasper, is crucial to ensure consistency and precision in EEG execution [27].

The 10-20 system holds paramount importance in clinical and scientific contexts. It provides a common framework for localizing recording sites, enabling clinicians to reliably compare EEG results across patients and over time. As technology has advanced, variants such as the 10-10 and 10-5 systems have been developed, offering a higher electrode density for more comprehensive brain mapping [28].

The 10-10 system represents a significant advancement, contributing to the improvement of spatial resolution in EEG recordings and allowing for a more detailed coverage of various brain regions, as depicted in Figure 1.8.

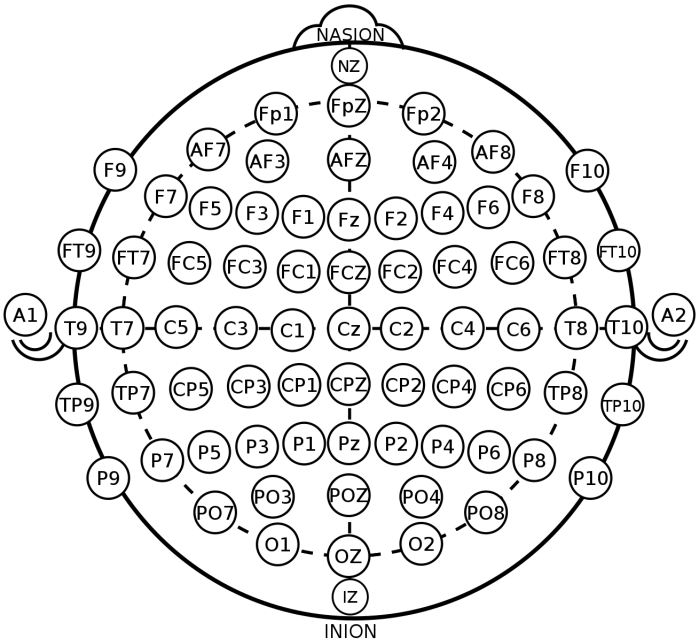

Figure 1.8. The positioning and naming of the 10-10 intermediate electrodes, as established by the standards of the American Electroencephalographic Society [29].

This increased precision in electrode placement across the extensive area of the head translates to a greater ability to map and analyze brain activity accurately.

The widespread adoption of the 10-10 system underscores its relevance and utility in neurophysiological research. Through its extensive use, it has proven to be an essential tool for the precise and reliable study of brain activity, significantly contributing to our understanding of neurological processes and clinical diagnosis.

1.3.4 EEG Signal Amplitude and Frequency Bands

The amplitude of the EEG signal, a key indicator of the intensity of brain electrical activity, is generally measured in microvolts (µV), typically ranging between 10 µV and 100 µV. This parameter reveals the power of intercepted neural signals, with a frequency band ranging from 0.1 Hz to 80 Hz.

It is important to note that the amplitude of the EEG signal can show significant variations not only among different individuals but also for the same person across various moments or in differing situations. Factors such as wakefulness or sleep states, the age of the subject, and the presence of neurological or psychiatric conditions can greatly influence these measurements [30].

Furthermore, brain rhythmic activity, reflected in the EEG, results from the temporal synchronization of cortical pyramidal neurons. This synchronization manifests in characteristic frequencies, leading to the traditional analysis of the EEG signal in terms of five main rhythms, classified based on their specific frequency bands and represented in Figure 1.9:

- Delta wave (δ): characterized by frequencies between 0.1 Hz and 4 Hz with amplitudes typically ranging from 20 µV to 150 µV. It is present in children and adults during deep sleep and is pathological during wakefulness.

- Theta wave (θ): with frequencies from 4 Hz to 8 Hz and amplitudes between 5 µV and 10 µV, theta waves are common in the early stages of sleep in adults and predominantly in children.

- Alpha wave (α): characterized by frequencies between 8 Hz and 13 Hz and amplitudes from 20 µV to 50 µV, these waves are detectable in healthy adults when in a relaxed state with closed eyes, mainly located in parietal and occipital regions.

- Beta wave (β): these waves, with frequencies between 13 Hz and 30 Hz and amplitudes between 5 µV and 30 µV, emerge in response to sensory stimuli, eye opening, or during states of increased concentration

and cognitive activity. They can be further divided into $\beta 1$ (13 Hz - 22 Hz) and $\beta 2$ (23 Hz - 30 Hz) waves.

- Gamma wave (γ): with frequencies between 40 Hz and 80 Hz, gamma waves manifest during cognitive activities that require the integration of activity across different brain areas and are linked to phenomena such as memory consolidation and brain plasticity [26, 31].

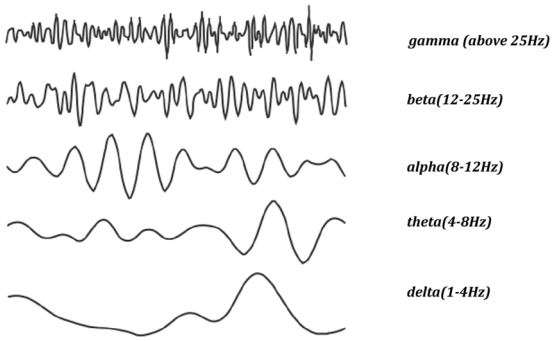

Figure 1.9. Representation of the different frequency contents of the EEG signal [32].

1.3.5 EEG Artifacts

In the context of EEG, artifacts pose a significant challenge, impacting the quality and interpretability of data. These unwanted signals, often originating outside of brain activity, can mask or distort true EEG signals, leading to incorrect interpretations or imprecise conclusions. Despite the refinement of EEG techniques over time, the presence of artifacts remains a crucial issue, especially in clinical and research studies.

These artifacts can be divided into different categories, such as physiological artifacts (e.g., eye movements, muscle activity), environmental artifacts (e.g., electromagnetic interference), or equipment-related artifacts (e.g., electrode connection issues). Each type of artifact exhibits unique characteristics in terms of frequency, amplitude, and morphology, necessitating specific approaches for identification and removal [33].

Physiological Artifacts

Muscular: caused by muscle contractions, especially in facial and neck muscles. Characterized by high amplitudes (50-300 µV) and high frequencies

(20-100 Hz). Due to their high-frequency contribution, they can be easily removed through a low-pass filter [34].

Ocular: arise from eye movements and blinking, which can be voluntary or involuntary. Typically detected by frontal electrodes (F7 and F8). Produce amplitudes ranging from 50 to 200 µV with low frequencies (<4 Hz for slow movements, up to 20-30 Hz for rapid movements). Eye movements can overlap with the delta band, and artifact removal techniques often involve simultaneous acquisition of an Electrooculogram (EOG).

Cardiac: the electrical activity of the heart can be picked up by EEG electrodes. Manifests as regular peaks with variable amplitudes. Since the source is distant from the recording point, cardiac electrical activity is nearly equipotential on the scalp, and thus not present in bipolar derivations but clearly recognizable using monopolar derivations. A simple method for their removal is to simultaneously acquire an ECG channel to identify the QRS complex and then remove the portions containing the artifact [26].

External Artifacts

Electrical: caused by electromagnetic interference, such as electrical equipment or unshielded cables. Often have fixed frequencies, such as 50 or 60 Hz (power line frequency). Removal of such artifacts is achieved, for example, with a Notch filter.

Motion: movements of the electrodes can cause impedance variations and transient artifacts appearing as a rapid increase and slow decrease in potential. Also called pop artifact [34].

Technical Artifacts

Baseline Drift: slow, low-frequency variations (<0.5 Hz) due to amplifier instability or impedance changes.

Electrode Jumps: sudden changes in EEG signal due to poor electrode contact. These can appear as sharp spikes or sudden signal dropouts. If they occur, it is necessary to reposition the electrode correctly before proceeding with new acquisitions [33].

In Figure 1.10 the visualization offers a detailed analysis of the impacts of common artifacts, contributing to the understanding and mitigation of interferences in recording brain activity through EEG.

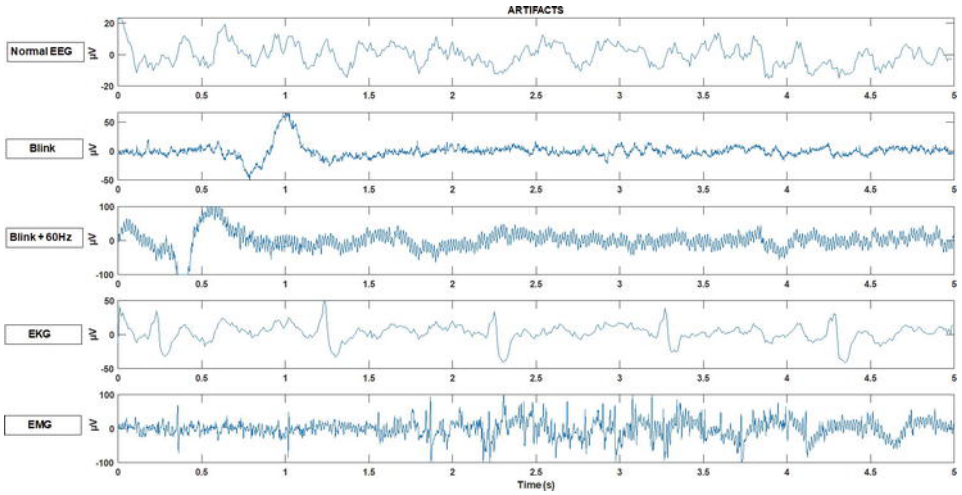

Figure 1.10. Graphic representation of major artifacts in EEG the five traces depict: 1) Normal condition, 2) Blink Artifact, 3) Blink + 60Hz Interference, 4) ECG Artifact, and 5) EMG Artifact [34].

1.4 Working Memory

Working memory is an essential cognitive function that enables the temporary processing and manipulation of information. Essential for reasoning, learning, and understanding, working memory is the mental 'workspace' we use to carry out daily cognitive tasks. It acts as a bridge between perception, long-term memory, and action, allowing us to maintain information 'online' while engaging in complex mental processes. This section explores its theoretical foundations, the cognitive models that describe its structure and functioning, and how age and pathologies impact this critical ability.

1.4.1 Theoretical Models in Working Memory

Working memory, a fundamental concept in cognitive psychology, has been the subject of intense study and research over the years.

Success in working memory tasks requires more than just undivided attention; it demands an intricate blend of several mental processes. The initial steps involve paying attention and recognizing incoming stimuli, setting the groundwork for further cognitive engagement. The journey continues with the encoding and storage of information, transforming and maintaining the stimuli in a usable form. Active rehearsal helps keep this information fresh and accessible, ensuring it remains at the forefront of our minds. The complexity

increases as we must constantly monitor and match this stored information against new inputs, maintaining a vigilant comparison. Meanwhile, the ability to inhibit irrelevant details and update the memory with pertinent data becomes crucial. This cycle of comparison, suppression, and renewal is a delicate balancing act, reflecting the sophisticated interplay of cognitive functions necessary for handling intricate tasks [35].

Among the various models proposed, two have had a significant impact: Baddeley and Hitch's multi-component model and Cowan's integrated processes model [36].

Multi-Component Model of Baddeley and Hitch

Introduced in the 1970s, this model revolutionized the understanding of working memory. It proposes that working memory consists of three primary components: the phonological loop, the visuospatial sketchpad, and the central executive.

The phonological loop is responsible for the manipulation and maintenance of verbal information. It is further divided into two subcomponents: a phonological store that preserves information in verbal form and an articulatory rehearsal buffer that repeats this information to maintain it in memory.

The visuospatial sketchpad, on the other hand, manages visual and spatial information. This component allows individuals to mentally visualize objects or paths, playing a crucial role in activities such as navigation and spatial understanding.

The central executive acts as a control system, coordinating and directing attention among various cognitive tasks and the other two components of working memory. Its function is crucial in multitasking and solving complex problems [36].

Cowan's Integrated Processes Model

In an attempt to integrate and expand on Baddeley and Hitch's model, Cowan proposed a different approach. His integrated processes model suggests that working memory is not a separate system but rather a subset of interconnected cognitive processes that include both short-term memory and elements of long-term memory.

According to Cowan, working memory consists of the temporary activation of a portion of long-term memory and the attentive control over this activation. From this perspective, the capacity of working memory is influenced not

only by the amount of information that can be actively maintained but also by an individual's ability to control attention and inhibit distractions [36].

Both models have provided fundamental insights into the functioning of working memory but differ in terms of emphasis and proposed mechanisms. Baddeley and Hitch's model focuses on specific subsystems and their functions, while Cowan emphasizes the role of attention and integration with long-term memory.

1.4.2 Aging and Working Memory

Aging leads to significant changes in working memory. These changes are due to neurobiological and structural factors, such as the reduction in gray matter volume and alterations in neuronal connectivity. Studies show that working memory capabilities decrease with age, affecting the ability to retain and manipulate information. These declines are often related to reduced efficiency in brain areas involved in multitasking and problem-solving [36].

Working Memory and Brain Pathologies Neurological and psychiatric conditions such as ADHD (attention deficit hyperactivity disorder), major depression, and traumatic brain injuries can significantly impact working memory. These conditions lead to a decline in the ability to actively manage and manipulate information. Changes at the neuronal level in these conditions can be identified through brain imaging, providing insights into the underlying mechanisms affecting working memory [36].

Rehabilitation and working memory training can be fundamental tools to counteract cognitive decline associated with aging and brain pathologies. Some studies [37] have shown that cognitive training can significantly improve working memory capabilities in children with ADHD. Another research [38] indicates that adults can also benefit from working memory exercises, with observed improvements in general cognitive functions. These studies suggest that structured training programs, which include activities such as memory exercises and cognitive tasks, can be effective in enhancing working memory capabilities in both young people and adults.

1.4.3 Improving Working Memory

From the variety of studies analyzed in [39], it is evident that different frequencies of brain waves influence various aspects of cognitive processes and memory, with variable effects. In particular, the alpha, beta, and theta frequencies exert a certain degree of influence on our domains of working memory.

During tasks involving working memory, alpha and theta waves coexist in different brain regions, where theta increases in the frontal region, and alpha increases in the posterior and bilateral regions of the brain.

It is essential to emphasize that the nature of brain waves plays a crucial role in shaping behavioral outcomes, especially in cognitive activities such as memory and attention. For example, theta waves are associated with the process of assimilating new information, while beta waves reflect cognitive control. Additionally, the role of alpha waves is noteworthy, often correlated with promoting a state of mental relaxation. However, recent research suggests that an effective increase in alpha amplitude may also contribute to improving performance in updating working memory. This suggests a potentially significant role of alpha waves in enhancing working memory capacity during complex cognitive tasks.

Chapter 2

Biofeedback, Neurofeedback and Neurostimulation

Within the realm of neurophysiology, beyond the exploration and description of the intricate human brain, there is a considerable interest in enhancing and modulating its activity for various purposes, ranging from therapeutic applications for illnesses to performance enhancement in healthy individuals. The focus will then shift to neurofeedback and neurostimulation (NS). In the following sections, we will delve into the characteristics of both approaches, highlighting their respective differences. However, before delving into neurofeedback, let us commence from an earlier point by closely examining the concept of biofeedback.

2.1 Biofeedback

In the late 1950s, a number of disciplines and fields came together to form biofeedback in the United States. These included behavioral therapy, psychophysiology, instrumental training for autonomic nervous system responses, and stress coping techniques [40]. Biofeedback is primarily used to offer instruments for the detection and control of psychophysiological arousal processes, including electrodermal activity, peripheral vasoconstriction, and muscle tension. Three activities in particular are performed by a biofeedback instrument: 1) observe a relevant physiological process; 2) give an unbiased measurement of the process under observation; 3) provide meaningful information based on

what is being tracked and measured.

Biofeedback is an advanced medical methodology that melds principles from complementary and alternative medicine with the latest developments in biotechnology [41]. It is a non-invasive method that empowers individuals to acquire the skills to modify their physiological activities, aiming to improve their overall performance, general health, and the physiological alterations often associated with behavioral, emotional, and cognitive changes. During biofeedback sessions, individuals are attached to electrical sensors that are subsequently connected to biofeedback apparatus, as in Figure 2.1. They provide information about physiological processes back to the user, helping them become more conscious of these processes and take deliberate control of their body and mind. It is possible to monitor blood pressure, heart rate, heart rate variability, muscle contraction, skin temperature, electrodermal activity (sweat gland activity), blood flow and electrical activity of the brain (EEG). According to research, biofeedback is useful for treating a wide range of medical and psychological conditions, including headache, hypertension, temporomandibular disorders, and attentional problems. It can also be used alone or in conjunction with other behavioral therapies [41].

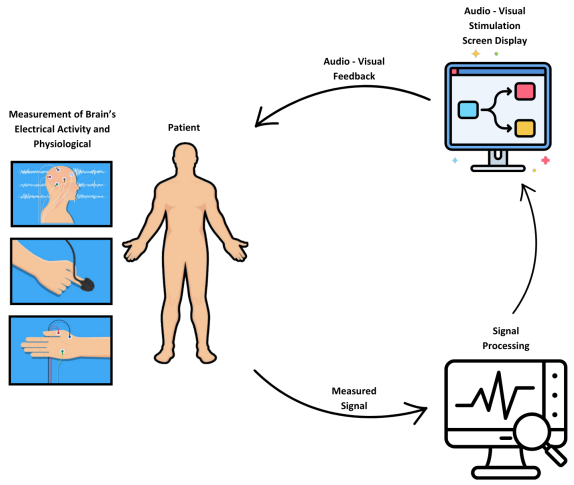

Figure 2.1. Biofeedback protocol

2.2 Neurofeedback

Neurofeedback, also known as EEG Biofeedback, is a non-invasive method that was developed from biofeedback: it focuses on teaching individuals how to take control of the electro-physiological functions of the human brain. EEG

data is used in neurofeedback to display current patterns in the trainee's cortex. Aberrant cortical activity patterns are present in many neurological and medical conditions. A baseline EEG and occasionally a multi-site quantitative EEG (QEEG) are used in neurofeedback assessment to detect defective patterns. The person is then able to adjust those patterns through clinical training using EEG feedback, regulating or optimizing brain activity. With the most acceptability for applications for ADHD, learning difficulties, seizures, depression, acquired brain injuries, substance misuse, and anxiety, neurofeedback treatment is expanding quickly [42]. Several treatment methods are available for neurofeedback training (NFT), summaries in a review [43]: *alpha training* is typically used to treat a variety of diseases including pain relief, anxiety and stress reduction, memory and, specifically, working memory enhancement, cognitive performance enhancement, and brain injury treatment. The purposes of *beta training* include enhancing cognitive processing, focus, and attention. Additionally, it results in a decrease in anxiety, obsessive compulsive disorder (OCD), overthinking, drinking, and insomnia. In the meanwhile, this kind of neurofeedback lessens stress and exhaustion while also enhancing sleep-related cognitive function. Beta waves with a frequency range of 12–15 Hz (sensorimotor rhythm) are known to alleviate stress, anxiety, and epilepsy [43]. One of the most commonly used neurofeedback trainings for reducing stress is *alpha/theta training*. In addition, this therapy is utilized to treat severe cases of anxiety, addiction, and depression. It also facilitates recovery from traumatic reactions and improves musical performance, creativity, and relaxation [43]. *Delta waves* are applied to treat strong and sharp muscle contractions, learning difficulties, headaches, and traumatic brain damage. They also reduce worries and enhance sleep [43]. *Gamma training* is intended to enhance problem-solving abilities, mental acuity, brain activity, short-term memory and information processing speed. Lastly, it decreases the frequency of migraine attacks [43]. *Theta training* has been found to alleviate emotional disorders, ADHD, depression, anxiety, daydreaming, and distractibility. Additionally, it has been observed to be associated with enhanced information encoding during working memory tasks [43].

2.3 Brainwave Entrainment

Brainwave entrainment, which is also called brainwave synchronization or neural entrainment, describes the observation that periodic external stimuli such flickering lights, speech, music, or tactile stimuli will cause brainwaves to automatically synchronize to their rhythm [44]. The concept of entrainment

is rooted in the principles of complex systems theory. This theory elucidates a phenomenon in which two or more autonomous oscillators, each possessing its distinct rhythm or frequency, can exert mutual influence on one another. The extent of this interaction is contingent upon the potency of the coupling force and materializes when these oscillators are in close proximity for an extended period, facilitating a gradual synchronization of their rhythms or frequencies. Consequently, they adjust to oscillate harmoniously at the same frequency [45]. Thus, brainwave entrainment is thought to be able to generate a desired state since different dominant brainwave frequencies can be linked to distinct conscious states. Numerous research show the benefits of applying this technique to various populations, indicating that different brain entrainment states may have distinct consequences on behavior and cognition [44].

2.4 Neurostimulation

Non-invasive brain stimulation methods, such as transcranial magnetic stimulation, transcranial direct current stimulation, and different forms of sensory stimulation, are effectively employed as therapeutic instruments in neurology and psychiatry. Additionally, they have been used extensively in recent years on healthy subjects in an effort to improve their cognitive ability [46]. To do this, the most consolidated and widely used frequency bands in the literature for sensory stimulation correspond to those previously outlined for NFT.

In order to better understand the neuronal mechanisms underpinning cognition, treat neuropsychiatric illnesses, and enhance cognitive rehabilitation following a stroke, non-invasive brain stimulation, for instance, is being employed more and more in clinical settings [47]. Brain-computer interface devices can be used to effectively use tactile, auditory, and visual stimulation as well as other sensory brain stimulation modalities to give paralyzed people an alternate channel of communication [48]. Electroencephalography and transcranial magnetic stimulation combined provide a non-invasive way to examine changes in cortical connection and signal propagation from healthy to disordered brains [49]. It also allows for an investigation of responses and cortical connectivity in the human brain.

Open Loop - Neurostimulation. The first generation of brain stimulation systems operated in an open loop mode, meaning that the stimulation parameters (such as amplitude, duration, and frequency) did not change over time in response to any physiological variables that occur in real-time [50].

However, depending on the underlying condition, the same stimulus may have different consequences due to the dynamic nature of the nervous system's or the modulated organ's physiology. Open-loop stimulation may therefore not be able to restore the intended function or result in adverse effects [51].

Closed Loop - Adaptive Neurostimulation. Based on closed-loop technologies, second-generation brain stimulation methods can dynamically modify therapeutic stimulation in real-time in response to the patient's brain activity [46]. This method, called closed-loop therapy, uses an algorithm or device to control stimulation, allowing for more specialized and targeted treatments. A closed-loop system synchronizes stimulation with the patient's instantaneous brain state by only initiating stimulation in response to abnormalities in brain activity. When compared to open-loop therapy, this type of neurostimulation may have advantages like higher efficacy, better clinical outcomes, and fewer side effects [46].

It is noteworthy that neurofeedback training, in which participants are given instructions to adjust a sensory measure of their brain activity, also employs closed-loop sensory stimulation. However, a number of issues, such as accurately interpreting human cognition and utilizing efficient learning techniques, limit the effectiveness of NFT. Automated adaptive stimulation structures, which can dynamically adapt to the changing properties of the brain, are proposed as a solution to these constraints. Customizing these treatments can be made easier by using the closed-loop neurostimulation technology, in which stimulation parameters are automatically adjusted based on feedback from biomarkers. In the development of closed-loop systems, choosing appropriate biomarkers to guide stimulation parameters has become a top priority [46].

Numerous research [52, 53] proposed the use of online automatic sensory stimulation, with parameters controlled by the patient's endogenous rhythms, such as heart rate, respiration rate, and EEG rhythms, to close the feedback loop in adaptive neurostimulation methods. These rhythms are interdependent and necessary for physiological efficiency, balance, and flexibility in response to environmental and internal changes. They are essential for recovering cerebral plasticity, training, and regulation of brain activity, as well as for the rhythmic facilitation of sensory processing. Remarkably, these rhythms are essential interoceptive signals for an individual's emotional state [52].

Chapter 3

Artificial Intelligence, Machine Learning and Deep Learning

3.1 Artificial Intelligence

The term "**Artificial Intelligence**" (AI) is generally used to describe the capacity of a machine to carry out tasks that are often associated with human minds, such as "learning" and "problem solving" [54]. Ensuring a machine can efficiently do a complex human task is the aim of any AI system. AI technology is widely employed in industry, government, and science. Historically, AI research has been centered on various core domains, including reasoning, the representation of knowledge, planning, learning, processing natural language, perception, and providing support in robotics [54]. Machine Learning (ML) and Deep Learning (DL) are subsets of Artificial Intelligence: this relationship is illustrated in Figure 3.1.

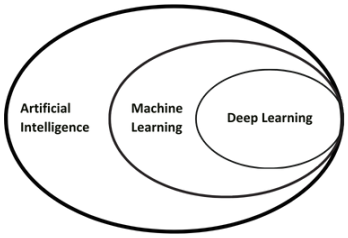

Figure 3.1. Relationship between AI, ML and DL.

3.2 Machine Learning

The discipline of creating statistical models and methods that enable computer systems to carry out complicated tasks without explicit guidance is known as **Machine Learning** [55]. Several algorithms are used in ML to solve data-related issues. The optimal kind of algorithm to tackle an issue is never a one-size-fits-all solution, as data scientists like to emphasize [55]. The type of method used will vary depending on the type of problem you want to solve, how many variables there are, what form of model works best, and other factors. Machine learning algorithms can be classified based on the type of output they produce: if a categorical output is desired, a **classifier** is employed; whereas, for a continuous output, a **regressor** is more suitable.

ML algorithms can also be categorized based on their learning approach, distinguishing between supervised and unsupervised learning.

3.2.1 Supervised Learning

The ML task of learning a function that translates an input to an output using exemplar input-output pairs is known as supervised learning. From labeled training data, which consists of a collection of training instances, it infers a function. Algorithms for supervised machine learning are those that require outside support. The train and test datasets are separated from the input dataset. An output variable from the train dataset needs to be classified or predicted. Every algorithm uses the training dataset to identify patterns of some sort, which it then applies to the test dataset for classification or prediction. Most famous supervised ML algorithms are Decision Tree, Naive Bayes and Support Vector Machine.

3.2.2 Unsupervised Learning

In contrast to the supervised learning described above, unsupervised learning lacks both an instructor and right responses. It is up to the algorithms to find and display hidden patterns in unlabeled data. Few features are learned from the data by the unsupervised learning algorithms. It recognizes the class of the data when it is introduced by using the previously learned features. Its primary applications are in feature reduction and clustering. Some examples of these two applications are, respectively, Principal Component Analysis and K-Means Clustering.

3.3 Deep Learning

Deep Learning is a subset of Machine Learning. In contrast to shallow Machine Learning, Deep Learning extracts and transforms features via a cascade of layers of nonlinear processing units, based on neural networks. With a hierarchical data representation, where higher level features are generated from lower level features (backpropagation algorithm [56]), it enables computers to learn [57]. A basic example of a deep neural network is shown in Figure 3.2, where inputs from DL algorithms are processed through several hidden layers, with the outputs coming from the computation of those layers.

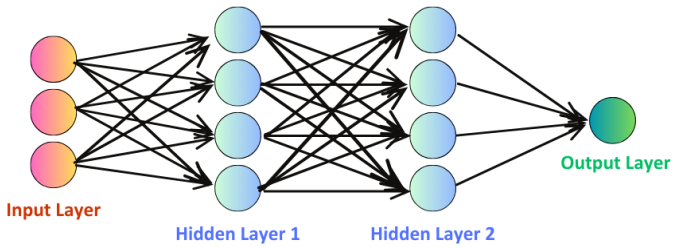

Figure 3.2. A Deep Neural Network is made up of at least two hidden layers.

When provided with an image, for example, a deep neural network can discern various features at each hidden layer. To illustrate, when given the pixels of an image as input, the initial layer can pinpoint edges by contrasting colors or brightness among neighboring pixels. Subsequently, the second hidden layer has the capability to identify corners and contours based on the edge descriptions. Following this, specific object components can be identified through the examination of particular collections of contours and corners. Ultimately, the objects within the input image can be successfully recognized [58].

Chapter 4

Materials and Methods

In this chapter, we will present the tools and methods used during the development of this thesis, outlining a clear and structured path. We will start with the presentation of the signal acquisition systems, then move on to the development environments for virtual reality tasks, and the calculators and visualization systems used. We will continue by examining the communication protocols established between the actors involved in the process and will provide a detailed description of the adopted experimental protocol. Subsequently, we introduce signal preprocessing, highlighting all the extracted features and delving into the adopted methodology. We will also delve into feature selection and the algorithm used, and then move on to a detailed discussion of regression and Support Vector Regression. We will conclude the chapter with an overview of the statistical methods employed for the analysis of the results.

4.1 Software and Instrumentation

The devices used in this research includes the 8-channel Enobio to take the EEG signal on the test subjects, NIC2 software downloaded to the computer to be able to communicate with the Enobio, the Oculus Meta Quest 2 visor for playing the virtual reality scenario developed on Unity, and a computer with certain specifications necessary to communicate properly with the virtual reality viewer.

4.1.1 Enobio

The 8-channels Enobio is a portable wireless device for monitoring EEG signals. It has a bandwidth of 0 to 125 Hz and a sampling rate of 500 SPS.

This system includes many accessories: a **neoprene headcap** with 64 holes, in which to place a maximum of 8 electrodes, according to the 10-10 system; **Ag/AgCl electrodes** for each of the 8 channels to fill with **conductive electrolyte gel**, **adhesive electrodes** for CMS and DRL references; conductive gel is injected inside the electrodes with a **curved syringe**; to these electrodes will be connected a **8-channel connector**, which actually consists of 10 cables, i.e., the 8 for signal monitoring and two for reference ones; the **Enobio Necbox** (**Neuroelectrics Control Box**) that is the actual device, to which the 8-channel connector is linked. It has an internal rechargeable battery, and thus also has its own charger in the kit. The complete system can be seen in the Figure 4.1.

Figure 4.1. 8-channels Enobio [59].

4.1.2 NIC2 Software

Neuroelectrics' NIC2 software [60] is designed to control devices—including the Enobio—from a computer. There are three modes available to connect it to a suitable device: USB cable, Bluetooth, and Wi-Fi. Once it's connected to the device, various settings can be set, among which the main ones are the **Line noise filter** to remove line interference at 50 or 60 Hz and the **TCP connection**, to send the collected data to other software (in this case, Matlab). In addition, **Default visualisation filter (Hz)** can be enabled to set the filter cutoff values for real-time signal display. These and other settings are visible in the Figure 4.2.

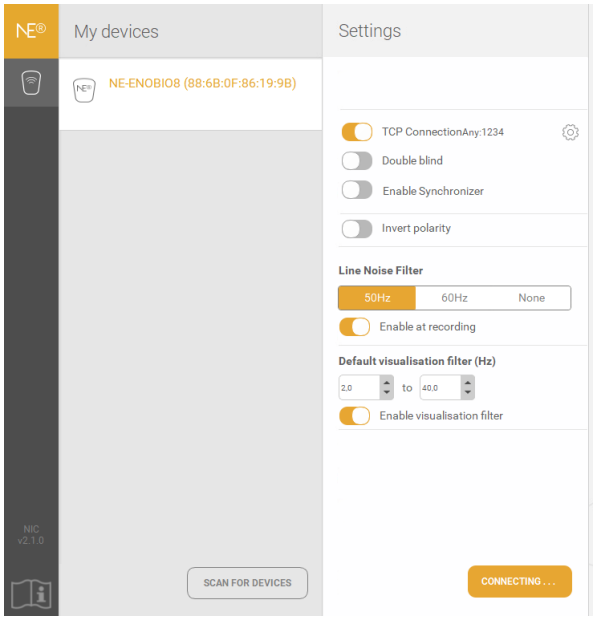

Figure 4.2. NIC2 settings.

There is also the possibility of including **markers** in the settings, so that they can be entered via the keyboard, to mark the signal and then be able to segment it later thanks to them. After all this has been set up, a new acquisition protocol can be created, in which you enter the name of the step, the step total duration and you select the desired channels in the order in which they will be mounted on the subject. Then you can finish and save the protocol. It can be seen in Figure 4.3.

The Figure 4.4 shows EEG signal for each of the 8 channels chosen: here it is possible to see the goodness of the signals acquired in real-time, having as an indication of this also the colors related to the signals (green if it is a very good signal, orange if it is good, red if of bad quality) and their corresponding quality index. There are three options available for signal display: amplitude scale in µV/div, time window in seconds, and channel reference (CMS or any other suitable channel). The protocol can be started, stopped and its name can be modified at the top of the screen.

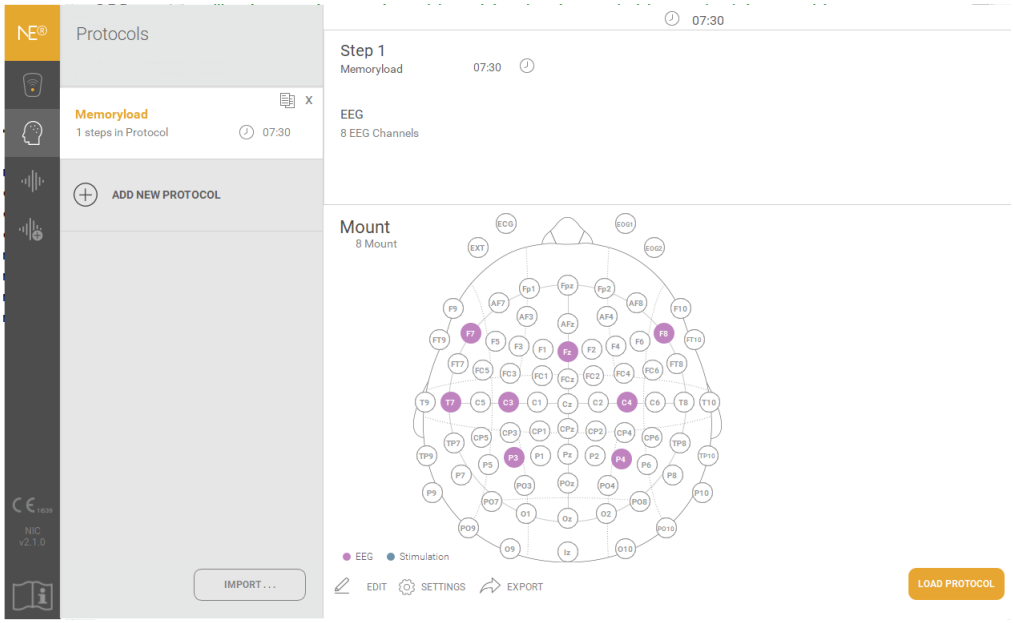

Figure 4.3. NIC2 protocol.

Figure 4.4. NIC2 channels.

4.1.3 Unity and Visual Studio

Unity Technologies has created a platform called Unity that facilitates the real-time development of interactive games and simulations in two- and three-dimensional spaces. Its use has grown over time to include a wide range of industries, including engineering, the film business, and the automobile industry. One of its main benefits is that, because of its easy-to-use editing features, its sophisticated visual editor and easy-to-use drag-and-drop feature let developers create complex virtual environments without requiring a lot of coding experience. The Unity Asset Store, a marketplace where creators may exchange or sell the environments and resources they have made, is another feature that improves its usability [61].

Unity utilizes the C# (C Sharp) programming language to cater to more experienced users who are interested in undertaking intricate projects and defining specific actions. C# is an object-oriented language that enables developers to script complex functionalities within Unity [62]. The process of writing scripts is made easier with the assistance of Visual Studio, a development environment created by Microsoft [63]. Visual Studio supports various programming languages, including C#, C++, Java, and JavaScript. This integration of user-friendly editing, a thriving marketplace for shared resources, and the ability to delve into advanced scripting languages positions Unity as a versatile tool that caters to a wide range of users, from beginners to seasoned developers, across multiple industries beyond gaming [64].

Unity Interface

Unity's interface is a sophisticated and versatile toolset, serving as the cornerstone for the creation of interactive multimedia and game development projects. The intuitive design and adaptability of Unity's interface, particularly highlighted through its Hierarchy and Inspector components, plays a pivotal role in enhancing the user experience and efficiency in interactive multimedia and game development, as visually represented in the Figure 4.5.

Hierarchy: The Hierarchy, a hierarchical representation of every element in the scene, is the central component of Unity's interface. This part gives developers a structural perspective of the game objects, making it easier for them to manage and arrange the many components in their project. The foundation for a logical and well-organized project structure is laid by the relationships between different game elements, which are established in large part thanks to the Hierarchy.

Scene: A dynamic, interactive depiction of the virtual world under development is provided by Unity's Scene View. This part gives developers real-time scene navigation and manipulation capabilities, giving the placement and interaction of game items a visual backdrop. A key element of level design is the Scene View, which enables programmers to see and maximise the spatial arrangement of their creations.

Game: The Game View, which provides a preview of the project as it will appear to end users, complements the Scene View. This part is essential for assessing and testing the interactive features of the programme, giving developers instant access to information about how users engage with it. For visual aspects to be refined and the final product to be seamless and immersive, the Game View is essential.

Inspector: One dynamic element that is essential to Unity's UI is the Inspector panel. It displays the attributes, parts, and scripts of the game item that is presently selected and offers comprehensive information about it. The Inspector is a tool that developers use to adjust and modify the properties of materials, game objects, and other scene elements. This fine-grained control enables developers to precisely iteratively improve their works.

Console: Developers rely heavily on the Console component in Unity's UI to monitor and troubleshoot their projects. It offers immediate feedback on problems, warnings, and log messages that are produced while the application is running. To guarantee the stability and robustness of the development process, the Console is a vital tool for problem-solving.

Project: The Unity interface's Project panel acts as a complete storehouse for all project-related resources and assets. It makes asset management easier by providing an organised view of directories, scripts, textures, and other project components. The Project panel is utilised by developers to arrange, import, and modify project materials, guaranteeing an efficient workflow and productive teamwork.

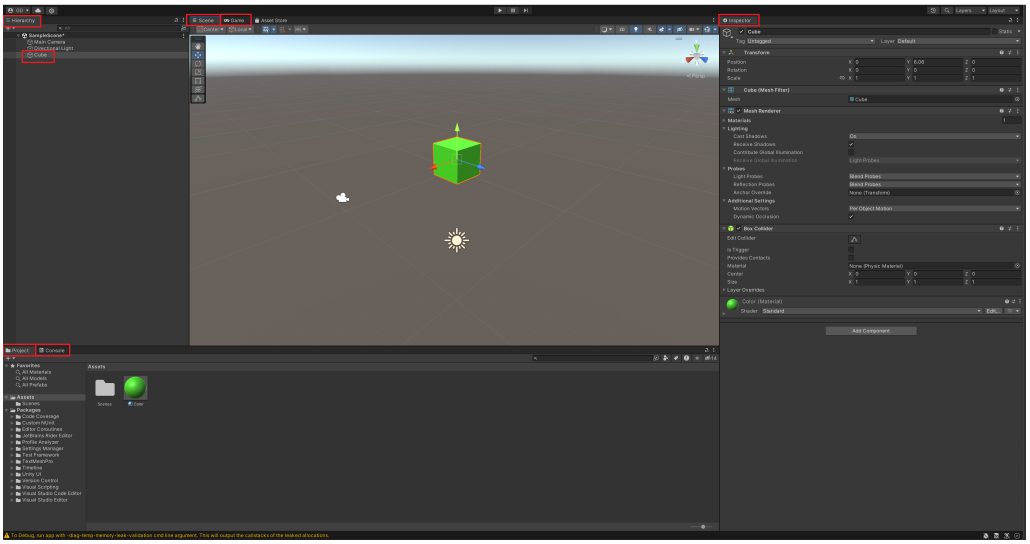

Figure 4.5. Example of a Unity interface in which the main components have been highlighted.

4.1.4 Virtual Reality

Virtual Reality (VR) represents an innovative technology that transports individuals into digitally simulated environments, providing an engaging and immersive experience. This advanced technology has found applications in various areas, from gaming to the simulation of complex training scenarios. In the context of scientific and psychological research, VR is utilized to explore and understand human behavior in controlled environments. In the current context, we delve into the design of a virtual reality scenario, focusing on the goal of creating an environment that emulates a study or workplace, with the aim of facilitating concentration and enhancing participants' cognitive performance. The combination of realistic and relaxing elements aims to provide an authentic experience, while also enabling the observation of mind-environment interactions under controlled conditions.

Virtual Reality Scenario

The design of the virtual reality scenario began with the intent to create an environment reminiscent of a study or workplace, where daily tasks requiring focus can be performed. This approach aims to immerse participants in a setting that mirrors real-life, offering familiarity and comfort to facilitate easier and more immediate concentration. In the Figure 4.6, it is possible to observe the set of elements that make up the virtual scenario. Instead of a bland and

sterile office environment, which could be unengaging and monotonous, the room includes elements that convey tranquility. This is expected to positively impact the participants' ability to achieve greater concentration. Therefore, objects reminiscent of work and study, such as a desk, a computer screen, and various books, were incorporated. At the same time, the room features a sofa, a fireplace, and various decorative items. Additionally, a large window allows participants to view a natural landscape, creating a sense of calm and promoting well-being.

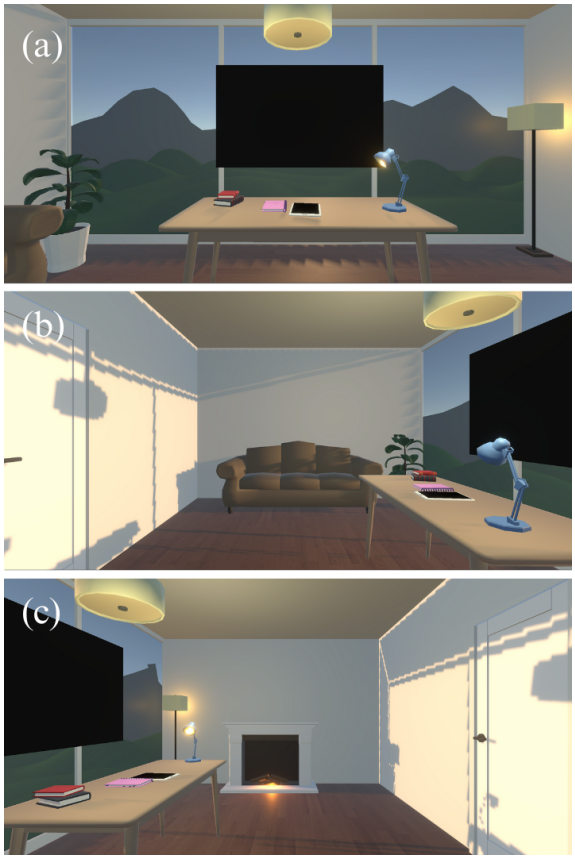

Figure 4.6. Virtual reality scenario: (a) Front View; (b) Left Side View; (c) Right Side View.

Research has shown that creating conditions for relaxation can enhance cognitive processes and, consequently, improve working memory levels. To amplify this effect, calm and soothing music is played throughout the virtual reality stimulation phase. This not only makes the sessions more immersive but also minimizes potential external distractions [65].

Oculus Meta Quest 2

Meta Quest 2 is a revolutionary virtual reality headgear represented in Figure 4.7. This technical analysis will examine the architecture, processing power, user interface, and underlying engineering principles of the Quest 2, delving into the complexities of its hardware and software components and their astounding performance [66, 67].

Figure 4.7. Meta Quest 2 [68].

The Snapdragon XR2 processor, which powers the Meta Quest 2, is a key component that contributes to the headset's powerful processing capacity. The XR2 CPU is designed with extended reality (XR) applications in mind. It offers better graphics rendering, lower latency, and increased energy efficiency. This technological development is essential for giving consumers a smooth and engaging virtual reality experience, especially in demanding applications like intricate simulations and high-fidelity games [69, 70]. The Meta Quest 2's engineering achievement is the use of inside-out tracking technology. Without the use of external sensors, the headset's array of integrated sensors—which includes gyroscopes and accelerometers—allows it to precisely trace the user's movements in three dimensions. This engineering solution increases the overall resilience and reliability of positional tracking during dynamic VR experiences, while simultaneously improving user comfort by removing the setup complications associated with additional sensors [66, 67]. The wireless capabilities of the Meta Quest 2, made possible by state-of-the-art communication protocols, is an important engineering aspect. Wi-Fi 6

technology integration ensures a snappy VR experience by minimizing latency and enabling high-speed data flow between the headset and the host device. This wireless feature, along with the device's portability, opens up new possibilities for the user's range of motion. It's an important engineering accomplishment that increases the VR system's total versatility [66]. Meta Quest 2 also shows great promise for rehabilitation and cognitive training, which makes it a flexible instrument for improving human well-being. The engineering principles that are integrated into the headset are in perfect harmony with the needs of applications that are designed to improve cognitive skills and motor rehabilitation [71, 72]. Furthermore, the immersive quality of virtual reality makes it a perfect medium for practicing working memory. The robust processing capabilities of the Meta Quest 2 make it easier to develop cognitive training programmes that test and enhance users' working memory. Interactive exercises in a virtual setting can be made to target particular cognitive functions, encouraging neuroplasticity and possibly helping people with illnesses that impact cognitive functions, like age-related cognitive decline or attention deficit disorders [72]. The Meta Quest 2's wireless and portable design increases its suitability for use in rehabilitation environments. Rehabilitation programmes are more flexible and accessible when patients can carry out prescribed exercises or cognitive training routines in a variety of settings. This feature is especially helpful for home-based rehabilitation since it makes it possible for patients to easily incorporate therapeutic activities into their regular routines [73]. Enabling Developer Mode in the Meta Quest 2 presents an amazing opportunity for users to fully utilise Unity's capabilities and dive into the virtual reality realm. This feature opens up the possibility of developing experiences and apps that are specifically suited to a user's interests, needs in terms of education, or leisure. Turning on Developer Mode on the Meta Quest 2 basically lets you create games with Unity, a powerful game engine that's highly regarded for its adaptability and streamlined user interface. Unity is the perfect platform for individuals who are eager to learn about VR creation but do not have a strong experience in coding because it makes it very simple for developers to build immersive and interactive content. Custom app development for the Meta Quest 2 has an almost infinite range of possibilities, from entertainment and educational applications to realistic simulations and experiences. The communication between a computer and the Meta Quest 2 is achieved either through a USB 3.0 cable or via WiFi. This connection is known as Quest Link, enabling access to the Rift interface, allowing users to launch their Unity-developed applications directly on the VR headset.

4.1.5 Computer

The connection via Oculus Link requires a computer with good performance and a compatible graphics card for the connection. In this study, a Personal Computer in Figure 4.8 with the following specifications was used:
CPU: Intel I7 12700F, 4.9 GHz.
GPU: NVIDIA 4060Ti 8GB.
RAM: DDR4 32GB.
Memory: SSD NVMe 1TB.
OS: Windows 11 Pro.
Cooling System: 240mm liquid cooling system.

Figure 4.8. Breunor Avalon [68].

4.1.6 Matlab Toolkit

MatNIC2 For advanced researchers, MatNIC2 is a Matlab toolkit for flexible, programmatic control of Neuroelectrics devices. You can receive and process EEG data, for example, and change any stimulation setting in real-time [74].

Functions from the MatNIC2 library must be loaded and started in order to connect Matlab to the NIC2. The TCP/IP protocol previously described is used to accomplish remote control. In this instance, the NIC2 functions as the server and Matlab as the client. The NIC2 Remote Stimulation Server is accessed with the function `MatNICConnect`. The server is running on the machine where the NIC2 application runs on the port 1235. This function

accepts the host, or IP address, as input and outputs three variables: socket, status, and ret. Whether the connection was successful (ret = 0) or not (ret < 0) is indicated by the value of "ret". On the other hand, the connection is identified by the "socket". Then, the functions `MatNICLoadProtocol` and `MatNICStartProtocol` respectively send to NIC2 the name of the protocol to be loaded and request NIC2 to start the protocol. After establishing the connection, you can utilize `MatNICEEGConnectLSL`, which creates an "inlet" for initiating the retrieval of "chunks".

4.2 Communication Protocols

Two types of communication protocols were utilized in this work, which are TCP/IP protocol, to ensure communication between Matlab and Unity, and LSL protocol, to enable communication between NIC2 software and Matlab. These are described as follows.

4.2.1 Transmission Control Protocol/Internet Protocol

The communication protocols known as TCP/IP, or Transmission Control Protocol/Internet Protocol, are used to link network devices on the internet. In this study we used those for a real-time communication between Matlab and Unity. This protocols provide end-to-end data communication [75]. In reality, TCP/IP is actually composed of two protocols, the Transmission Control Protocol (TCP) and the Internet Protocol (IP), often referred to as the TCP/IP suite. Each of these two protocol has a distinct purpose. Applications can establish communication channels over a network according to *TCP* specifications. Additionally, it controls the process of breaking up a message into smaller packets so that they may be sent across the internet and assembled correctly at the destination address. Each computer or device connected to the network is assigned a unique *IP* address (Internet Protocol address) by TCP/IP. This allows each IP address to establish a connection on one or more ports, up to a maximum of 65535, for the purpose of sending and receiving data to and from other network devices. This creates a private, two-way channel of communication between devices that are referenced by an IP address. To ensure that a packet reaches its intended location, IP specifies how to address and route each packet. This IP address is checked by each network gateway computer to determine where the message should be forwarded [76]. In order to make a connection over TCP/IP, a device known as the client—in our study, Matlab—and the server— i.e. Unity—are required. The server (or

listener) is the computer that "listens" for all incoming connections from the various clients. The client must know the port number via which it intends to send and receive data, in addition to the IP address of any server it wants to connect to. The server waits for connections to arrive and decides whether to accept or reject them. A connection is open until either the client or the server chooses to break it. Data can be transferred and received via the designated port number between the Client and the Server during this time [76].

4.2.2 Lab Streaming Layer

A set of libraries and tools known as the Lab Streaming Layer (LSL) provide multi-modal time-synchronization, real-time data streaming, and triggering. Several computer languages (C, C++, Python, Java, C#, Matlab) and operating systems (Mac, Windows, Unix) can be used to control the connection. Any software sending or receiving data must be connected to the same network in order for LSL to function [77]. The liblsl library is used in the communication protocol. The following abstractions are available for usage by client applications through the liblsl library [77]:

- *Sample.* It is a single measurement of every channel from a device.
- *Chunk.* For better latency, a sample can be transferred alone; for better throughput, it can be transferred in segments comprising many samples, called chunks.
- *Metadata.* In addition to the raw data, XML data—which is similar to a file header—are stored and transferred with information about the stream. They are known as Metadata.
- *Stream.* A stream is made up of the Metadata and sampled data from a device. A stream may consist of one or more channels with either a regular or irregular sampling rate. A stream's data must all be of the same type (integers, floats, doubles, or strings).
- *Stream Outlet.* Its function is to provide lab network users with access to time series data streams. Sample-by-sample or chunk-by-chunk, the data is sent into the outlet. A group of computers (specified by the network configuration) can see the stream when an outlet is created, and they can subscribe to it by using a Resolver to locate it and connecting a Stream Inlet to it.

- *Stream Inlet.* Receiving time series data from a single connected outlet is done using a stream inlet. It permits the orderly retrieval of samples from the stream, along with optional failure recovery, type conversion, and dependable (re-)transmission. In addition to the samples, the Metadata is also available.

- *Resolver.* Streams on the lab network can be resolved using LSL functions based on content-based queries (e.g., by name, content-type, or meta-data queries).

- *Built-in clock.* It enables mutual synchronization of the sent samples by providing a time-stamp.

4.3 Study Protocol

4.3.1 Memory Task

The n-back test, an integral part of neuropsychological assessments, serves to evaluate working memory and its capacity. It challenges participants to monitor and respond to sequences of stimuli, with difficulty levels adjusted by altering 'n', the number of steps back in the sequence for recall. This test offers crucial insights into an individual's cognitive functions, particularly in working memory and executive function. Originating as a simple memory test, the n-back task has evolved into a pivotal tool in cognitive psychology and neuroscience research, with applications in clinical diagnosis. It caters to a diverse demographic, including children, adults, and the elderly, and is used for understanding cognitive processes in both healthy individuals and those with impairments, such as ADHD, schizophrenia, and dementia [78, 79]. The simplicity of the n-back task design belies its execution complexity. In a typical setup, participants are shown stimuli like letters or numbers and must identify matches with those presented n steps earlier. For example, in a 2-back task with a sequence of 5-8-5, the participant identifies the second 5 as matching the first. This task assesses not only memory capacity but also attention control and response inhibition. Its adaptability allows researchers to tailor the task for specific needs, like using different stimuli types or increasing the n-back level for greater challenge. This has led to a variety of n-back task versions, enhancing its utility in cognitive assessments. Furthermore, the n-back task has been key in mapping brain areas involved in working memory through functional MRI studies, enhancing understanding of how these areas function in various neurological conditions [80]. Overall, the n-back test is

not merely a memory measurement tool; it provides a comprehensive view of the human brain's complex functioning, offering valuable insights for both theoretical and practical applications in cognitive health.

2-back

In this thesis, the 2-back memory task is employed to challenge and assess working memory. Participants are presented with a sequence of digits from 1 to 9, identifying if the current digit matches the one shown two steps back. This task necessitates continuous memory updating and monitoring, exemplified by identifying a repeating digit in a sequence like 3-5-3. It effectively tests attention, concentration, and the ability to manage and manipulate temporary information in the mind.

3-back

The 3-back task, a more demanding version of the n-back, is also included in this thesis to rigorously evaluate working memory. Participants see a series of digits from 1 to 9, determining if the current digit matches the one three steps prior. This task, exemplified by recognizing a digit repeating after two intermediate digits, like in 4-2-7-4, demands a higher level of cognitive processing, challenging participants to retain and manipulate information over an extended period.

4.3.2 EEG Acquisition

The EEG signal acquisition is the starting point and a crucial part of the entire study. Using the NIC2 acquisition software, connected via Bluetooth to the Enobio Necbox device, two protocols are set up: one for calibration and the other for real-time operation. These protocols, identical in terms of electrode placement, differ in their duration and operating type.

Open-Loop Phase

During the calibration phase, the signal is recorded 'offline' by NIC2 using an *open-loop* protocol and stored in .easy format files. These files can be easily loaded into Matlab for further processing. Markers, detailed in the 'NIC2 software' section, are inserted during recording to temporally align the signal with the VR viewer test performed by the subject. This temporal alignment is crucial for the functionality of the calibration phase, upon which the overall system's performance heavily relies.

Following this offline recording obtained through Bluetooth communication between Enobio Necbox and NIC2, the signal is imported and processed in Matlab. Relevant features specific to the user are now extracted from the EEG signal, and a regression model is trained to be used in the subsequent real-time phase.

Closed-Loop Phase

To initiate the real-time phase, the TCP/IP protocol must be activated on the NIC2 interface. This enables direct communication between Matlab and NIC2 using the MatNIC functions (described in the corresponding section). These functions allow the loading and initiation of a new recording protocol on the NIC2. Following this setup, Matlab establishes a connection via LSL to receive data packets (chunks) comprising approximately 250 samples each, acquired at 500Hz. Matlab processes the received chunks and then transmits parameters to Unity through the TCP/IP protocol for modulating various stimulations. Unity subsequently delivers the modulated stimuli in the virtual reality environment. This protocol is then defined as a *closed-loop* system. The following Figure 4.9 schematically depicts the operational difference between the open-loop and closed-loop phases, highlighting the various modes of interaction and data flow among the system components.

4.4 EEG Signal Preprocessing and Analysis

This thesis incorporates a comprehensive approach to EEG signal preprocessing and analysis using a custom Matlab script, designed to extract and evaluate various EEG parameters. The script initiates with an environment setup, followed by detailed steps for signal preprocessing, feature extraction, and data analysis. The preprocessing of the EEG data is a critical step, involving several sub-processes.

4.4.1 Signal Filtering Process

Filtering is a pivotal process in EEG signal preprocessing, crucial for enhancing signal quality and isolating meaningful data for analysis. This section describes the filtering techniques applied to EEG data, focusing on the types of filters used and their role in the preprocessing workflow.

Interpreting the EEG signal is challenging due to its non-linear and non-stationary characteristics. Simply examining the EEG trace visually does not

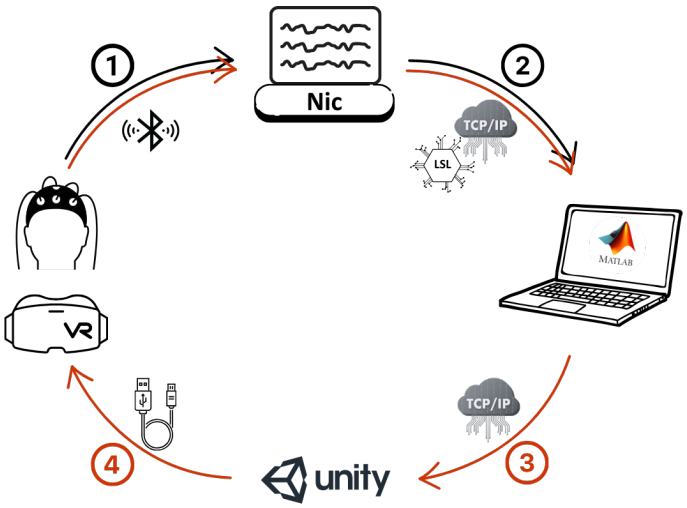

Figure 4.9. Representative diagram of the open loop phase (indicated by black arrows) and the closed loop phase (indicated by red arrows) in the communication between Enobio Necbox, NIC2, Matlab, and Unity. (1) Acquiring the EEG signal using Enobio Necbox and recording via NIC2. (2) Transferring the signal from NIC2 to Matlab for processing. (3) Transmitting data from Matlab to Unity. (4) Delivering the stimulus in virtual reality.

provide enough information for meaningful analysis. The complexity arises primarily because the raw signal (referenced in Figure 4.10) contains overlaid non-brain-related signals. These include artifacts from eye movements (EOG), artifacts from movements of facial muscles (EMG), electrical noise, and disruptions resulting from incorrect placement of electrodes.

Types of Filters Used

Chebyshev filters play a significant role in refining the EEG data for accurate analysis. These filters are a type of digital filter with distinct characteristics, making them particularly suitable for specific EEG processing needs. Chebyshev filters are part of the IIR (Infinite Impulse Response) filter class and are categorized as ARMA (autoregressive moving average) types, as their transfer function includes both poles and zeros. Chebyshev filters come in two types: Type I and Type II. Both are known for their sharp cutoff characteristics, which means they can more precisely separate the desired signal from unwanted frequencies.

1. **Type I Chebyshev Filters**: These filters exhibit a ripple effect in their passband, which refers to the range of frequencies they allow to

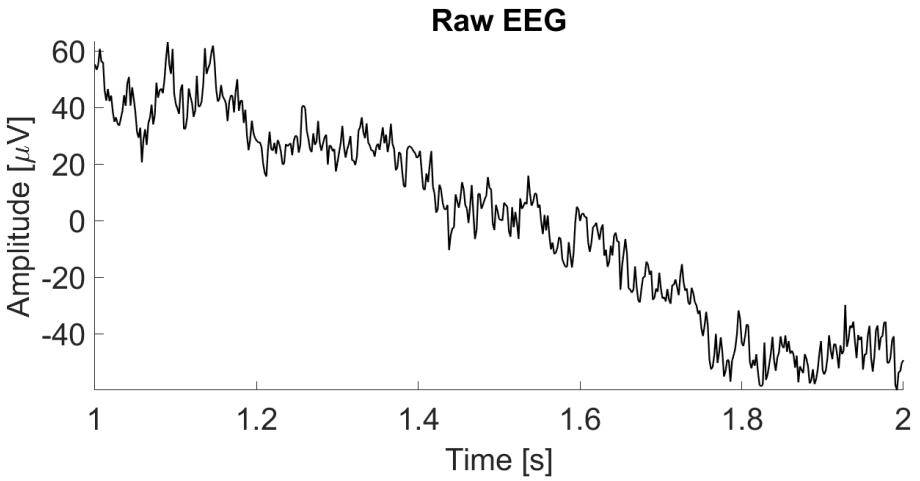

Figure 4.10. Raw EEG Signal. The graph represents a raw EEG signal over a time period of seconds. The x-axis represents time in seconds and the y-axis represents amplitude in µV.

pass through. The ripple is a series of peaks and troughs in the filter's response, offering a sharper cutoff at the expense of a less uniform passband. This feature can be advantageous in EEG processing when a sharp delineation between frequency bands is needed, such as sharply differentiating between alpha and beta waves.

2. **Type II Chebyshev Filters**: In contrast, Type II filters, also known as inverse Chebyshev filters, show a ripple in the stopband instead of the passband. This means they maintain a flat response within the frequency range of interest (passband) but have a variable response in the range of frequencies being filtered out (stopband). This characteristic is beneficial when a uniform signal within a specific band is crucial, and variations in the stopband are less of a concern.

Both types of Chebyshev filters are characterized by their fast roll-off, meaning they transition quickly from the passband to the stopband. This makes them highly effective in EEG applications where separating closely spaced frequency bands is essential, such as distinguishing between overlapping neural oscillations.

In this thesis, the choice was made to utilize two Chebyshev Type I filters, as it was crucial to distinctly eliminate frequencies not pertinent to the study, which could include artifacts such as muscular and ocular movements. Therefore, a high-pass filter (HPF) and a low-pass filter (LPF) are employed in a cascading sequence:

1. **High-Pass Filter (HPF) using Chebyshev Type I**: The function `[b_high, a_high] = cheby1(n, Rp, wp, 'high')` is utilized to design the high-pass filter. The `cheby1` function in Matlab is specifically tailored for creating a Chebyshev Type I filter. The parameters of this function are:
    - *n*: This determines the order of the filter, influencing the steepness of the filter's response curve. A higher order indicates a more abrupt cutoff at the designated frequency.
    - *Rp*: This is the pass-band ripple, defining the maximum permissible ripple within the pass band, measured in decibels (dB). It balances the sharpness of the cutoff with the pass-band's frequency response uniformity.
    - *wp*: This represents the cutoff frequency for the high-pass filter, marking the frequency below which signals are attenuated.
    - *'high'*: This parameter specifies the filter type as high-pass.
2. **Low-Pass Filter (LPF) using Chebyshev Type I**: The function `[b_low, a_low] = cheby1(6, Rp, wp, 'low')` is used for generating the coefficients of the low-pass filter. This function is similar to the previous one, with the only change being the last parameter switching from 'high' to 'low'. In this context, `wp` indicates the frequency above which the signal's components will be attenuated, playing a vital role in defining the frequency range the filter will effectively allow. The function returns `b_low` and `a_low`, arrays that contain the numerator and denominator coefficients of the filter's transfer function, respectively. These coefficients are crucial for the implementation of the filter in digital signal processing tasks.

The integration of high-pass and low-pass Chebyshev Type I filters in this thesis constitutes a cascading system, pivotal for the precise isolation of target frequency ranges in EEG signal analysis. This meticulously designed system ensures the elimination of extraneous frequencies and artifacts, thereby enhancing the purity and relevance of the data. A notable aspect of this approach is the preference for IIR (Infinite Impulse Response) filters over FIR (Finite Impulse Response) filters. This choice is strategically made due to the IIR filters' proficiency in achieving the desired specifications with a lower order, resulting in a significantly reduced transient response. However, a challenge with IIR filters is their inherent non-linear phase characteristic, which can introduce phase distortion into the signal. To adeptly counteract

this issue, the study employs anticausal zero-phase rotation filters, exemplified by the utilization of Matlab's 'filtfilt' function, which effectively negates any phase distortion, ensuring the fidelity of the signal processing. The dual arrangement of the Chebyshev filters brings forth multiple advantages. Enhanced precision in frequency isolation is achieved as each filter's cutoff frequency can be finely tuned. This level of control is invaluable in EEG analysis for the accurate identification of specific brainwave frequencies.

Moreover, the system offers a flexibility surpassing that of a single bandpass filter, allowing for tailored adjustments to suit various research needs and EEG data types. The cascading structure also significantly elevates the integrity of the EEG signal. By dedicating each filter to a specific task – filtering out either high or low-frequency noise – the system yields a cleaner, more accurate representation of the desired signal. This approach effectively minimizes the risk of artifact-induced distortions, a critical factor in the validity of EEG data analysis.

In addition to these technical merits, the stability of the filter system is paramount. Stability is verified through Matlab's 'freqz' function, which provides a detailed visual representation of the frequency response masks, as illustrated in Figures 4.11 and 4.12. These visualizations are not just graphical representations but are instrumental in affirming the filter's performance and stability over the intended frequency range. They are vital in ensuring that the filters operate as intended, thereby upholding the accuracy and reliability of the EEG data analysis.

After undergoing the described processing steps, the filtered signal is presented as shown in Figure 4.13. This graph illustrates the impact of filtering across time, where the x-axis denotes time in seconds and the y-axis measures the amplitude in microvolts.

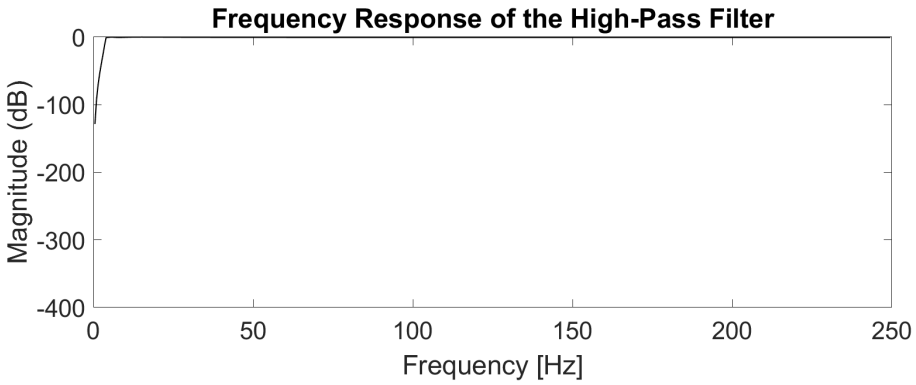

Figure 4.11. Frequency response of HPF.

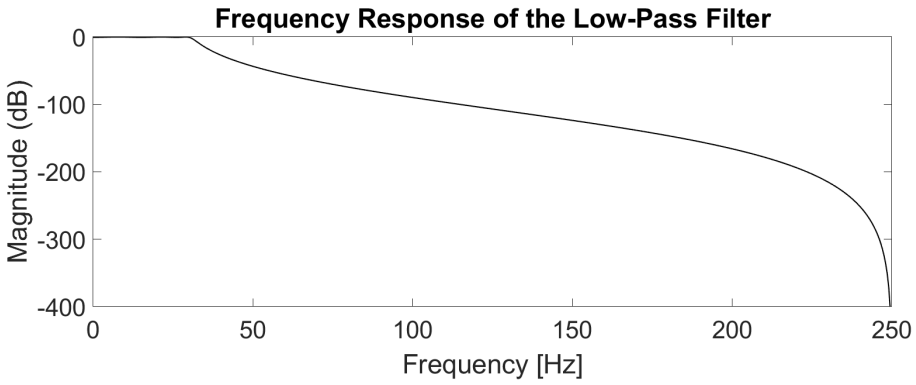

Figure 4.12. Frequency response of LPF.

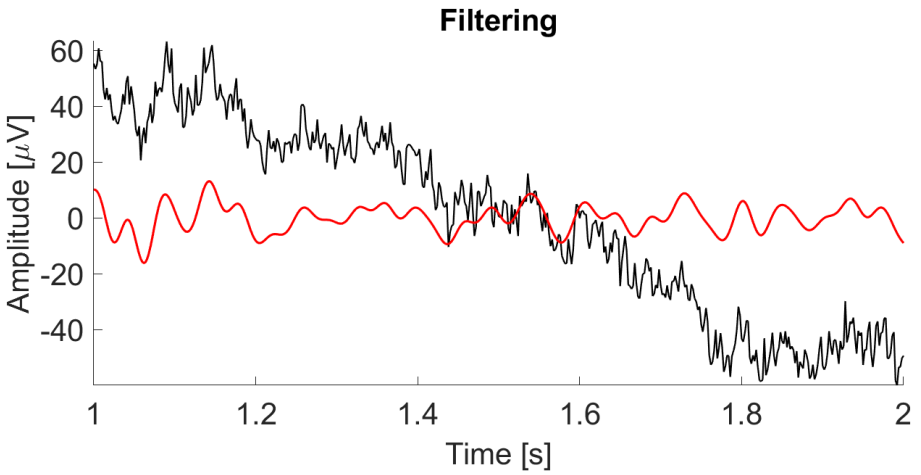

Figure 4.13. Comparison of the Raw Signal (in black) and the Filtered Signal (in red).

4.4.2 Power Spectrum Analysis

The EEG signal, a mirror of neural activity, exhibits oscillations across a range of frequencies. Spectral analysis, often employed for its quantification, is rooted in extensive research linking the EEG's frequency spectrum to various cognitive states and neurological pathologies. The core aspects of this analysis are the measurement of power and its spatial distribution within the brain. Here, 'power' measures the intensity of specific frequency bands in the signal, while 'spatial distribution' addresses the dispersion of this power throughout different brain regions, a key factor for decoding certain cerebral functions. The process of spectral estimation typically relies on the Fourier Transform (FT). This technique breaks down a signal into separate sinusoidal components, each with its own frequency and phase. Together, these components form the signal's power spectrum. The goal is to determine the power spectral density (PSD), essentially the frequency-wise distribution of the signal's power. A common approach for this analysis is the periodogram, offering a non-parametric PSD estimation by computing the squared magnitude of the signal's FT. It's important to note, however, that spectral analysis is ideally suited for signals that are stationary or at least 'weakly' stationary. The EEG signal, inherently random and non-stationary, does not fulfill this criterion, thus posing unique challenges in its spectral analysis. Nonetheless, a viable approach involves segmenting the signal into sufficiently short epochs (a few seconds) to at least ensure quasi-stationarity. In this thesis, power calculations were performed using a simple periodogram with 1-second signal epochs, equivalent to 500 samples. The implementation of the simple periodogram in Matlab utilizes the function:

$$\texttt{[P, f]} = \texttt{pwelch(x, w, noverlap, NFFT, f c)}$$

Where the input variables are:

- x: the time-series data, representing the signal for which the power spectrum is to be estimated.

- w: the windowing function applied to each data segment. This function mitigates the spectral leakage effect, enhancing the accuracy of the estimation.

- noverlap: the number of points by which consecutive data segments overlap. A higher overlap can increase the resolution but also the computational load.

- NFFT: the number of Fast Fourier Transform points used to calculate the power spectrum. This determines the frequency resolution of the analysis.
- f_s: the sampling frequency of the signal. This is crucial for correctly scaling the frequency axis of the power spectrum.

The function outputs two variables:

- P: the power spectral density estimate of the signal, providing insights into the power present at different frequencies.
- f: the frequency vector corresponding to the PSD estimates, facilitating the mapping of power distribution across the frequency spectrum.

This function is integral in analyzing EEG data, particularly in understanding the distribution of power across different frequency bands within the signal. In this study, it was decided to introduce no overlap in the spectral analysis, setting the `noverlap` parameter to zero. This approach ensures distinct and independent evaluation of each signal segment. The sampling frequency employed is 500 Hz, providing a detailed capture of the EEG signal's nuances. Furthermore, the `NFFT` was set to 500, aligning the apparent resolution with the theoretical resolution. This configuration allows for a precise and consistent analysis of the frequency components within the EEG signal, crucial for the accurate interpretation of the spectral characteristics.

$$\text{Theoretical Resolution} = \frac{1}{T} = \frac{f_c}{N} \tag{4.1}$$

where `T` represents the duration of the window in seconds, and `N` is the length of the window in samples.

$$\text{Apparent Resolution} = \frac{f_c}{\text{NFFT}} \tag{4.2}$$

To achieve an apparent resolution equal to the theoretical resolution, it is necessary to set `NFFT` equal to `N`, the length of the signal segment. In this study, the selection of a 1-second window length ensures a theoretical resolution of 1 Hz. This resolution is particularly effective for the EEG signal, allowing for the discrimination of frequencies that are typically 1 Hz apart within the various EEG frequency bands. Upon estimating the power spectral density of the EEG signal, the next step involves calculating the relative power within specific frequency bands. These include the theta band (4 Hz - 7 Hz), alpha

band (8 Hz - 14 Hz), beta 1 band (15 Hz - 21 Hz), and beta 2 band (22 Hz - 30 Hz). They can be seen in Figure 4.14.

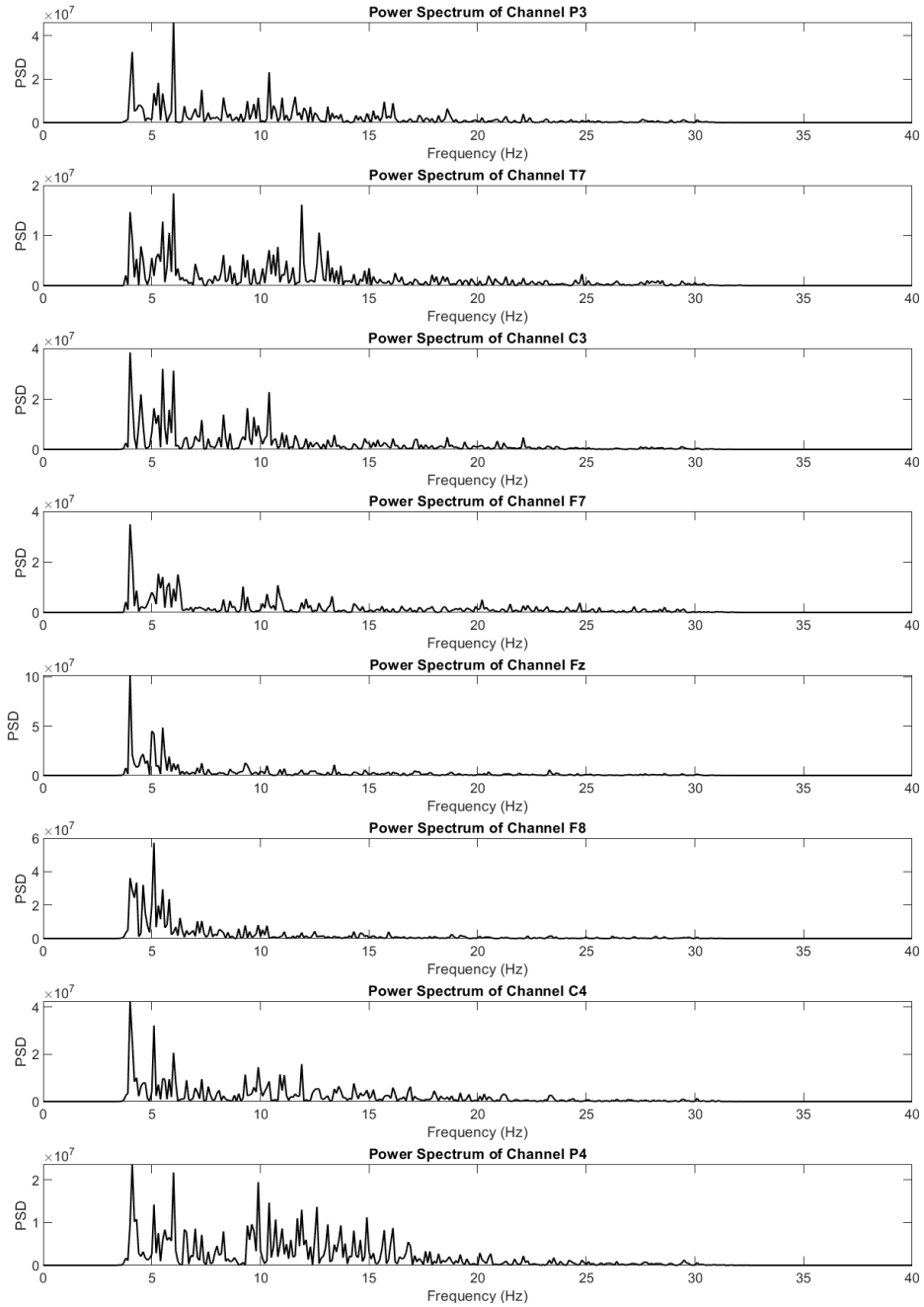

Figure 4.14. Power Spectral Density of the 8 Channel.

This process is crucial for understanding the distribution and dominance of different frequency bands in the EEG signal, which can be indicative of various cognitive states or neurological conditions

4.4.3 Feature Extraction

The primary objective of this study is to enhance the performance of working memory in the subjects participating in the research. To achieve this, the chosen strategy involves the development of an index through regression algorithms. This index aims to capture the trajectory of each subject's memory performance while they engage in the n-back memory task. To construct this index, it is essential to first extract predictive features from the EEG signals that are relevant to the phenomenon under investigation. Specifically, for all 8 channels recorded using the Enobio system, 348 total features are extracted. These features will be discussed in greater detail in the subsequent paragraphs, offering a comprehensive insight into their relevance and application in improving working memory performance.

Time Domain Features

This segment of the thesis examines the mathematical and statistical attributes extracted from the EEG signals in the time domain, offering a multifaceted understanding of their characteristics. Each feature extracted is pivotal for comprehensive EEG analysis:

1. *Mean*: the mean of the data, calculated as the average value of the EEG signal in a given segment. Mathematically, it is expressed as:

$$\bar{x} = \frac{1}{n} \sum_{i=1}^{n} x_i \tag{4.3}$$

   where x_i represents the signal values and n is the number of values.

2. *Variance*: this represents the extent to which the signal values deviate from the mean. Computed as

$$\sigma^2 = \frac{\sum_{i=1}^{n} (x_i - \bar{x})^2}{n-1} \tag{4.4}$$

   it measures the dispersion of the EEG signal values.

3. *Standard Deviation*: the square root of the variance, it provides a measure of the signal's volatility around the mean.

4. *Minimum Value*: the smallest value in the EEG signal segment, indicative of the lowest signal amplitude observed in the given time-frame.

5. *Maximum Value*: conversely, this is the highest value in the signal segment, representing the peak amplitude within the segment.

6. *Range*: computed as the difference between the maximum and minimum values, this feature reflects the overall amplitude variability of the EEG signal in the segment.

7. *Kurtosis*: a measure of the 'tailedness' of the signal's probability distribution. Kurtosis indicates how outlier-prone the signal distribution is, with higher values suggesting more outliers.

8. *Skewness*: this feature measures the asymmetry of the signal distribution. A skewness value different 5from zero indicates a distribution that is not symmetric around the mean.

9. *25th Percentile (Lower Quartile)*: this statistic represents the value below which 25% of the data falls, providing insights into the lower range of the EEG signal distribution.

10. *75th Percentile (Upper Quartile)*: analogously, this is the value below which 75% of the data falls, offering a perspective on the upper range of the EEG signal distribution. It helps in understanding the distribution's higher amplitude characteristics.

11. *Median*: the median provides a robust measure of the central tendency of the signal, representing the value at the middle of the dataset when ordered from lowest to highest. It is less sensitive to outliers than the mean, often giving a better representation of a 'typical' value in skewed distributions.

Each of these features contributes to a comprehensive understanding of the EEG signal's characteristics in the time domain. The mean, variance, and standard deviation offer insights into the signal's central tendency and variability. In contrast, the minimum and maximum values, along with the range, provide information about the signal's amplitude fluctuations. Kurtosis and skewness offer deeper insights into the shape of the signal's distribution, indicating the presence of outliers and the symmetry of the distribution, respectively. The percentiles and median give a more nuanced view of the signal's distribution, especially in the presence of non-normal distributions.

Collectively, these time-domain features provide a multi-faceted view of the EEG signals, facilitating a more nuanced analysis and interpretation. This detailed approach to feature extraction lays a solid foundation for subsequent analyses, such as feature selection and regression.

Mobility e Complexity

In the nuanced study of cognitive states using EEG signals, the metrics of Mobility and Complexity are invaluable for their detailed insight into signal characteristics. Mobility, represented mathematically as M, is defined by the formula

$$M = \sqrt{\frac{\text{var}(dX(t))}{\text{var}(X(t))}}. \tag{4.5}$$

Here, $\text{var}(dX(t))$ is the variance of the first derivative of the EEG signal $X(t)$. This derivative represents the rate of change of the signal, which is indicative of its frequency content. Therefore, Mobility is a measure of the average frequency or the 'speed' of the EEG signal, with higher values indicating more rapid fluctuations.

Complexity, denoted as C, builds upon this concept and is calculated as:

$$C = \frac{\text{Mobility}(dX(t))}{\text{Mobility}(X(t))}. \tag{4.6}$$

This ratio compares the Mobility of the signal's first derivative to the Mobility of the signal itself. Essentially, Complexity measures the relative smoothness of the signal's waveform; a higher Complexity value suggests a more intricate and less smooth waveform. This is particularly useful in EEG analysis as it reflects the intricacies of the neural activities and interactions underpinning different cognitive processes.

By applying these measures to EEG signals, researchers can gain a nuanced understanding of brain activities associated with specific cognitive tasks. For instance, variations in Mobility and Complexity across different tasks can reveal how neural dynamics change in response to cognitive load or attentional focus. This deeper analysis paves the way for advanced interpretations and applications in the field of cognitive neuroscience and related disciplines [81].

Power Domain Features

In the pursuit of understanding the complex states of the human mind through EEG analysis, we have extracted power measures across various frequency

bands that are indicative of distinct cognitive states. The bands of particular interest in our study are theta, alpha, beta 1, and beta 2. Theta activity typically emerges during deep sleep or profound relaxation, alpha waves are prominent during wakefulness and moments of relaxation, while beta waves are associated with concentration and attentiveness. For each channel, power within these four bands was extracted, resulting in a set of 32 features that encapsulate the power distributions.

However, these power features, while emblematic of certain mental states, do not suffice to accurately differentiate between relaxed states and those involving active working memory tasks, nor do they precisely predict performance. This limitation necessitated a multimodal approach through machine learning, which enables the integration of diverse variables and datasets to form a more complete picture of mental state transitions.

To enhance the interpretative power of our analysis, we combined these power measures to create ratios that could more sensitively reflect shifts in mental states. Notably, we focused on the ratios between theta and alpha powers, theta and beta powers, as well as beta and theta powers, aiming to cover the full spectrum of possible combinations. These ratios, particularly the beta/theta ratio, have been implicated in various cognitive phenomena, including attention and mental workload. During the computational analysis, it became evident that the power in the beta 1 band was particularly influential in the machine learning model training process. This finding underscored the significance of the beta 1 frequency band in relation to cognitive effort and attentional states.

Figure 4.15, with its topographic maps for different frequency bands, illustrates this complex interplay of brain activities during resting states and cognitive tasks. The visual representation vividly demonstrates the spatial power variations that correspond to the engaged mental processes, providing a compelling confirmation of our analytical findings.

This integrative approach, combining raw power features with calculated power ratios , offers a potent method for delving into the intricacies of EEG data and deciphering the nuanced patterns that underlie cognitive function and mental state transitions.

Resting-State Topographic Maps for Different Frequency Bands

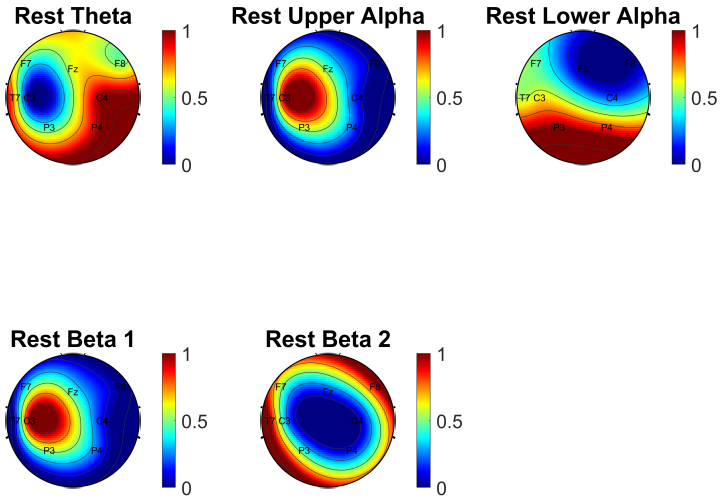

2-Back Topographic Maps for Different Frequency Bands

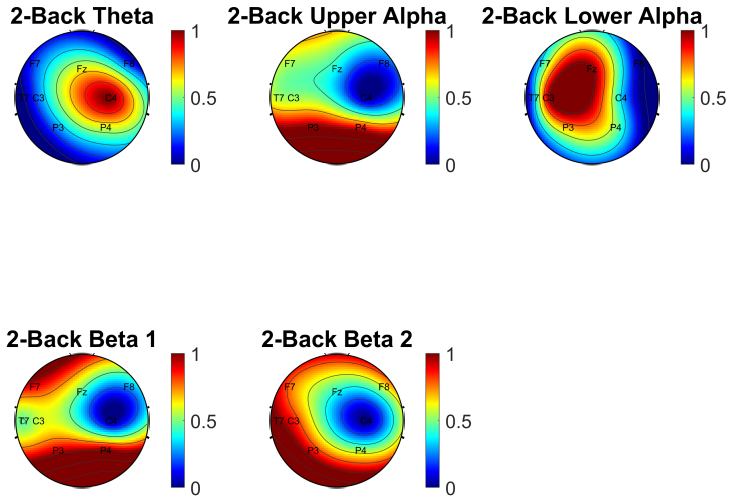

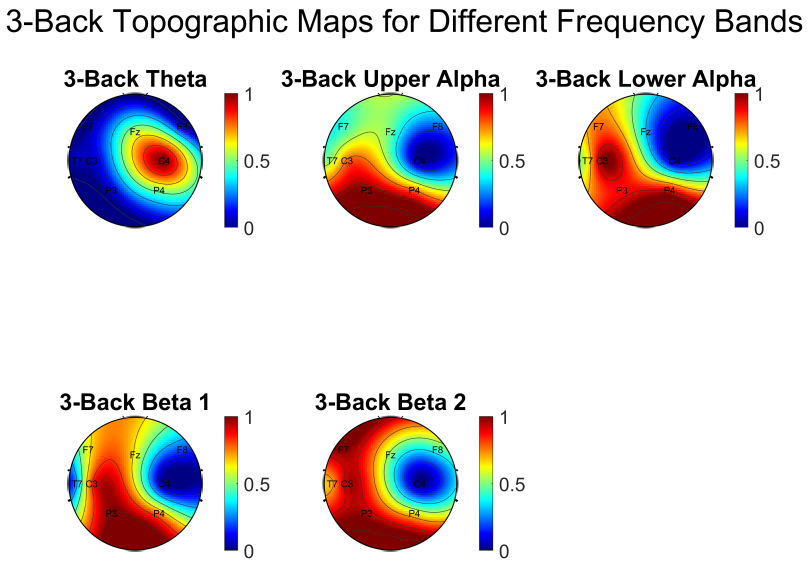

Figure 4.15. Topographic distribution of EEG power across various frequency bands during different cognitive states. EEG Power Distribution at P3, T7, C3, F7, Fz, F8, C4, P4 electrodes during from top to bottom respectively:rest, 2-back, and 3-back.

In addition to calculating power in various frequency bands, two other crucial features were extracted: the *Individual Alpha Frequency* (*IAF*) and the *Individual Theta Frequency* (*ITF*). The IAF, a term introduced in 1999 by Klimesh [82], represents the peak frequency in the alpha band and is obtained by selecting, from the frequency spectrum between 9 and 13 Hz, the frequency corresponding to the maximum power. More precisely, it was calculated as the average IAF during the task phase, further averaged across electrodes P3 and P4, following the recommendations of recent studies [35], which suggest that alpha power is prominently observable in the parietal region.

On the other hand, the ITF represents the counterpart of the IAF but in the theta band. This frequency was extracted from the Fz channel (frontal midline area), as proposed in [83].

Imaginary Coherence Index

In the domain of electrophysiological studies, particularly those investigating the neural substrates of cognitive functions like attention and working memory, Imaginary Coherence (ICH) stands out as a sophisticated analytical

tool. ICH is used to gauge the linear relationship, or the degree of synchrony, between two EEG signals at specific frequencies, thus providing insights into the frequency-specific interactions among different brain regions. Unlike traditional coherence measures, ICH is not influenced by volume conduction, thus offering a more genuine depiction of connectivity by negating false correlations arising from extraneous coherence or self-interaction [84].

To compute ICH, the cross-power spectral density (CPSD) between two channels is determined, and the imaginary part of this complex quantity is taken:

$$ICH = \frac{\text{imag}\{CPSD(x, y)\}}{\sqrt{P_{xx}P_{yy}}} \tag{4.7}$$

Here, $CPSD(x, y)$ represents the cross-power spectral density between channels x and y, while P_{xx} and P_{yy} denote the power spectral densities of channels x and y, respectively. The ICH can manifest as either positive or negative values; a positive $ICH_{x\to y}$ implies a flow of information from channel x (source) to channel y (sink), while a negative $ICH_{x\to y}$ suggests that channel x acts as a sink [84].

To procure these measures, the Welch's averaged modified periodogram method is employed. The frequency resolution achieved is a function of NFFT, set at 500 in the referenced study to obtain a resolution of 1Hz with a sampling rate of 500 Hz [84].

The absolute values of ICH are indicative of the strength of connectivity, while the sign delineates the directionality of the flow, adding a layer of interpretation to the data. By separating and averaging the absolute values of ICH across channels within specific frequency bands—theta (4–7 Hz), alpha (8–14 Hz), beta1 (15–21 Hz), and beta2 (22–30 Hz) it is possible to infer the intricate patterns of neural interactions that underlie cognitive processes [84].

In the context of our thesis, the application of ICH to EEG data reveals nuanced insights into the neurodynamics associated with working memory and attentional states. As Fig. 4.15 illustrates, the topographic maps of EEG power in various frequency bands during resting and cognitive engagement states are complemented by the ICH analysis, which elucidates the inter-regional connectivity that underpins these power distributions. This multi-faceted approach, combining topographical and connectivity analyses, permits a comprehensive understanding of how different brain regions coordinate and communicate during cognitive tasks, furthering our grasp of the underlying neural mechanisms.

Spectral Entropy

Spectral Entropy (SE) serves as a profound measure of complexity within a signal's spectral power distribution, deeply rooted in the concept of Shannon entropy from information theory. Shannon entropy, often regarded as a cornerstone of communication and complexity science, quantifies the amount of information or uncertainty present in a signal. In the context of Spectral Entropy, the power spectrum of a signal, when normalized, is treated akin to a probability distribution. This normalization is fundamental because it allows the signal's power distribution across frequencies to be interpreted probabilistically, where the sum of all probabilities equals one, reflecting the complete signal energy.

Mathematically, for a given signal $x(n)$, the power spectrum $S(m)$ is derived from the magnitude squared of its discrete Fourier transform $X(m)$, given by $S(m) = |X(m)|^2$. From this power spectrum, the probability distribution $P(m)$ is obtained through normalization:

$$P(m) = \frac{S(m)}{\sum_i S(i)}. \tag{4.8}$$

Subsequently, Spectral Entropy H is computed as:

$$H = -\sum_{m=1}^{N} P(m) \log_2 P(m), \tag{4.9}$$

where N is the total number of frequency points. To ascertain the normalized Spectral Entropy H_n, which allows for comparison across different systems or signals, we use:

$$H_n = \frac{-\sum_{m=1}^{N} P(m) \log_2 P(m)}{\log_2 N}, \tag{4.10}$$

with the denominator $\log_2 N$ representing the maximal Spectral Entropy achievable by white noise, which exhibits a uniform distribution in the frequency domain [85].

In our thesis, the exploration of Spectral Entropy extends to EEG signals during cognitive tasks, where SE provides an objective metric to assess the distribution of electrical power across various brain frequencies. The entropy values serve as an index of mental workload and cognitive complexity, differentiating between states of focused attention and rest. As such, SE becomes a crucial feature in the construction of predictive models that seek to interpret and classify cognitive states based on EEG data.

To compute SE in Matlab, the function:

```
[se] = pentropy(Data, Fs, 'Instantaneous', false)
```

is employed, which adheres to the principles outlined above. This function simplifies the computational process, taking a time-domain signal as input and returning its Spectral Entropy as in Figure 4.16 that displays the Spectral Entropy fluctuations over a duration of 400 seconds, as recorded from the T7 electrode, positioned in the temporal region of the scalp. Each point on the horizontal axis marks a second in time, while the vertical axis represents the Spectral Entropy value, reflecting the complexity and unpredictability of the EEG signal at that instant. The data illustrates a characteristic pattern of entropy variation, which may correlate with shifts in cognitive states and underlying neural activity during the EEG session. The application of `pentropy` aligns with the methodological rigor required in advanced signal processing, granting us a robust feature that encapsulates the dynamism of brain activity.

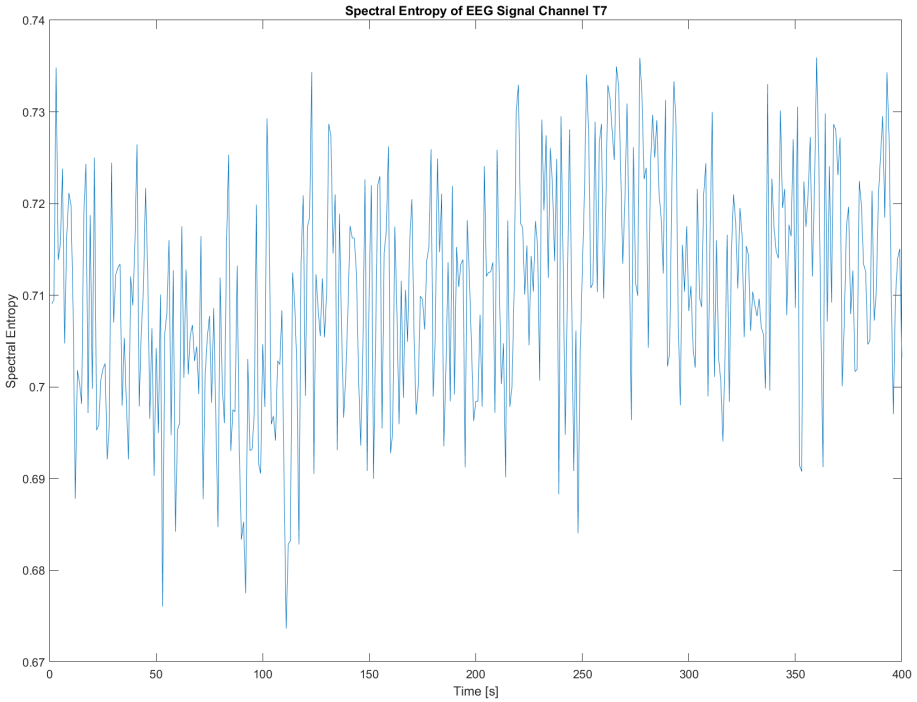

Figure 4.16. Temporal Variation of Spectral Entropy in EEG Channel T7.

Phase Locking Value

The Phase Locking Value (PLV) is a robust statistical tool used in EEG to quantify the phase synchronization between different neuronal populations. It serves as a measure of the consistency with which two signals, or signal components, lock in phase, irrespective of their amplitude. This synchronization is particularly telling of the functional connectivity within the brain, which is central to understanding how different regions communicate during various cognitive tasks.

In mathematical terms, starting from a signal $x(t)$, the analytic signal is obtained by applying the Hilbert transform:

$$x_a(t) = \text{Hilbert}(x(t)) \tag{4.11}$$

The instantaneous phase $\phi(t)$ is calculated from the analytic signal:

$$\phi(t) = \text{angle}(x_a(t)) \tag{4.12}$$

In the same manner, the process is applied to the signal $y(t)$. Therefore, for two signals $x(t)$ and $y(t)$ with instantaneous phases $\phi_x(t)$ and $\phi_y(t)$, PLV is defined as the absolute value of the average phase difference between the signals over time:

$$PLV = \left| \frac{1}{N} \sum_{t=1}^{N} e^{i(\phi_x(t) - \phi_y(t))} \right| \tag{4.13}$$

where N is the total number of samples, and i is the imaginary unit. This formula captures the extent to which the phase difference remains constant over time; a PLV of 1 indicates perfect phase synchronization, while a PLV close to 0 suggests no synchronization.

In the computational exploration of our thesis, the PLV serves as a pivotal measure, and its calculation is executed through a custom Matlab function `computePLV`. This function is adeptly designed to process filtered EEG data, iterating over defined epochs to calculate the phase synchronization between channels.

The function `computePLV(eeg_filt, num_iterations, Ns, Fs)` takes a matrix of EEG data, `eeg_filt`, with dimensions [num_samples x num_channels] and other parameters such as the number of iterations `num_iterations`, the number of samples per iteration `Ns`, and the sampling frequency `Fs`. Within each iteration, it selects an epoch for analysis and applies the Hilbert transform to compute the instantaneous phase. This phase information is then used to determine the phase differences between every pair of channels.

The function intricately constructs a matrix of PLV values, capturing the essence of neural connectivity. By concentrating on the lower triangular portion of this matrix, the function efficiently compiles a vector of unique PLV values, thus avoiding redundancy as phase locking between channels is symmetric.

This custom function `computePLV` embodies the methodological sophistication necessary for advanced EEG signal processing, granting a nuanced analysis of the phase relationships intrinsic to cognitive processes. By incorporating this function into our signal processing pipeline, we ensure a robust, repeatable computation of PLV, a critical step in establishing a reliable biomarker for cognitive state differentiation based on EEG data.

Higuchi Fractal Dimension

The Higuchi Fractal Dimension (HFD) serves as a pivotal tool in the mathematical analysis of time series data, particularly EEG signal analysis, to understand the complexity of brain activity. This technique quantifies the irregularity or complexity of signals, shedding light on the intricate dynamics of neural oscillations. It is particularly effective in revealing subtle changes in EEG recordings associated with different cognitive states [86].

To compute the HFD, a time series is segmented into subsequences:

$$(X(1), X(2), \ldots, X(N)). \tag{4.14}$$

From these, new sequences are formed for each initial time m and time interval k, creating k new series:

$$X_{mk} = X(m), X(m+k), X(m+2k), \ldots, X\left(m + \left[\frac{N-m}{k}\right] \cdot k\right) \tag{4.15}$$

where m ranges from 1 to k. For each k, the length $L_m(k)$ is the normalized sum of the absolute differences between consecutive points spaced k units apart:

$$L_m(k) = \left(\sum_{i=1}^{\left[\frac{N-m}{k}\right]} |X(m+ik) - X(m+(i-1)\cdot k)| \right) \times \frac{N-1}{\left[\frac{N-m}{k}\right] \cdot k} \tag{4.16}$$

The HFD is derived from the proportionality of $L_m(k)$ to k^{-FD}:

$$FD = -\frac{\log L(k)}{\log k} \tag{4.17}$$

In this thesis, the HFD is utilized to evaluate working memory regions in the brain during task performance. A higher HFD indicates increased complexity, suggesting a higher cognitive load or concentration. This aligns with the observation that EEG signals become more irregular with increased cognitive demand.

Our empirical analysis employs HFD to assess EEG data during specific working memory tasks, such as the n-back task. Variations in HFD reflect changes in cognitive load, with higher dimensions indicating periods of heightened working memory engagement.

Katz Fractal Dimension

The Katz Fractal Dimension (KFD) is instrumental in EEG signal analysis within cognitive neuroscience, enabling the assessment of structural complexity in neural oscillations. This thesis applies KFD to quantify the complexity of EEG waveforms, correlating fractal dimensionality with cognitive states during working memory and concentration tasks.

The Katz method calculates the fractal dimension as a scalar index, reflecting the waveform's form and dimensionality. Typically, fractal dimensions range between 1 and 1.5, where lower values indicate simpler waveforms and higher values denote increased complexity [87].

The KFD is calculated from the total length of the waveform, L, the sum of distances between consecutive points, and d, the maximum distance from the waveform's origin to its furthest point:

$$L = \sum \text{dist}(i, i+1) \tag{4.18}$$

$$d = \max \text{dist}(1, i) \tag{4.19}$$

The fractal dimension (FD) is determined by the logarithmic ratio of L to d:

$$FD = \frac{\log(L)}{\log(d)} \tag{4.20}$$

For EEG analysis, scale normalization is essential, where an average interpoint distance a is used to adjust the FD calculation:

$$FD = \frac{\log(L/a)}{\log(d/a)} \tag{4.21}$$

This thesis hypothesizes that increased cognitive activity, as in working memory tasks, corresponds to higher KFD values. Cognitive engagement is believed to induce less regular and more complex signal patterns, elevating the KFD.

Computational analysis confirms the KFD's effectiveness in differentiating cognitive workload levels. It provides insights into brain activity dynamics as subjects perform tasks challenging their working memory. KFD not only deepens our understanding of signal processing but also aids in developing predictive models reflecting the brain's functional state.

Modified Approximate Entropy

Traditional complexity measures like Approximate Entropy (ApEn) have significantly contributed to the study of electroencephalogram by providing stable insights into the irregular patterns of EEG signals, especially when dealing with short and noisy data epochs [88]. However, the efficacy of ApEn in EEG analysis is often hampered by its sensitivity to a variety of parameters, such as sampling rate, embedding dimension, tolerance, and epoch duration. These parameters, if not optimally set, can lead to inconsistent and even contradictory results, posing a significant challenge in the interpretation of EEG studies [88].

To overcome these challenges and enhance the reliability of EEG complexity analysis, the concept of Modified Approximate Entropy was introduced. This innovative approach fine-tunes the original ApEn formula, resulting in more stable and consistent measurements. Such stability is particularly crucial for the nuanced analysis of EEG data during cognitive tasks, where subtle changes in complexity can yield significant insights into brain function.

One of the key improvements in Modified ApEn lies in its approach to handling the parameters that significantly influence the original ApEn's results. The time delay τ between coordinates in Modified ApEn is adjusted to be in linear relation to the sampling frequency. This change addresses the issue of oversampling that can skew ApEn results and ensures that the time delay is optimally set to match the specific frequency of the EEG data.

Furthermore, the tolerance level r in Modified ApEn is dynamically chosen to ensure a specific percentage of recurrence points are found in the embedding dimension m. This approach avoids arbitrary selection and guarantees an adequate number of recurrences for reliable complexity estimation, a method

that aligns with approaches like the minimum numerator count method, which has been proven to provide stable estimations even with short data series [88].

Additionally, the Modified ApEn maintains a uniform number of embedded vectors across two embedding dimensions (m and m+1). This uniformity is achieved by discarding the last vectors in the lower dimension, thus ensuring that the index remains non-negative and stable.

Incorporating a high-pass filter to remove low frequency trends is another critical adjustment in the Modified ApEn algorithm. This filter, with a cutoff frequency proportional to the inverse of the epoch duration, tailors the analysis to the specific time frame of the EEG data, ensuring that only relevant frequency components are considered.

A Theiler window is also introduced in the Modified ApEn calculation to address the issue of self-recurrences. By ensuring that points too close in time are not considered neighbors, this modification is particularly crucial in EEG data analysis, where temporal proximity can lead to false indications of complexity.

Mathematically, Modified ApEn can be expressed as:

$$ApEn(m, r, N) = \Phi^m(r) - \Phi^{m+1}(r) \tag{4.22}$$

Here, $\Phi^m(r)$ represents the correlation integral, m is the embedding dimension, r is the tolerance (distance) threshold, and N is the number of data points. The modifications in Modified ApEn revolve around optimizing these parameters to enhance the stability of the measure.

In the broader context of this thesis, applying Modified ApEn to EEG data during cognitive tasks, such as working memory exercises or attention tests, offers a more accurate and reliable measure of complexity; an example of this measure in Figure 4.17 that illustrates the complexity of EEG signals during 'Relax', '2-back', and '3-back' cognitive tasks, and during a 'Pause' period. The x-axis represents the progression of time in seconds (s), while the y-axis indicates the Modified ApEn values, reflecting the complexity of the neural oscillations. The vertical red lines demarcate the distinct phases of the experiment, showcasing the variations in signal complexity associated with each task and rest period. This enhanced measurement allows for a deeper understanding of how the brain's functional state changes in response to varying cognitive loads.

Moreover, the Modified ApEn extends the range of parameters for which stable complexity indications can be achieved, adapting to the variability inherent in cognitive neuroscience.

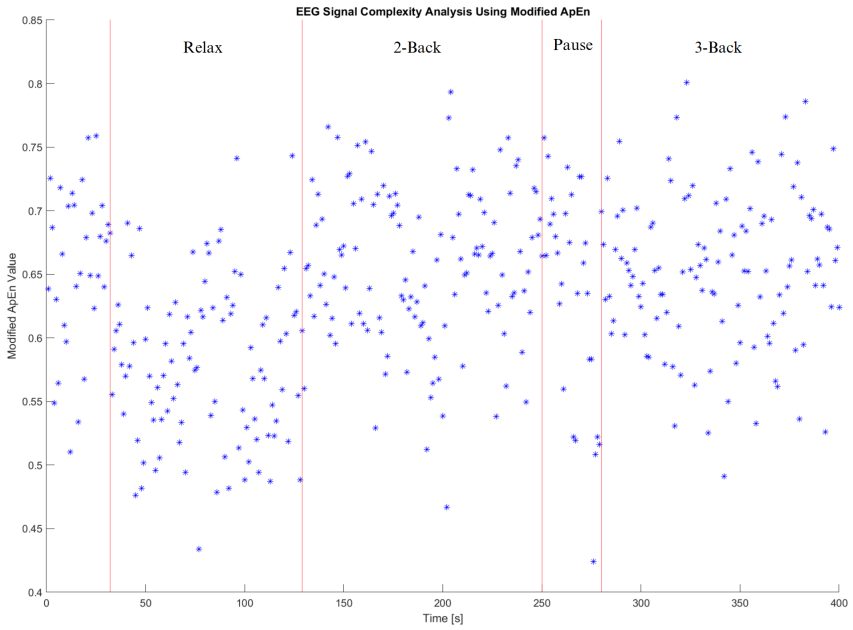

Figure 4.17. Distribution of Modified Approximate Entropy (Modified ApEn) values across different cognitive states.

4.4.4 Outlier Detection and Elimination

In data analysis, the presence of outliers can significantly skew results and impede accurate interpretations. An outlier is an observation that significantly deviates from the majority of data, suggesting it may have been generated under different conditions or by a different mechanism. In EEG data, outliers can arise due to various factors, such as external noise, artifacts from subject movements, or equipment malfunctions.

To address this issue, Matlab's 'isoutlier' function offers a robust solution for identifying and removing outliers, specifically through the Median Absolute Deviations (MAD) method. The MAD method is particularly effective in handling outliers in data that may not be normally distributed. This method calculates the median of the absolute deviations from the data's median, providing a measure of variability. An observation is typically classified as an outlier if a value is more than three scaled median absolute deviations (MAD) from the median [89] .

The `isoutlier` function in Matlab, when configured to use the MAD method, identifies outliers by evaluating how far data points deviate from the median in terms of MAD. The function's syntax for employing the MAD

method is as follows:

```
TF = isoutlier(A, 'median')
```
(4.23)

In this command, `A` represents the input data set (such as a vector or matrix of EEG signal values). The specification `'median'` directs the function to use the MAD method for outlier detection. The function then returns a logical array `TF` of the same size as `A`, where `true` indicates an outlier.

In our EEG data analysis, we utilized the `isoutlier` function with the MAD method to preprocess the data. This step was crucial for ensuring the integrity of our data set. By effectively identifying and removing outliers as in figure , we improved the reliability of subsequent analyses, including the computation of various complexity measures and the interpretation of EEG signals in relation to cognitive states.

4.5 Feature Selection

Feature selection, or "feature selection" in English, in the context of machine learning, is a critical process that involves choosing the most relevant features to use in building a predictive model. This process is critical for several reasons: it improves model performance, reduces model complexity by making it faster to train and easier to interpret, and can also help avoid overfitting when a model is too complex by also capturing the "noise" in the data rather than just the relevant signal.

There are several feature selection techniques, which can be grouped into three main categories:

1. **Filter Methods**: filter methods evaluate features based on univariate statistics and select them independently of the machine learning algorithm that will be used later. These methods are generally fast and used as a preliminary step in feature selection. Examples of metrics used include the Chi-square test, Pearson correlation coefficient for continuous variables, and mutual information score. Filter methods are effective in removing irrelevant or redundant features but may not capture intricate connections between the target and features.

2. **Wrapper Methods**: wrapper methods approach feature selection as an issue of conducting searches, where different combinations are evaluated to determine the optimal one. They use a predictive model to evaluate the performance of a subset of features, iterating through different combinations to find the best subset. Examples of wrapper methods include

Forward Selection, Backward Elimination, and exhaustive search such as the RFE (Recursive Feature Elimination) method. These methods can be very efficient but are also computationally intensive, especially with a large number of features.

3. **Embedded Methods**: intrinsic methods integrate the process of feature selection as an integral part of model training, concurrently optimizing both feature selection and model training. These methods exploit specific algorithms that have feature selection "built in" to their construction. A classic example is LASSO regression, which adds an L1 penalty on the size of the model coefficients, pushing some coefficients to be exactly zero, which is equivalent to feature selection. Other examples include decision trees and tree-based models such as Random Forest and Gradient Boosting, which select features based on the importance of those features during tree construction [90].

4.5.1 Chi-Square Feature Selection Method

The Chi-square (χ^2) test provides a systematic method for ranking features based on their statistical significance. This method is based on the principle of conducting individual Chi-square tests between each feature and the corresponding class of an observation. The essence of this technique is quantified by computing p-values, which indicate the probability of observing the data if the null hypothesis (which suggests no association between the feature and the outcome) were true.

In mathematical terms, the χ^2 statistic for each feature is calculated as:

$$\chi^2 = \sum \frac{(O_i - E_i)^2}{E_i}, \tag{4.24}$$

where O_i represents the observed frequency and E_i denotes the expected frequency under the assumption of independence. The sum is taken over all categories or groups within the feature.

The method's applicability extends to both categorical and continuous variables. For continuous variables, the Chi-square method entails discretizing the data into intervals. This discretization process involves segmenting continuous values into bins, a step that necessitates careful optimization. The number of intervals or bins is a critical parameter that can significantly influence the model's final performance.

The Chi-square method is primarily employed for classification tasks. While it can be adapted for regression, its utility shines in classification problems

where the objective is to identify features that have the most significant relationship with the categorical outcome variable. The selection procedure assesses the independence of each predictor variable from a response variable through individual Chi-square tests. A low p-value from the test statistic suggests that the associated predictor variable is dependent on the response variable and is considered a significant feature. The output is represented as $-\log(p)$. Hence, a higher score value signifies the importance of the corresponding predictor, as in the Figure 4.18.

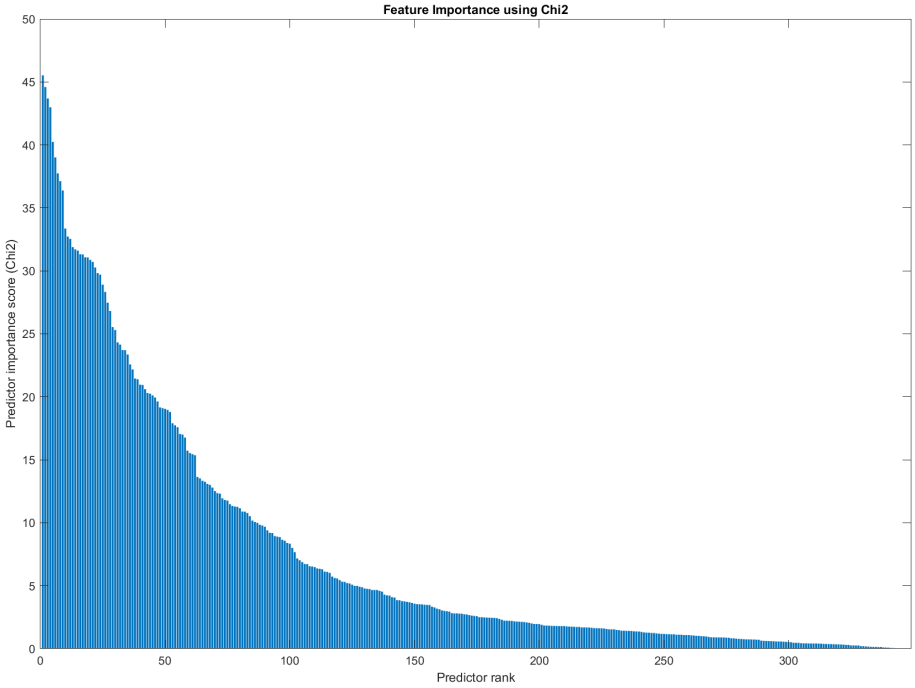

Figure 4.18. Feature Importance Ranking as Determined by Chi-square Scores.

This method provides a transparent and statistically sound approach to feature selection. By filtering out irrelevant or weakly associated features, the Chi-square method aids in reducing model complexity and improving interpretability. It ensures that the resultant predictive model is both efficient and robust, built upon features that are genuinely influential in determining the target variable [91].

4.6 Regression

In this thesis, a regressor was chosen instead of a classifier to compute the working memory level (WML), as a continuous output index was required to modulate parameters for neurostimulation. Various regressors were experimented with, and it was found that the Support Vector Machine was not only the most effective but also sufficiently fast and efficient to make real-time predictions.

4.6.1 Support Vector Machine

Support Vector Machines (SVMs) are a popular modern machine learning approach. They are supervised learning models that examine data for regression and classification and have learning algorithms linked with them. In the case of regression, they are called ε-Support Vector Regression (ε-SVR) [92]. Our task requires nonlinear regression, but to explain the operational complexity of this regressor, we begin with the description of the linear case.

Linear SVR: Primal Formula

Suppose we have a certain training set $\{(x_1, y_1), \ldots, (x_N, y_N)\}$, in ε-SVR the objective is to find a function $f(x)$ that is as flat as possible while deviating from y_n (in which $n = 1, \ldots, N$), by a value no larger than ε for each training data. We should find the linear function

$$f(x) = x'\beta + b \tag{4.25}$$

with the smallest norm value ($\beta'\beta$) to make sure it is as flat as feasible. The goal of this convex optimization problem is to minimize

$$J(\beta) = \frac{1}{2}\beta'\beta \tag{4.26}$$

while ensuring that every residual has a value less than ε, i.e.

$$\forall n : |y_n - (x'_n\beta + b)| \leq \varepsilon \tag{4.27}$$

In simpler terms, the optimization problem involves finding a kind of regression tube (with ε radius) such that all points are inside the tube, as it can be clearly seen in Figure 4.19. During the training process of an SVR model, *support vectors* are identified, which are data points contributing to the definition of the optimal margin. These support vectors directly influence the shape of the regression function.

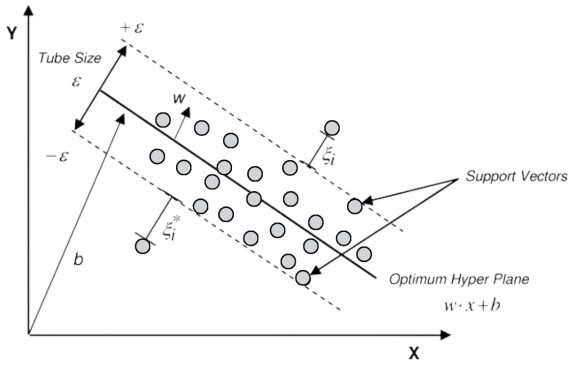

Figure 4.19. The illustration of SVM for linear regression problem.

It's possible, however, that there isn't a function $f(x)$ that can meet the above-mentioned requirements at every point. Consequently, for each point, introduce slack variables ξ_n and ξ_n^* to handle otherwise unfeasible constraints. Regression errors up to ξ_n and ξ_n^* are now permitted by the slack variables. Adding slack variables results in the *primal formula*, or objective function [93].

$$J(\beta) = \frac{1}{2}\beta'\beta + C\sum_{n=1}^{N}(\xi_n + \xi_n^*), \tag{4.28}$$

subject to the following constraints:

$$\begin{aligned}
\forall n: \quad & y_n - (x_n'\beta + b) \leq \varepsilon + \xi_n \\
\forall n: \quad & (x_n'\beta + b) - y_n \leq \varepsilon + \xi_n^* \\
\forall n: \quad & \xi_n^* \geq 0 \\
\forall n: \quad & \xi_n \geq 0.
\end{aligned}$$

The box constraint, represented by the constant C, is a positive number that regulates the penalty applied to observations outside of the epsilon margin ε, which is useful in avoiding overfitting. This number establishes the trade-off between the flatness of $f(x)$ and the tolerance limit for deviations greater than ε. Errors within ε of the observed value are ignored by the linear ε-insensitive loss function, which treats them as equal to zero. The distance between the observed value y and the ε boundary is used to calculate the loss function. This is explained in formal terms by

$$L_\varepsilon = \begin{cases} 0 & \text{if } |y - f(x)| \leq \varepsilon \\ |y - f(x)| - \varepsilon & \text{otherwise} \end{cases}$$

Linear SVR: Dual Formula

In its Lagrange dual formulation, the previously described optimization issue is computationally easier to solve. A lower bound on the primal (minimization) problem's solution is given by the *dual problem's solution*. The "duality gap" is the difference between the optimal values of the primal and dual issues, which need not be equal. However, the dual problem's solution provides the value of the optimal solution to the primal problem when the problem is convex and satisfies a constraint qualification condition. Create a Lagrangian function from the primal function and add nonnegative multipliers α_n and α_n^* for every observation x_n to get the dual expression. This results in the dual formula, where we minimize

$$L(\alpha) = \frac{1}{2}\sum_{i=1}^{N}\sum_{j=1}^{N}(\alpha_i-\alpha_i^*)(\alpha_j-\alpha_j^*)x_i'x_j+\varepsilon\sum_{i=1}^{N}(\alpha_i+\alpha_i^*)+\sum_{i=1}^{N}y_i(\alpha_i^*-\alpha_i), \quad (4.29)$$

subject to the constraints

$$\begin{aligned}&\sum_{n=1}^{N}(\alpha_n-\alpha_n^*)=0\\ &\forall n: \quad 0\le\alpha_n\le C\\ &\forall n: \quad 0\le\alpha_n^*\le C.\end{aligned}$$

The following equation can be used to fully characterize the β parameter as a linear combination of the training observations:

$$\beta=\sum_{n=1}^{N}(\alpha_n-\alpha_n^*)x_n. \quad (4.30)$$

Only the support vectors are necessary for the function that predicts new values to work:

$$f(x)=\sum_{n=1}^{N}(\alpha_n-\alpha_n^*)(x_n'x)+b. \quad (4.31)$$

The optimization constraints necessary to achieve optimal solutions are the Karush-Kuhn-Tucker (KKT) complementarity conditions. These requirements apply to linear SVR and are

$$\begin{aligned}&\forall n: \quad \alpha_n(\varepsilon+\xi_n-y_n+x_n'\beta+b)=0\\ &\forall n: \quad \alpha_n^*(\varepsilon+\xi_n^*+y_n-x_n'\beta-b)=0\\ &\forall n: \quad \xi_n(C-\alpha_n)=0\\ &\forall n: \quad \xi_n^*(C-\alpha_n^*)=0.\end{aligned}$$

Under these circumstances, all observations that are rigidly contained inside the epsilon tube have Lagrange multipliers of $\alpha_n = 0$ and $\alpha_n^* = 0$. A support vector is the equivalent observation if either α_n or α_n^* is non-zero. A trained SVM model's attribute *alpha* stores the difference between two support vectors' Lagrange multipliers, $\alpha_n - \alpha_n^*$. *SupportVectors* and *Bias* are two properties that store x_n and b, respectively.

Nonlinear SVR: Primal Formula

A linear model is not sufficient to capture some regression situations, such as the one in this study. However, the previously mentioned method can be extended to nonlinear functions using a technique known as the "kernel trick". This permits SVMs to effectively conduct non-linear regression by implicitly translating their inputs into high-dimensional feature spaces. Replace the dot product $x_1' x_2$ with a nonlinear (Gaussian or Polynomial) Kernel function $G(x_1, x_2) = \langle \phi(x_1), \phi(x_2) \rangle$ to create a nonlinear SVR model. $\phi(x)$ is a transformation that maps x to a high-dimensional space. In this thesis we use a *Gaussian*, or *RBF Kernel*, which has the formula: $G(x_j, x_k) = \exp\left(-\|x_j - x_k\|^2\right)$. The elements of the *Gram matrix*, which is an n-by-n matrix, are $g_{i,j} = G(x_i, x_j)$. Every element $g_{i,j}$ is equivalent to the predictors' inner product after being converted by ϕ. Nevertheless, since we can create the Gram matrix directly using the kernel function, we do not need to know ϕ.

Nonlinear SVR: Dual Formula

The corresponding element of the Gram matrix $g_{i,j}$ is substituted for the inner product of the predictors $x_i' x_j$ in the dual formula for nonlinear SVR. Regression using nonlinear SVM determines thus the coefficients that minimize

$$L(\alpha) = \frac{1}{2} \sum_{i=1}^{N} \sum_{j=1}^{N} (\alpha_i - \alpha_i^*)(\alpha_j - \alpha_j^*) G(x_i, x_j) + \varepsilon \sum_{i=1}^{N} (\alpha_i + \alpha_i^*) - \sum_{i=1}^{N} y_i (\alpha_i - \alpha_i^*), \tag{4.32}$$

subject to the same constraints as before:

$$\begin{aligned} &\sum_{n=1}^{N} (\alpha_n - \alpha_n^*) = 0 \\ &\forall n: \quad 0 \leq \alpha_n \leq C \\ &\forall n: \quad 0 \leq \alpha_n^* \leq C. \end{aligned}$$

In the same way, the prediction function for new values is equal to

$$f(x) = \sum_{n=1}^{N} (\alpha_n - \alpha_n^*) G(x_n, x) + b. \tag{4.33}$$

The conditions for KKT complementarity are

$$\begin{aligned} \forall n: \quad & \alpha_n(\varepsilon + \xi_n - y_n + f(x_n)) = 0 \\ \forall n: \quad & \alpha_n^*(\varepsilon + \xi_n^* + y_n - f(x_n)) = 0 \\ \forall n: \quad & \xi_n(C - \alpha_n) = 0 \\ \forall n: \quad & \xi_n^*(C - \alpha_n^*) = 0. \end{aligned}$$

4.7 Performance Metrics

In the context of ML, evaluating a model's performance is a crucial step to understand its behavior and generalization capability. Various metrics are employed to measure different perspectives of a model's performance. The key metrics for a classifier are described below:

- *Recall* focuses on the correct identification of positive examples, while *precision* assesses the accuracy of positive predictions. Striking a balance between these metrics is often crucial in scenarios where classes are imbalanced. Recall $= \frac{\text{True Positives}}{\text{True Positives+False Negatives}}$, Precision $= \frac{\text{True Positives}}{\text{True Positives+False Positives}}$.
- *F1 Score* represents the harmonic mean between precision and recall. It is particularly useful in scenarios where balancing the accuracy of positive predictions and the ability to correctly identify positive examples is important. F1 Score $= 2 \cdot \frac{\text{Precision} \cdot \text{Recall}}{\text{Precision+Recall}}$.
- *Sensitivity* (True Positive Rate) and *Specificity* (True Negative Rate) measure, respectively, the model's ability to correctly identify positive and negative examples. Sensitivity $= \frac{\text{True Positives}}{\text{True Positives+False Negatives}}$, Specificity $= \frac{\text{True Negatives}}{\text{True Negatives+False Positives}}$. They represent critical aspects in situations where the cost of errors can vary considerably.
- *Accuracy* provides a global assessment of correct predictions relative to the total predictions. However, it can be misleading in the presence of imbalanced classes. Accuracy $= \frac{\text{True Positives+True Negatives}}{\text{Total Predictions}}$. *Balanced accuracy* offers a corrected version of accuracy by considering imbalances between classes, providing a fairer evaluation of the model's performance. Balanced Accuracy $= \frac{\text{Sensitivity+Specificity}}{2}$.

- *Receiver Operating Characteristic (ROC) Curve* is a graphical tool used to evaluate the performance of a binary classifier on a dataset by varying the decision threshold. The ROC Curve illustrates the trade-off between Sensitivity and Specificity as the decision threshold changes. The ROC curve is particularly useful for assessing the model's ability to discriminate between classes in different threshold scenarios. An ideal classifier will have an ROC curve extending towards the upper-left corner of the graph (Figure 4.20) , indicating high Sensitivity and Specificity across all possible decision thresholds. The *Area Under the Curve (AUC)* of the ROC curve provides a quantitative measure of the classifier's ability, with an AUC of 1 indicating perfect performance and an AUC of 0.5 suggesting random performance.

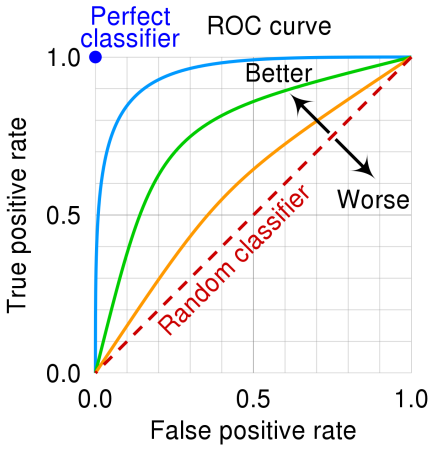

Figure 4.20. Comparison between a "better" and "worse" classifier in the ROC space [94].

The main metrics for a regressor are instead:

- The coefficient of determination R^2 quantifies the fraction of variance in the data explained by the model. The coefficient of determination, R^2, spans from 0, indicating no explanatory power, to 1, signifying perfect prediction. $R^2 = 1 - \frac{\sum_{i=1}^{n}(y_i - \hat{y}_i)^2}{\sum_{i=1}^{n}(y_i - \bar{y})^2}$, where n is the total number of observations, y_i are the observed values, $\hat{y}_i$ are the values predicted by the model, $\bar{y}$ is the mean of the observed values.

- *MSE (Mean Squared Error), RMSE (Root Mean Squared Error), e MAE (Mean Absolute Error)* assess the discrepancy between the model's predictions and the actual data. MSE penalizes larger errors, while RMSE

provides a square root version. MAE is less sensitive to outlier errors, offering a robust perspective on the model's accuracy. The related formulas are as follows: MSE $= \frac{1}{n}\sum_{i=1}^{n}(y_i - \hat{y}_i)^2$, RMSE $= \sqrt{\frac{1}{n}\sum_{i=1}^{n}(y_i - \hat{y}_i)^2}$, MAE $= \frac{1}{n}\sum_{i=1}^{n}|y_i - \hat{y}_i|$, where n is the total number of observations, y_i are the observed values, $\hat{y}_i$ are the values predicted by the model.

The choice of metrics depends on the specific nature of the problem and the desired objectives. A thorough analysis of these metrics will contribute to a comprehensive and informative evaluation of the machine learning model's performance.

4.8 Stimuli

This thesis makes use of the following kinds of stimulus, which are *binaural beats* and *pulsed light* for user's neurostimulation, while a *bar* is used as neurofeedback.

4.8.1 Binaural Beats

A binaural beat is a type of **auditory beat stimulation** (ABS), a widely used method to enhance mood and cognitive function. It is believed to cause a frequency-following response in brainwaves [95]. Thus, it's one of several ways to achieve brain entrainment.

A *binaural beat* (BB) occurs when one tone is played to one ear and the other tone is played to the other ear independently. The brain interprets the sounds as having a frequency that is equal to the difference between the two frequencies, which results in a binaural beat. This phenomenon has the potential to induce neural entrainment. It's important to note that these auditory sensations are generated by the brain, and they do not represent overlapping physical waves. To avoid the perception of two distinct sounds (which is the actual nature of the input), it is recommended to keep the frequencies not too high and not too far apart. According to studies [96, 97], the largest behavioral and psychological impacts are caused by frequencies around 400 Hz with a maximum difference of up to 35 Hz between two frequencies. For instance, a BB sound of 10 Hz is produced when tones of 400 Hz and 410 Hz are delivered to the left and right ears, respectively, as in Figure 4.21.

Figure 4.21. Functioning of binaural waves.

4.8.2 Pulsed Lights

Another technique to induce brain entrainment is with pulsed light. A rhythmic flickering light at a certain frequency can serve as a stimulating source.

Numerous research [98, 99] have already documented the psychophysiological effects of naturalistic light stimulations on physical and mental well-being, including sleep quality, as well as subjective well-being and cognitive performance. However, there are two characteristics of rhythmic light stimulations that need be taken into account from the standpoints of neuroergonomics and user experience:

1. Constant exposure to the flickering light sources overloads the sensory system, causing discomfort and weariness in the user both physically and subjectively.

2. According to a number of studies [100, 101], the flickering light source is most likely to elicit strong power modulations when it is positioned in the center of the visual field and directly fixated (i.e., with focused attention). However, because this configuration is so disruptive, it is not recommended for use in the majority of everyday tasks and environments.

As such, it is imperative to investigate appropriate protocols that are typified by:

1. Reduced user discomfort and non-intrusiveness (e.g., by employing less noticeable flickering stimulations);

2. Integration feasibility (e.g., by investigating entrainment effects during a stimulation that does not necessitate the direct fixation on the light source).

Numerous investigations [102] have shown that brain entrainment effects persist even in the absence of direct fixation of the stimulation source and when stimulated below the individual perceptibility threshold.

Therefore, protocols that enable non-perceptible rhythmic stimulation are particularly beneficial since they reduce eye fatigue and user discomfort.

Furthermore, it is important to investigate inter-individual variations (such as age) in entrainment effects as well as traits of people who are not responsive to or appropriate for rhythmic light stimulation (such as in the case of an epileptic diagnosis [103].

4.8.3 Neurofeedback Bar

As explained in the section on neurofeedback, during the NFT, the EEG is recorded, and key components are extracted. These components are then fed back to the individual through a feedback loop, employing audio, visual, or a combination of both. This format enables the distinct representation of relevant electrophysiological components, such as a bar graph where the amplitude of a frequency corresponds to the bar's size. The individual's task may then be to increase the size of the training-frequency bar while concurrently reducing the size of bars associated with inhibitory frequencies. This process provides real-time feedback, allowing the individual to learn and adapt their neural responses to improve control over specific electrophysiological patterns.

4.9 Inverse Efficiency Score

In experimental cognitive psychology studies, participants often engage in specific tasks, yielding two key dependent variables (DVs): the proportion of errors (PE) and the reaction time (RT), which represents the time elapsed between the stimulus onset and the initiation of the correct response. Typically, these variables are analyzed separately, introducing complexities in interpretation.

To enhance clarity and simplify the interpretation, researchers have explored the integration of PE and RT into a unified DV. Townsend and Ashby [104] proposed a solution known as the 'Inverse Efficiency Score' (IES). This score serves as an observable metric that assesses the average energy consumption or power of the cognitive system over time. The IES is calculated by dividing RT by either (1-PE) or by the proportion of correct responses (PC). In practical terms, for a given participant, the mean (or median) RT of correct responses in a specific condition is computed and then divided by (1-PE) or by PC. This approach aims to provide a comprehensive measure that appropriately balances the influence of both speed and accuracy in cognitive

tasks.

$$IES = \frac{RT}{1 - PE} = \frac{RT}{PC} \tag{4.34}$$

The IES is represented in milliseconds, same like RTs are. The execution of a test associated with better performance (low RT and high PC) is reflected in a lower value of IES.

However, it is crucial to verify, prior to employing this index, whether the observations derived from the PE and RT are congruent or if there are indications of a potential trade-off between speed and accuracy. In this latter scenario, where faster responses are associated with higher error rates, reaching definitive conclusions becomes particularly challenging. Furthermore, other exceptions arise when error rates are exceptionally elevated (surpassing 25%). In such instances, a more comprehensive examination is imperative to ensure robust and accurate interpretations.

4.10 Statistical Tests

In the realm of empirical research and data analysis, statistical tests play a pivotal role in drawing meaningful conclusions from collected data. These tests provide a structured framework for making inferences about populations based on sample data, helping researchers assess the reliability and significance of their findings. Statistical tests are essential tools for hypothesis testing, enabling researchers to make informed decisions about the generalizability of their results. The choice of a statistical test depends on various factors, such as the nature of the data, the research question, and the underlying assumptions. In this thesis, we explore two key statistical tests: the Shapiro-Wilk test and the Wilcoxon test. Each test serves a specific purpose and is applicable in different scenarios, providing researchers with versatile tools to analyze data across various research domains.

4.10.1 Shapiro-Wilk Test

The Shapiro–Wilk test is a test of normality. It tests the null hypothesis, according to which a sample $x_1, ..., x_n$ represents a population with a normal distribution. The test statistic is

$$W = \frac{\left(\sum_{i=1}^{n} a_i x_{(i)}\right)^2}{\sum_{i=1}^{n}(x_i - \overline{x})^2} \tag{4.35}$$

where

- $x_{(i)}$ represents the i-th smallest value in the sequence.
- $\overline{x} = \frac{x_1 + \cdots + x_n}{n}$ is the sample mean.
- The constants a_i are given by

$$(a_1, \ldots, a_n) = \frac{m^\top V^{-1}}{(m^\top V^{-1} V^{-1} m)^{1/2}}$$

where

$$m = (m_1, \ldots, m_n)^\top$$

and $m_1, \ldots, m_n$ are the expected values of the ranks of a standardized random variable, and V is the covariance matrix of these ranks [105].

The population's normal distribution is the null hypothesis for this test. The test can yield values of 1 (true) or 0 (false) respectively, based on whether the null hypothesis can be rejected or not. Therefore, the null hypothesis is rejected and there is evidence that the tested data are not normally distributed if the *p value* is smaller than the selected significance *alpha* level. Conversely, the null hypothesis cannot be rejected if the p value exceeds the selected alpha level.

For instance, a dataset with a p-value below 0.05, at an alpha level of 0.05, leads to the rejection of the null hypothesis, suggesting that there is evidence against the assumption that the data is derived from a normally distributed population; on the other hand, a data set with a p value greater than the 0.05 alpha value is unable to do so.

4.10.2 Wilcoxon Test

The Wilcoxon Test is a nonparametric statistical procedure used to compare two paired samples. It is particularly useful when the data do not follow a normal distribution, a common condition in many practical applications. The test was developed by Frank Wilcoxon in 1945 [106].

Test Description

Wilcoxon's Test is based on the ordering of differences between pairs of observations. Let $X_1, X_2, \ldots, X_n$ and $Y_1, Y_2, \ldots, Y_n$ be two paired samples. The first step is to calculate the differences $D_i = X_i - Y_i$. Next, we order these differences in absolute value and assign ranks, from 1 to the smallest absolute value to n to the largest.

Calculation of Statistics

The Wilcoxon statistic, W, is obtained by summing the ranks of differences. Traditionally, only the ranks of positive differences are summed. However, a more comprehensive approach involves calculating two sums separately: one for the ranks of positive differences (W^+) and one for the ranks of negative differences (W^-). The test statistic W is then the lower of W^+ and W^-. This method ensures that the test is sensitive to differences in either direction and reduces the risk of bias. The formula for W becomes:

$$W = \min\left(\sum_{i:D_i>0} R_i^+, \sum_{i:D_i<0} R_i^-\right) \tag{4.36}$$

where R_i^+ and R_i^- are the ranks of positive and negative differences, respectively.

Bicaudal and Monocaudal Testing

Wilcoxon's Test can be applied in either bicaudal or monocaudal form. In a bicaudal context, one tests the null hypothesis that the median of differences is zero against the alternative hypothesis that it is nonzero. In a monocaudal context, the alternative hypothesis may be that the median of differences is greater (or less) than zero.

Chapter 5

Virtual Reality Experimental Protocol

Within this chapter, a detailed account of all phases of the experimental protocol is provided. The journey begins with calibration, a fundamental process in establishing the foundation for subsequent personalized regression model training. The latter represents a crucial step as it allows the development of an ad-personam model tailored specifically to individual characteristics.

Subsequently, the focus shifts to threshold calculation. This step is of particular importance as thresholds determine key parameters for modulating neurostimulation. Understanding and adapting these thresholds based on individual needs are essential for optimizing the effectiveness of neurostimulation within the experiment's context.

Finally, the chapter concludes with a comprehensive analysis of real-time testing phases. This process represents the pivotal moment where the experimental protocol undergoes practical verification, allowing for the assessment of the effectiveness and accuracy of measurements and adjustments made during the preceding phases. In summary, the chapter provides a complete overview of experimental activities, from the initial calibration phase to real-time evaluation, thus offering an in-depth perspective on the overall experimental process. All this process is visible in Figure 5.1.

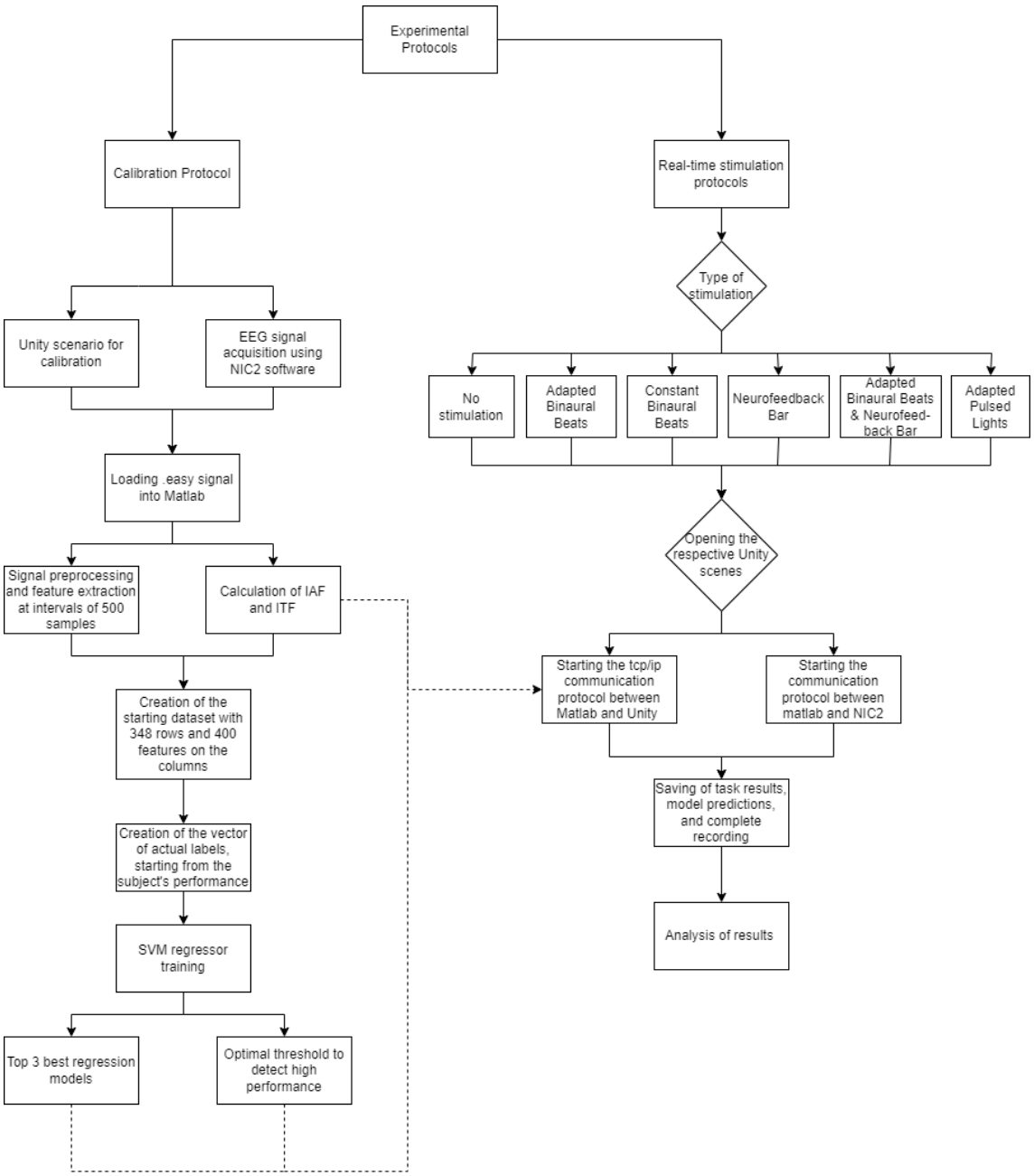

Figure 5.1. Flowchart of the experimental protocol.

5.1 System Calibration Acquisition

This subsection outlines the protocol employed for acquiring the recording used during the system calibration phase. In this critical stage, the primary objective is to capture a prolonged and interference-free signal to ensure the collection of high-quality data. These data serve as a crucial foundation for the subsequent training of the regression model, which is essential for obtaining an accurate index of working memory activity.

Mounting EEG System and Oculus on the User The arrangement of the 8 electrodes follows the layout depicted in Figure 4.3, which displays a snapshot of the NIC2 software interface. The elastic neoprene cap of the Enobio allows for the insertion of electrodes in Ag/AgCl NG Geltrode, adhering to the 10-10 positioning system. The decision regarding the electrode placement was made through a meticulous review of scientific literature in the field of working memory analysis through EEG signal acquisition. Specifically, the selection was made to position the electrodes at P3, P4, T7, F8, F4, Fz, C3, and C4 locations. Initially, participants are instructed to wear the positioning cap. Subsequently, using cotton swabs soaked in medical disinfectant, hair is gently moved to the predetermined positions of the electrodes. With the same swab, the skin is disinfected and lightly rubbed to remove any superficial layers of grease, thus improving the contact between the electrodes and the skin. Following this, Ag/AgCl electrodes are carefully filled with conductive gel and positioned in their designated locations. Before connecting the 8-channel connector to the electrodes, participants are asked to wear the Meta Quest 2 headset, previously initialized by creating a physical space. Once the participant has donned the headset, the 8-channel connector and the Necbox device are connected, as shown in the Figure 5.2.

EEG Signal Recording After verifying all connections and ensuring the electrode-skin connections are sound, the recording begins using the NIC2 software. Participants, through the VR headset, find themselves immersed in the scenario as they prepare for the memory task. Following a brief 20-second orientation and button trial phase, where participants familiarize themselves with the controls, they are guided to relax for 100 seconds Following this, two tasks of 120 seconds each are presented, separated by a 30-second break, resulting in a total protocol duration of 6 and a half minutes. The initial memory task involves a 2-back, succeeded by a 3-back. With the Oculus controllers, participants can interact by selecting between two options (Yes

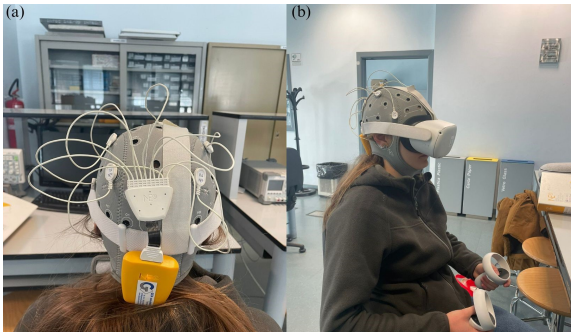

Figure 5.2. Illustration of the Assembly of the EEG System and the Oculus on the User: (a) Rear View; (b) Side View.

or No), with only one being correct. A 2-second response time is allowed, after which the question updates. The outcomes "Correct" or "Try again" are displayed based on the participant's response.

5.2 Calibration Signal Preprocessing and SVR Training

After this offline registration phase, signal pre-processing can be carried out. The signal undergoes initial processing through a tandem arrangement of two Chebyshev filters, each of order 6. The first filter serves as a high-pass filter, allowing frequencies from 4 Hz and above to pass through. Subsequently, the second filter, configured as a low-pass filter, permits frequencies below 30 Hz to pass while attenuating higher frequencies. The signal is then segmented based on markers manually inserted via the keyboard in the NIC2 software during acquisition. Subsequently, parameters are extracted from the acquired EEG signal, calculating a total of 348 features from the selected 8 channels and concatenating them into a 2D matrix. The matrix will have the number of rows equal to the number of features and the columns representing the total seconds. Now, outliers are being removed: for each feature, outliers are replaced with the value of that specific feature from the previous second. In addition to these features, which will be used to train the model, the IAF and the ITF are extracted. These frequencies will serve as starting frequencies to be modulated for real-time neurostimulation. Afterward, the matrix, now free from outliers, is standardized with respect to the baseline, which is the 100-second resting phase with open eyes conducted before the two tasks. Now, labels are being created to train the model: during the initial relaxation phase

and the pause between the two tasks, the assigned label is zero. However, during each task, a label is assigned based on the subject's performance. This information is derived from the report saved by Unity, which includes a number for each response. The number is zero if the user's response was incorrect or not given, and one if it was correct. Subsequently, a sliding window of 3 samples is generated, and these samples are averaged to obtain a number reflecting the subject's average performance in that specific time interval. Once the labels are obtained, the process moves on to the data: a feature selection is performed using the Chi-square method, selecting the top 30 features to be used as input, along with their corresponding labels, for the SVR.

5.2.1 SVR

Hence, an SVM model has been trained to estimate the user's WML in successive real-time tests, using the following options:

K-fold cross-validation is performed to avoid potential overfitting of the model to the training data. This approach helps the model generalize better for subsequent real-time predictions on test data.

The *radial basis function* (RBF) is used as the Kernel Function.

The *Bayesian optimizer* is used as the algorithm for hyperparameter optimization, employing the *expected-improvement-plus* acquisition function. A maximum of 100 objective functions are evaluated. The hyperparameters include ranges for Box Constraint and Kernel Scale exploration, both constrained within the limits of $[1 \times 10^{-2}, 1 \times 10^{2}]$.

To speed up the training process, we also utilize the parallel pool process, enabling the simultaneous use of 12 cores, reducing the total time to approximately 10 seconds.

In the Table 5.1, there are the regression metrics for the just-mentioned training.

Table 5.1. Regression metrics on Users' Training Set

	R^2	**RMSE**
User 1	0,65	0,27
User 2	0,56	0,31
User 3	0,39	0,36
User 4	0,57	0,29
User 5	0,82	0,20
User 6	0,71	0,24
User 7	0,84	0,19
User 8	0,71	0,25
User 9	0,42	0,34
User 10	0,86	0,18
User 11	0,34	0,35
User 12	0,34	0,36
User 13	0,73	0,25

5.2.2 Classification

Moreover, an associated classifier has been developed to differentiate between relaxation and task states. This classifier employs an optimal threshold determined by maximizing the separability between activity and relaxation states, to do this, the ROC curve was used. WML values below this cutoff are assigned a value of 0, while those above are set to 1, representing a relatively low-performance level.

Another threshold is added corresponding to the mean WML during the task phase, indicative of a high-performance level. This value is conveyed to Unity for reference in parameter modulation for neurostimulation. The final threshold is the mean of the first two thresholds, representing an average user performance level. The obtained values for each user are visually presented in the Figure 5.3.

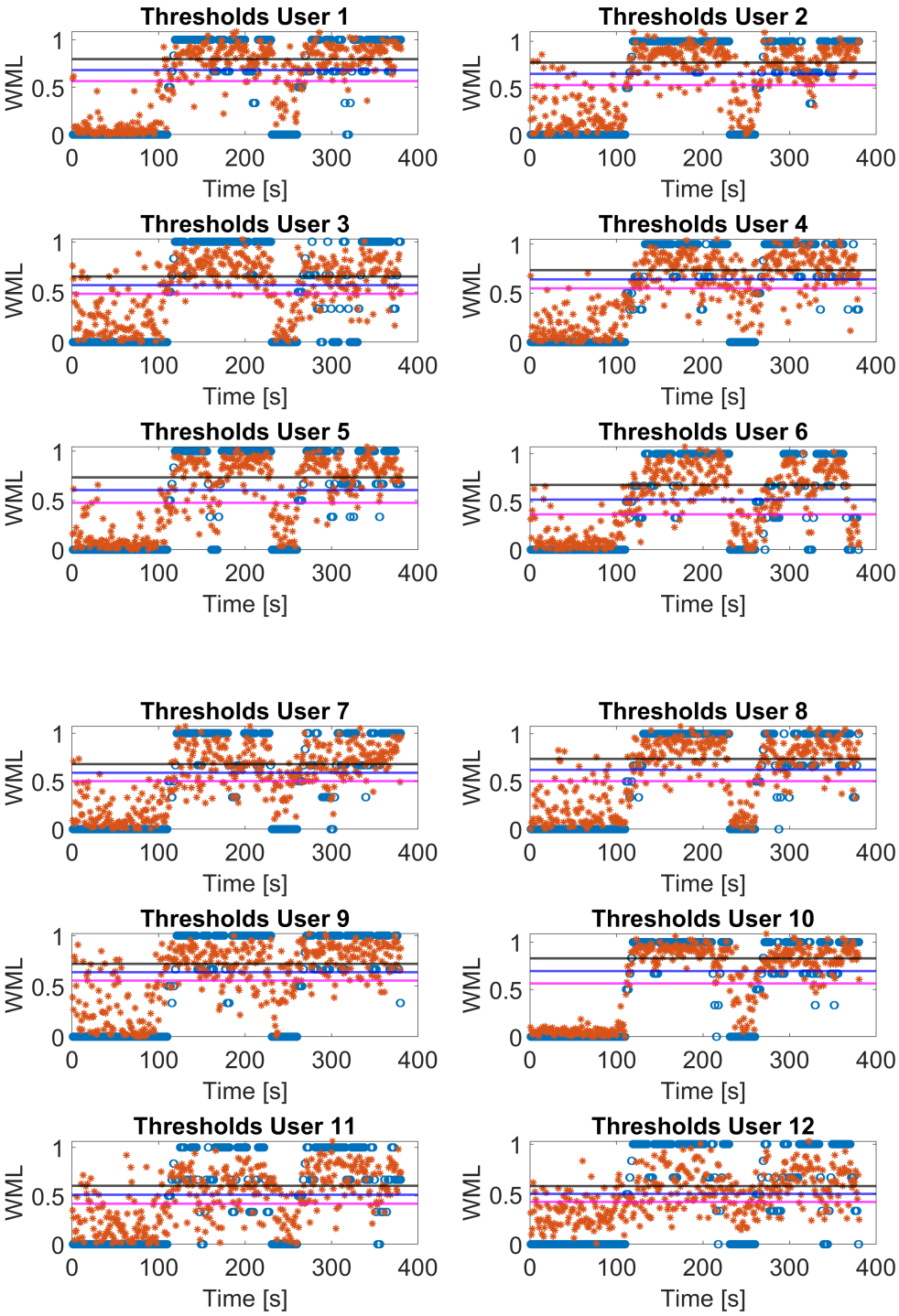
Thresholds User 1
Thresholds User 2
Thresholds User 3
Thresholds User 4
Thresholds User 5
Thresholds User 6
Thresholds User 7
Thresholds User 8
Thresholds User 9
Thresholds User 10
Thresholds User 11
Thresholds User 12
WML
Time [s]
0
0.5
1
0
100
200
300
400

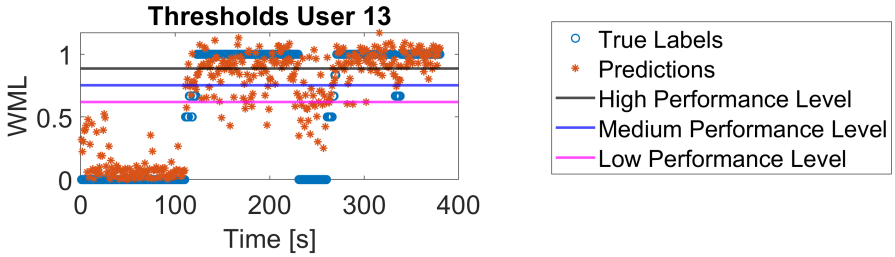

Figure 5.3. Users' Thresholds.

The classification metrics, along with the selected optimal thresholds for each user, are summarized in the Table 5.2.

Table 5.2. Classification metrics on Users' Training Set.

User	**AUC**	**Precision**	**Specificity**	**Recall**	**Optimal Threshold**
1	0,85	97%	96%	73%	0,74
2	0,82	92%	90%	73%	0,71
3	0,82	90%	85%	78%	0,54
4	0,86	92%	88%	84%	0,56
5	0,94	99%	99%	89%	0,54
6	0,87	95%	94%	81%	0,46
7	0,94	99%	98%	90%	0,49
8	0,91	94%	90%	91%	0,51
9	0,77	93%	92%	60%	0,72
10	0,95	98%	97%	93%	0,62
11	0,79	89%	86%	70%	0,52
12	0,76	88%	85%	66%	0,49
13	0,93	95%	92%	93%	0,67

Once the specific model associated with a particular individual, including the thresholds, is obtained, we proceed to the various phases of real-time processing, which will now be explained below.

5.3 Real-Time Phase

5.3.1 Virtual Reality Stimuli

In this thesis work, one type of neurofeedback-i.e., visual neurofeedback-and two types of neurostimulation, one visual and one auditory, were chosen. The chosen stimulation bands include:

- **Alpha band**, a frequency range that, as we delved into in the section on neurofeedback and neurostimulation, has been associated with enhancing working memory performance;
- **Theta band**, associated with enhanced information encoding for working memory.

Neurofeedback Bar

The neurofeedback chosen, which falls under visual neurofeedback, is a fill bar, implemented on Unity via a slider, which signals the subject's instantaneous working memory level. This coincides with the output of the SVR, which provides a continuous value: this is sent to Unity every 500 ms via the TCP/IP connection. The value is calculated over one second of signal, that is, over 500 samples, with a 50 percent overlap between one signal segment and the next, so that a value is given every half second. In this way the subject has immediate feedback, with negligible delay, on his level of memory and attention. He must then try to raise the level of bar filling during the task to try to improve his performance. The bar is placed vertically to the left in the screen, to be as unobtrusive as possible but at the same time to be seen out of the corner of the eye during the performance of the n-back test. It has the filled part in white color, on a gray background of the remaining unfilled area (Figure 5.4).

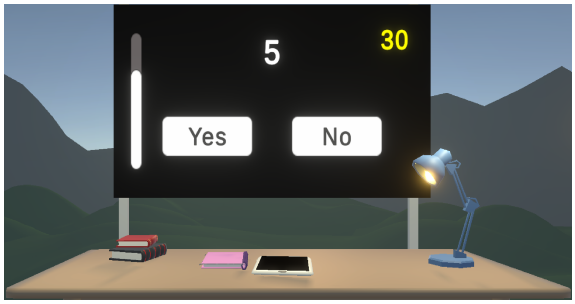

Figure 5.4. Visual feedback: fill bar.

It appears only during the task phases and disappears in the relaxation phases, as it could distract the subject and interfere with his or her state of relaxation.

Neurostimulation with Binaural Beats

One of the chosen neurostimulation techniques is binaural beats. Unlike the previous type of stimulus, which was obviously conscious, this subsequent stimulus is instead unconscious, as in most cases, the user will not be aware of the sound, which will serve to synchronize brain waves at a specific frequency without the user even noticing. The alpha band was selected as the preferred frequency range for implementing these stimuli among various available frequency bands. Binaural beats were here used in two different configurations: a *closed-loop* configuration, where the frequency of the sounds changed over time based on the real-time brain responses of the user, and an *open-loop* configuration, where the stimulation frequency remained fixed throughout the task.

Variable Alpha Band Frequency. The starting frequency of binaural beats (during the real-time test involving this stimulus), considered as the difference between the frequency sent to the right ear and that sent to the left ear, is the IAF extracted during the user's calibration phase. At the beginning of the real-time phase, the frequency sent to the left ear is 400 Hz and remains constant throughout the test, while the frequency sent to the right ear is 400 Hz + IAF, and it is this frequency that will be modulated based on performance. This modulation is achieved through an optimization algorithm implemented by us in a C# script assigned to the Binaural Beats object. The value of IAF will be updated by the algorithm with a new IAF value chosen by it. The value of IAF will be updated by the algorithm with a calculated IAF_NEW value based on the working memory level, as described earlier, and sent to Unity every 500 ms. More specifically, the IAF value is increased or decreased by 1 Hz if, in the last 10 seconds (i.e., among the last 20 received WML values), at least 8 values are below a certain threshold. Afterward, another 10 seconds are waited, and the number of indices below the threshold is compared to the previous count. If there are more indices below the threshold than before, the algorithm decreases the frequency by 1 Hz if it had previously increased it (or increases it by 1 Hz if it had decreased it), as it would mean that the change was not in the right direction. If there are fewer indices below the threshold compared to the previous step, the same type of modification is made because it would indicate that the direction of the

change was correct. Of course, the frequencies that the algorithm can choose range between 9 and 13 Hz, precisely within the alpha band. This process continues in this manner. By doing so, it should lead to a convergence condition, resulting in a lower number of indices below the threshold, indicating an improvement in performance. The threshold chosen for the comparison of indices is calculated during the calibration phase and represents and average level of user performance against which improvement can be sought during the stimulation. It has been sent to Unity using the LSL protocol, always through a specific port. Throughout the whole stimulation session, calming music was played with binaural beats superimposed on top. This is because there is a chance that these noises will cause pain for the subjects, and it is important to stimulate the subjects subconsciously to ensure that they are not affected by this element during the experiment. In the following graphs, depicted in Figure 5.5, several examples of frequency modulation of stimuli across six users are presented. These are overlaid on the graph alongside the temporal trends of WML for the same users. It is evident that changes in frequency align with periods of lower user performance within that specific timeframe.

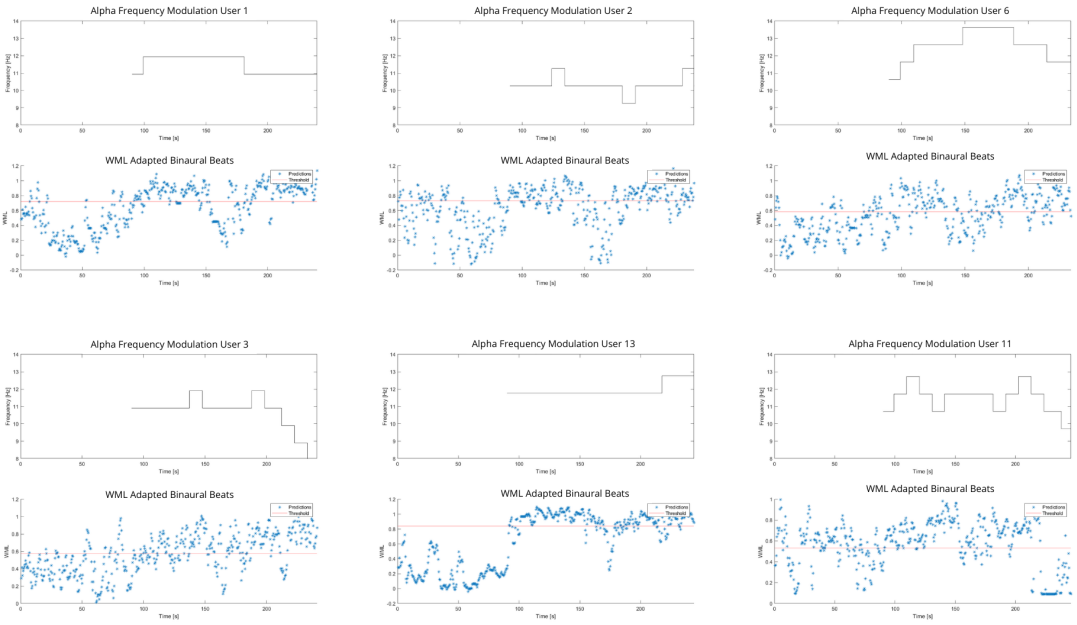

Figure 5.5. Alpha modulation for six example subjects.

Constant Alpha Band Frequency. In addition to previous variable alpha band stimulation, a phase of constant alpha band stimulation has also been tested to compare the effects of the two different configurations with each other. In this case as well, the binaural sounds will play only during the task phase, while they will stop during the relaxation phases. At a theoretical level, this type of configuration should be less effective than the previous one, as it is a fixed stimulation that does not adapt to the real-time needs of the user. The user's working memory level could decrease at any moment, requiring an almost instantaneous frequency modification to follow this change.

Neurostimulation with Pulsed Light

Regarding the pulsed light stimulation, we designed a Christmas tree with lights that flash at a certain frequency, adapted to the real-time performance of the subject, as explained in the previous paragraph about binaural sounds. Entrainment was performed in the theta band, following the same type of algorithm seen above, aiming to reach convergence for the highest possible performance. It follows the same principles just described, with the only difference being that instead of choosing IAF as starting frequency, it is chosen the ITF. In this case, the algorithm will explore frequencies ranging from 4 to 8 Hz, which correspond to the theta band. Flashing occurs only during the task phase, while in the relaxation phase, they are turned off to avoid interference with the relaxation phase, which is very sensitive/delicate. The tree is positioned on the desk and extends to the right side of the screen, ensuring it is visible or even just perceptible during the exercises (Figure 5.6).

Figure 5.6. Pulsed light stimulation using Christmas lights.

The following Figure 5.7 illustrates the changes in the pulsating light frequency over time for six users, overlaid with their instantaneous working memory level (WML) trends, similar to what was described earlier for binaural sounds. In the case of User 11, for instance, a consistently above-threshold

WML suggests that no changes in stimulation frequency are needed, as it is already appropriate for the user. Conversely, Users 1, 6, and 13 exhibit numerous adjustments in the pursuit of an optimal frequency, as their performances fall below the threshold for extended periods.

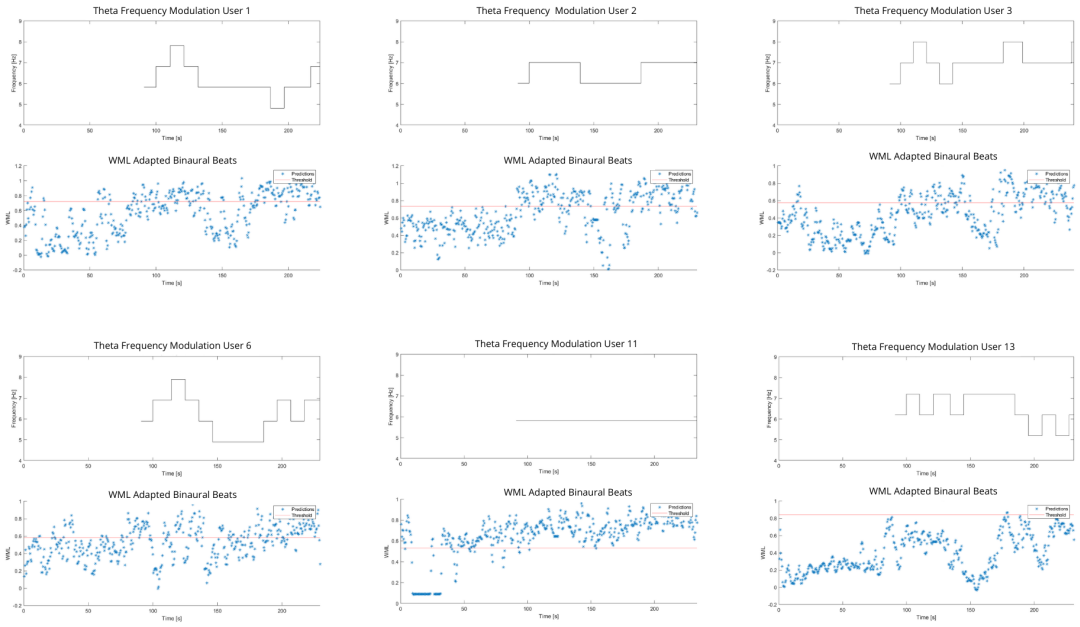

Figure 5.7. Theta modulation for six example subjects.

Neurofeedback and Neurostimulation

Finally, the combination of two different stimuli was also tested, which are the neurofeedback provided by the fill bar, and the neurostimulation through binaural beats in the alpha band. The expectations for this phase with combined stimuli are high because the beneficial effects of these two stimuli, taken separately, should here be positively summed. In this situation as well, an analysis was conducted on the changes in modulation frequencies of binaural sounds based on real-time user performance. Six sample users are represented in the Figure 5.8.

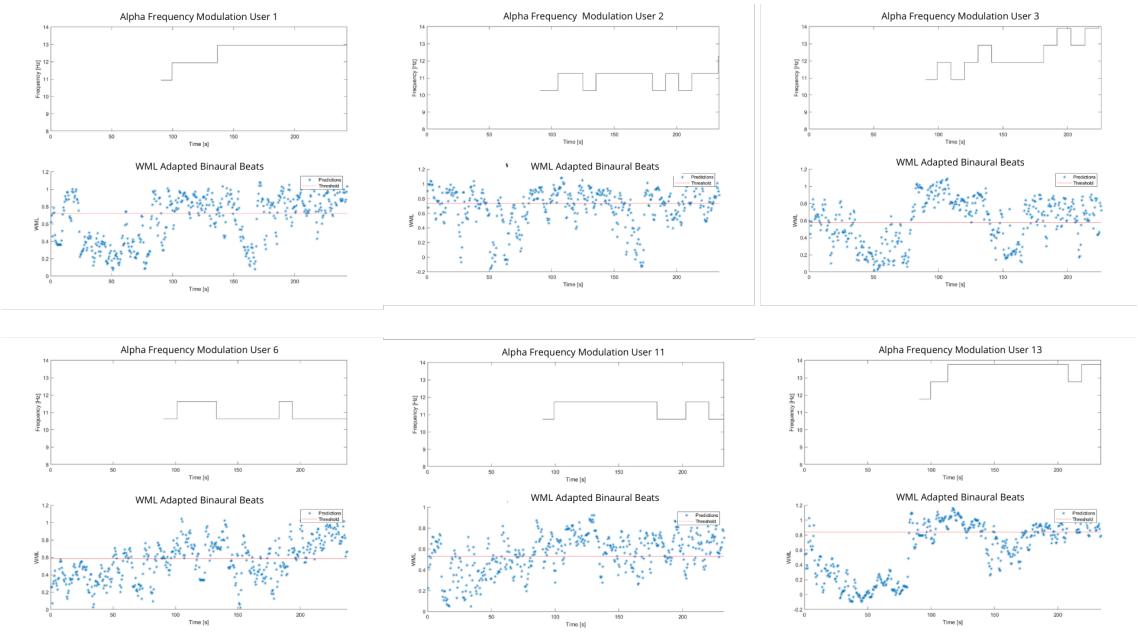

Figure 5.8. Alpha modulation for six example subjects.

5.3.2 Real-Time Acquisition

For each testing phase, the subject's model, IAF, ITF, the top 30 selected parameters, and the baseline from the calibration phase are loaded one by one. The mean and standard deviation of the features are then calculated on this baseline. These statistics are used to standardize the parameters that will be computed in real-time.

Using the MatNIC functions, connection is created between the NIC2 program and Matlab to enable real-time processing of the signal obtained through Enobio Necbox. The TCP/IP connection is necessary for these operations. Raw EEG data are transmitted utilizing an LSL protocol, where receives chunks of approximately 250 samples at a time. To conduct signal analysis, buffers of 500 samples are filled by concatenating incoming chunks and analyzing the latest 500. Through LSL connection, data can be received either sample by sample or in chunks. We chose to use chunks as they allowed for better script execution speed, i.e., better real-time performance. This is because, while we perform feature calculations on the latest arriving samples, the NIC2 is already collecting an entire chunk of 250 samples, saving us from having to wait for one sample at a time and concurrently executing these two

tasks. As soon as the new chunk arrives, we are ready to analyze it immediately, concatenating it to the previous one, and in the meantime, the NIC2 is collecting another chunk. And so on. This approach results in almost zero latency.

We use TCP/IP connection to send Unity some values that are used to modulate neurostimulation: before the task starts we send the IAF, ITF and the threshold corresponding to the average of the user's WML during the calibration phase. During the task we will send WML in real-time, every 500 ms.

After making these connections, reception of the signal within a `while` cycle begins, which allows samples to be acquired indefinitely until there is a stop by Unity, which, at the end of the task, will exit play mode and thus stop communication. As soon as a buffer of 500 initial samples is filled, the necessary calculations described below will begin. Filtering between 4 and 30 Hz is applied to each buffer, and the 30 parameters needed for the model to make predictions are extracted and standardized. From these parameters, the regressor outputs the WML values. This index is crucial for managing the modulation of neurofeedback and neurostimulation in Unity. WML is calculated over 1-second epochs with a 0.5-second overlap between successive epochs, resulting in an index every half-second. This approach ensures that the index is nearly instantaneous relative to the subject's condition, minimizing any significant delay. To avoid abrupt changes in visual and auditory stimuli and obtain cleaner data with less noise, the calculated parameters for the current second are averaged with those of the four previous ones. The resulting value is then input into the regressor, and its output is sent to Unity.

This entire real-time acquisition protocol is repeated six times, once for each designated Unity room, presented randomly to exclude any patterns related to training from subsequent statistical tests. All rooms share the same virtual reality scenario but have some different elements based on the type of stimulation for which they were created. The order of the various phases is the same as in the calibration, but the protocols have a shorter duration. The relaxation phase will last for 60 seconds instead of 100, and each of the two tasks will last 60 seconds instead of 120. In total, each complete protocol will last for 4 minutes.

The following rooms are thus present:

- One of them presents features elements called 'binaural beat objects', which provide binaural sounds with a variable frequency in the alpha band adapted to the user's instant WML. This can be defined as a closed-loop stimulation.

- Then, there is a room dedicated to stimulation with binaural sounds in the alpha band but with a constant frequency, corresponding to the IAF extracted during the calibration phase. It is useful for comparing the effects of adapted stimulation with those obtained at a fixed frequency.
- Another room introduces an additional visual element, a Christmas tree with lights that flash at a variable frequency in the theta band.
- An additional room features visual neurofeedback, consisting of a filling bar displayed on the screen, indicating the level of instant WML. This is useful for understanding whether neurostimulation leads to better improvements compared to simple neurofeedback.
- Then, a dedicated room was created to combine visual neurofeedback and neurostimulation, containing both the filling bar and binaural sounds with a variable frequency in the alpha band.
- Finally, there is a baseline room with no stimulation, providing a reference against which to compare the performance obtained with the various stimulations tried in the other rooms.

Chapter 6

Results and Discussions

This chapter details the results obtained in the course of the research and provides an in-depth analysis of the effects of the neurostimulations examined. Beginning with the calibration phase and ending with a discussion of the effectiveness of these stimulations on the subjects, the aim is to determine whether there is concrete evidence of improvement in cognitive abilities, with a particular focus on working memory. Comparison will be made between participants' basal working memory levels and those observed during the stimulation sessions, as described in the Materials and Methods section.

6.1 Real-Time Regression Results

This section delves into the analysis of the regression model's performance during real-time testing phases where subjects underwent neurostimulation. The evaluation employs regression metrics calculated across the real-time phase, leveraging actual user performance during tasks as reference labels.

In Figure 6.1, the regression model's output is illustrated in blue throughout the six sessions of the real-time phase, while a low-pass filter at 0.1 Hz applied to the same signal is shown in red, emphasizing the fluctuations in working memory level. This method of representation, using the same scale for modulating stimulations (every 10 seconds), allows for a clear visualization of the model's tracking ability with respect to the dynamic changes in working memory. Graphs of the regression results for all subjects analyzed in the thesis are given in Appendix A.

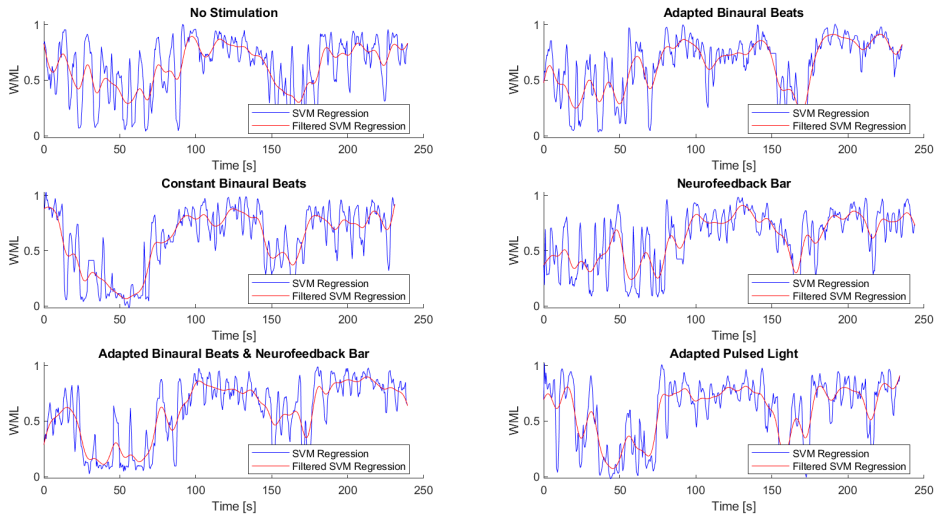

Figure 6.1. Regressor report for user 9 for all six test conditions.

The primary metrics used to evaluate the regression model's quality are the coefficient of determination (R^2) and the Root Mean Square Error (RMSE), computed across the full duration of the WM task.

The Table 6.1 below summarizes the average evaluation metrics for each subject across the six stimulation conditions, providing a comprehensive overview of the model's predictive performance.

The R^2 values across subjects reveal varied efficacy of the regression model in capturing the dynamics of working memory levels under different stimulation scenarios. Notably, the model achieved its highest R^2 value of 0.44 for User 8, suggesting a robust ability to predict working memory levels, particularly under certain conditions.

In contrast, the lowest value observed was 0.12 for User 12, indicating a substantial divergence between the predicted and actual working memory levels for this individual. Analyses of model metrics highlight how much can be done to increase the robustness of the protocol in order to make it more accurate and stable during forecasting.

Table 6.1. Classification metrics on Users' Training Set

User	R^2	**RMSE**
1	0,34	0,42
2	0,30	0,45
3	0,33	0,39
4	0,15	0,40
5	0,26	0,41
6	0,41	0,38
7	0,38	0,35
8	0,44	0,37
9	0,32	0,42
10	0,25	0,41
11	0,17	0,42
12	0,12	0,45
13	0,40	0,38

6.1.1 Predominantly Selected Features

In the context of a comprehensive analysis of the problem under study, an examination was conducted to identify signal features and channels most frequently selected by the feature selection method.

This approach aimed to pinpoint those features and channels that could warrant focused attention for future, more in-depth studies. Figure 6.2 presents a histogram of feature occurrences across the 13 subjects, which reveals that the developed method predominantly identifies the alpha power as the most significant feature for addressing the problem across subjects. Additionally, good performance is also observed in power ratios and phase locking value, demonstrating that synchronizations between cerebral areas are crucial for the proper functioning of working memory.

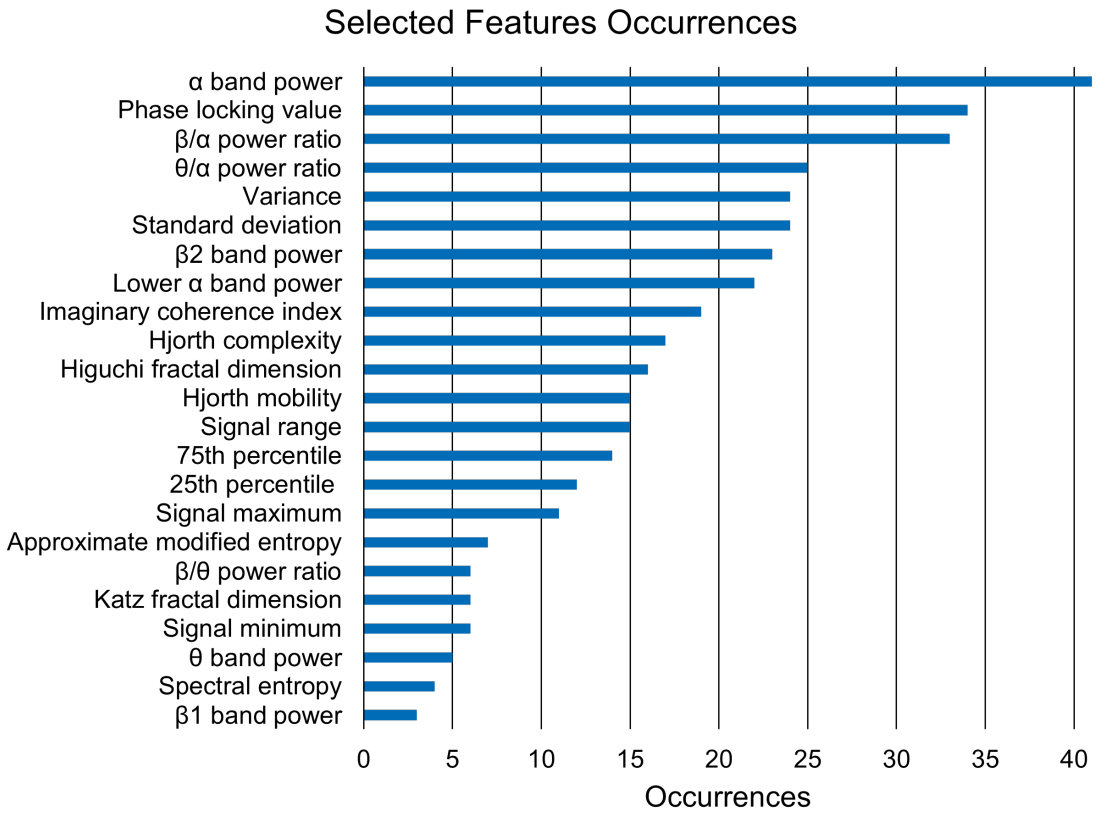

Figure 6.2. Histogram of feature occurrences across the 13 subjects.

Figure 6.3 illustrates that the predominantly selected channels are F7, T7, and P3, suggesting a higher involvement of the left lobe in this particular activity. This observation aligns with existing literature, since working memory tasks have shown hemisphere differences in parietal activations. Many studies have consistently found left-lateralized activity for verbal working memory and right-lateralized activity for spatial working memory, using behavioral assessments and PET scans during n-back tasks [107].

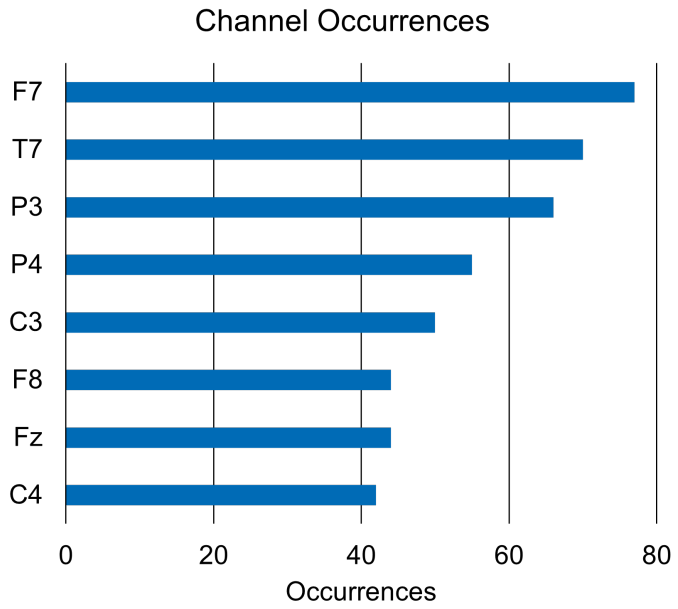

Figure 6.3. Histogram of channel occurrences across the 13 subjects.

It's worth noting that our n-back task employs numerical stimuli, establishing a connection with verbal working memory. This adds a layer of specificity to our findings, emphasizing the interplay between numerical processing and left-lateralized activations in the working memory context.

6.2 Evaluation of Treatment Effects

During the next phase of the project, different neurostimulation methodologies were applied in order to evaluate the impact of these interventions on working memory functions. Implementing a structured stimulation protocol across six experimental sessions, different combinations of neurostimulation and neurofeedback were examined and correlated with n-back cognitive tasks. Analysis of the results was aimed at verifying any improvements in cognitive performance, adopting statistical methods for significance analysis of the observed differences.

The stimulation protocol, detailed in the preceding chapters, aimed to evaluate the effectiveness of different interventional approaches, with a particular focus on their influence on working memory abilities. This phase of investigation assumes a critical role in exploring the potential effects of neurostimulations, as well as allowing for a comparative evaluation of the effect of various

neurofeedback techniques on cognitive performance.

Next, analysis of the collected data focused on identifying significant changes in working memory performance by comparing sessions with stimulation to control sessions, with the intent of quantifying the effectiveness of the applied stimulation techniques. Through the use of statistical approaches, it was possible to rigorously examine the experimental hypotheses, providing a solid quantitative foundation for the interpretation of the results.

The adoption of statistical analysis techniques proved indispensable in determining the statistical significance of the differences between stimulation and control sessions, offering the possibility of validating the experimental methodologies used in this pilot research. This process facilitated the identification of improvements attributable specifically to the stimulation modalities employed, contributing to the formulation of evidence-based conclusions regarding their actual impact on working memory functions.

Assessment of Subject Accuracy

To preliminary investigate participants' cognitive performance, accuracy was analyzed in the 2-back and 3-back tasks. Accuracy was defined as the ratio of the number of correct responses (NA) given by the subject to the total number of stimuli presented (TQ), according to the formula:

$$Accuracy = \frac{NA}{TQ} \tag{6.1}$$

This metric made it possible to quantify participants' performance in the different experimental sessions. The graphical analyses, shown in Figure 6.4, illustrate the results obtained by each subject in each test session.

Upon examination of the graphs, it is observed that for the 2-back task, no significant differences emerge between sessions, presumably due to the relative simplicity of the task that leads performance to saturate close to 100%. In contrast, the 3-back task, characterized by greater difficulty, allowed the effect of different stimulations to be more clearly distinguished. In particular, there was a tendency for improvement in sessions with both constant and adaptive binaural stimulation compared to control. This indicates that tasks of greater complexity are more likely to reveal changes in performance, suggesting the potential effectiveness of the neurostimulations examined.

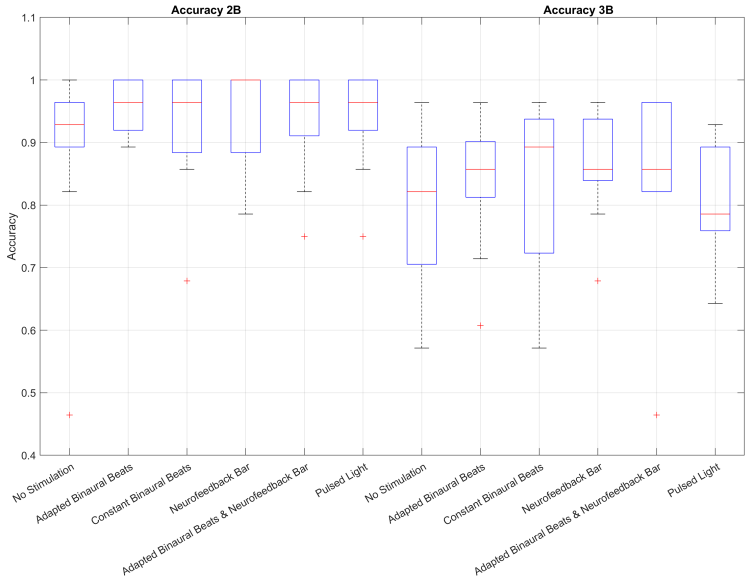

Figure 6.4. Distribution of subjects' accuracy in 2-back and 3-back tasks, illustrating changes in performance following different stimulations.

This observation underscores the importance of selecting appropriate tasks when evaluating the effect of neurostimulation interventions, highlighting how more demanding tasks can facilitate the identification of significant trends related to the application of stimulation techniques.

Analysis of the Reaction Time

Reaction time analysis represents a crucial index of cognitive processing speed. At this stage of the study, average reaction times associated only with correct responses were considered in order to exclude possible biases due to hasty and unreflective responses. The focus on correct reaction times ensured that the analysis reflected cognitive processing speed under optimal conditions.

The graph in Figure 6.5 exhibits the reaction times, measured in milliseconds, for the 2-back and 3-back tasks. Examination of the graph reveals a clear distinction in the average reaction times between the two tasks, with 3-back exhibiting greater variability than 2-back. In the case of 2-back, there are no substantial differences that would indicate a definite effect of the stimulations. However, in the more complex 3-back task, the data suggest the emergence of differential trends between the stimulation and control conditions.

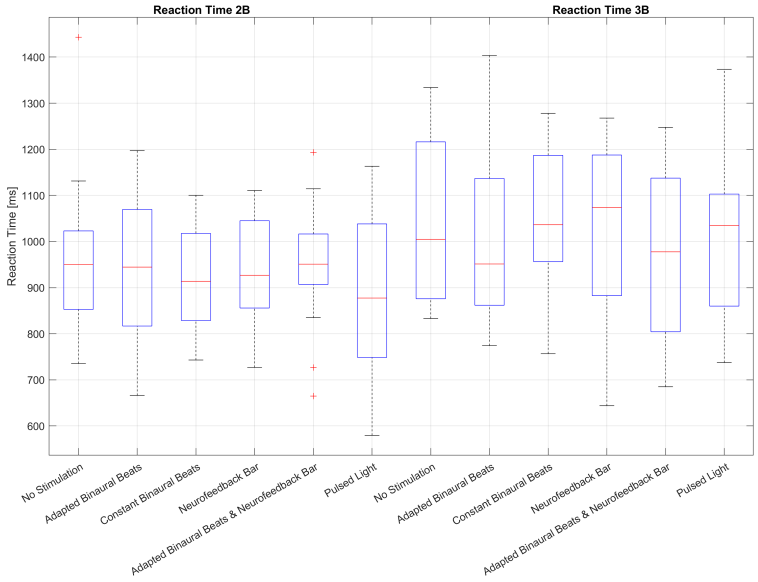

Figure 6.5. Comparison of average reaction times (RT) between 2-back and 3-back tasks under stimulation and control conditions.

In the detailed analysis of Figure 6.5, it is particularly evident how the median of reaction times tends to be affected by experimental conditions. It is observed that, for some stimulation modalities, the median of reaction times is lowered, suggesting a potential efficacy in improving processing speed. These results invite further investigation to establish the consistency of the observed trends and to explore the causal relationship between neurostimulation methodologies and cognitive performance as measured by reaction times.

Analysis of the Inverse Efficiency Score

In order to obtain a more holistic measure of cognitive performance that integrates information on both speed and accuracy, the Inverse Efficiency Score was employed. This index, previously defined in the Materials and Methods section, provides a composite assessment of cognitive performance by combining reaction time with subject accuracy. The IES is particularly useful in that it provides a measure of efficiency that penalizes both slow and inaccurate responses.

Figure 6.6 shows the distribution of IES for the 2-back and 3-back tasks in the different stimulation conditions. Visual analyses indicate considerable variation across sessions, with a general trend toward higher IES scores for the more complex 3-back task. This suggests that while the 2-back may not

have been sufficiently challenging to reveal significant differences, the 3-back elicited a wider range of efficiency in participants, thus allowing the effect of different stimulation techniques to be more clearly discriminated.

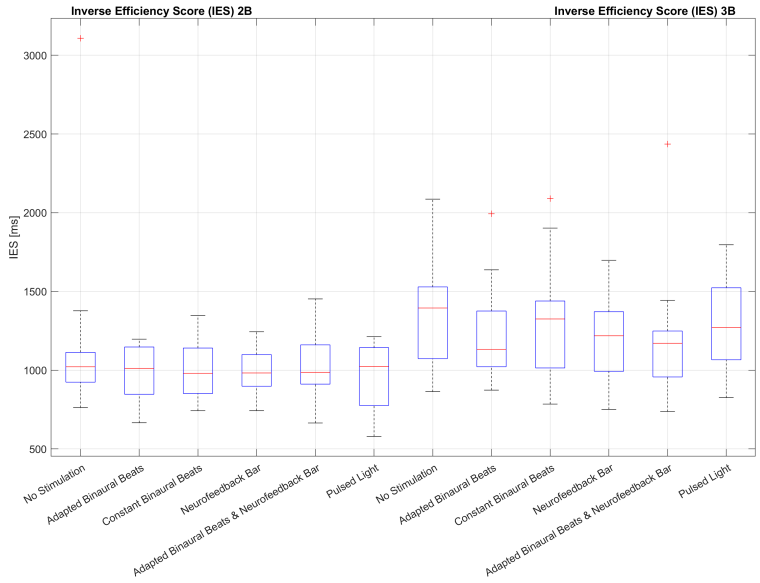

Figure 6.6. Distribution of the IES for the 2-back and 3-back tasks.

Detailed analysis of IES can reveal valuable information about the balance between speed and accuracy, offering additional perspective on cognitive performance beyond what could be inferred from accuracy or reaction times taken individually. These results underscore the importance of considering composite measures such as IES for a more comprehensive assessment of the impact of neurostimulation on cognitive function.

6.3 Study of Normality

In this section, the distribution of accuracy, reaction time and Inverse Efficiency Score data derived from the 2-back and 3-back tasks is examined. Determining the normality of the distribution is critical to the choice of the appropriate statistical test: for distributed data normally parametric tests such as Student's Test are preferred, while for non-normal distributions non-parametric methods such as Wilcoxon test are used.

The Shapiro-Wilk test, used to test normality, considers "0" as indicative of a normal distribution and "1" for a non-normal distribution. Below, the

results of the Shapiro-Wilk test applied to the averages of accuracy, reaction time and IES for each subject in the six evaluation sessions are shown in the Table 6.2.

Table 6.2. Shapiro-Wilk normality test summary table.

	2-back			3-back		
Stimulations	**PC**	**RT**	**IES**	**PC**	**RT**	**IES**
No Stimuli	1	0	1	0	0	0
Adaptive BB	1	0	0	0	0	0
Constant BB	1	0	0	1	0	0
NF Bar	1	0	0	0	0	0
Adaptive BB & NF	1	0	0	1	0	1
Pulsed Light	1	0	0	0	0	0

The results indicate variation in the normal distribution of the data among the variables analyzed. The presence of non-normal distributions for some variables suggests the need to use non-parametric statistical tests for analysis. Therefore, in the presence of mixed results regarding normality, Wilcoxon tests for paired data were used to examine differences between stimulation conditions.

This methodology ensures the reliability of the statistical analysis despite the variation in the data distribution, ensuring rigorous evaluation of the research hypotheses without assuming normality of the data.

6.4 Analysis of the Effects of Adaptive Neurostimulation

Through statistical tests, the effects of the various stimulation modalities tested on cognitive performance were evaluated.

The absence of complete normality in the data led to the use of a nonparametric statistical procedure, i.e., the Wilcoxon test for paired data, orienting the analysis toward a dual purpose: to deepen understanding of the effectiveness of adaptive neurostimulation and to provide an empirical basis for methodologically sound conclusions.

6.4.1 Wilcoxon Test

Wilcoxon test was used to determine the existence of statistically significant differences between the stimulation and non-stimulation conditions, as well as between the adaptive and constant stimulation conditions.

The results of this analysis are presented in the following Table 6.3, which summarizes the results obtained from the comparison tests for each parameter used between the unstimulated and stimulated conditions.

Table 6.3. Wilcoxon test summary table.

	2-back			**3-back**		
Stimulations	**PC**	**RT**	**IES**	**PC**	**RT**	**IES**
No Stimuli/ Adaptive BB	0,08	0,23	0,12	0,12	0,25	0,04
No Stimuli/ Constant BB	0,12	0,15	0,15	0,15	0,50	0,25
No Stimuli/ NF Bar	0,23	0,32	0,19	0,01	0,21	0,03
No Stimuli/ Adaptive BB & NF Bar	0,19	0,55	0,39	0,05	0,08	0,05
No Stimuli/ Pulsed Light	0,12	0,04	0,06	0,40	0,19	0,16
Constant BB/ Adaptive BB	0,31	0,73	0,53	0,75	0,34	0,42

Close examination of the results obtained from the 2-back test reveals the absence of significant changes in the parameters of accuracy, reaction time and Inverse Efficiency Score. It is hypothesized that the less complex nature of this test led to a reduced incidence of errors on the part of the participants, consequently limiting the possibility of observing noticeable improvements.

Otherwise, the analysis conducted on the 3-back test demonstrates a substantial change, showing statistically significant differences. In particular, the Inverse Efficiency Score analysis shows that the comparison between the conditions of no stimulation and those characterized by adaptive stimulation using binaural beats in the alpha band, both alone and in combination with neurofeedback, elicit statistically significant improvements ($p < 0.05$). These results are illustrated effectively through the use of boxplots, as shown in Figure 6.7.

However, this contrast between the results of the 2-back and 3-back tests suggests a greater sensitivity of the latter to variations in individuals' cognitive conditions, attributable to its greater complexity. This aspect underscores the importance of selecting appropriately challenging test protocols to evaluate the effectiveness of cognitive stimulation techniques.

There is evidence of statistically significant changes in reaction times, with a marked reduction observed in users subjected to adaptive stimulation conditions. Specifically, the stimulation mode employing binaural beats in the alpha band was shown to be particularly effective in facilitating faster response

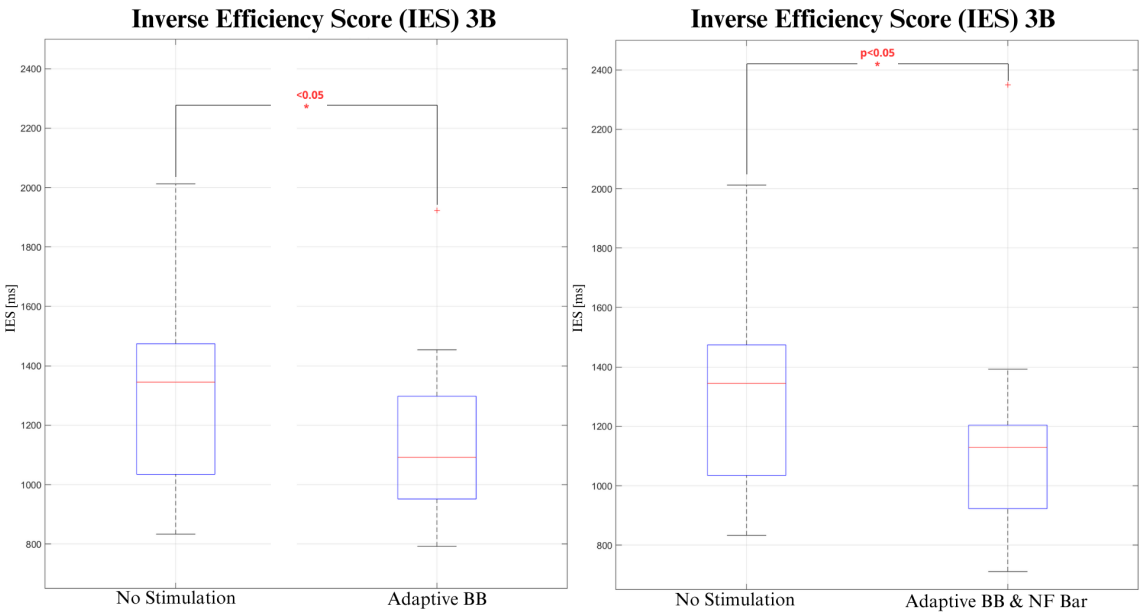

Figure 6.7. Boxplots comparing significative results for IES in 3-back: no stimuli condition vs adaptive BB on the left; no stimuli condition vs adaptive BB & neurofeedback bar on the right.

times to correct queries than the unstimulated condition.

These results are detailed in Figure 6.8, which represents a comparison between the two conditions. The statistical significance of this reduction in reaction time underscores the effectiveness of adaptive alpha-band stimulation in enhancing responsiveness, highlighting the potential of such approaches in optimizing cognitive function.

Comparative analysis of accuracy reveals differential improvements between the conditions without stimulation and those in which the Neurofeedback bar was applied, results that reach statistical significance ($p < 0.05$). Although these increases are small in magnitude, their statistical significance is clearly highlighted in Figure 6.9. This finding suggests that the use of Neurofeedback bar can positively influence the accuracy of users' responses, albeit to a moderate extent.

The main objective of the present research work is to examine the efficacy of the individual-adaptive neuronal stimulation approach, evaluating its improvements over unstimulated conditions and non-adaptive stimulation modalities, the latter of which are widely discussed in the scientific literature.

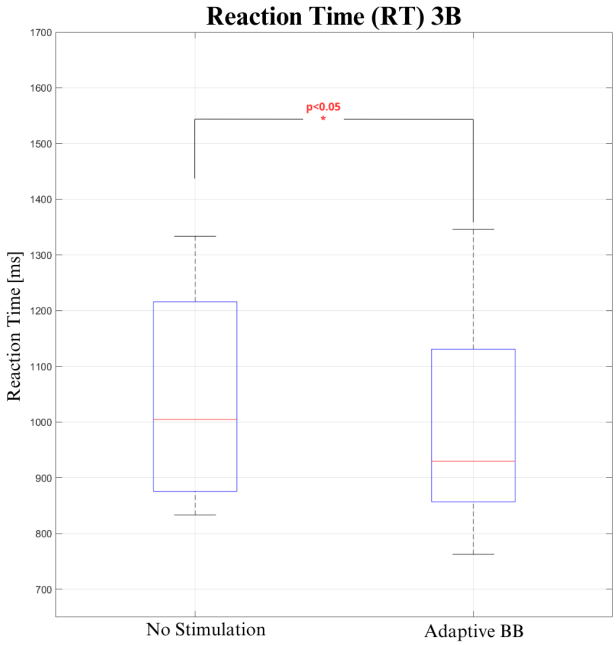

Figure 6.8. Boxplots comparing significative results for RT in 3-back: no stimuli condition vs adaptive BB.

To this end, comparative tests were conducted between the adaptive stimulation conditions and standard reference stimulation conditions in order to identify any improvements introduced by treatment personalization.

Specifically, analysis of the Inverse Efficiency Score, as illustrated in Figure 6.10, showed no statistically significant differences in improvement, although visual analysis of the boxplots suggests a slight tendency toward improvement that may merit further investigation.

This result lays the foundation for future research to explore the potential of adaptive stimulation in greater depth, with the aim of confirming or refuting the observed trends and expanding the understanding of the effect of such interventions on cognitive abilities.

Relative to reaction times, the analysis revealed the existence of statistically significant differences between the conditions of stimulation using constant binaural beats and those involving the use of adaptive binaural beats in the alpha band ($p < 0{,}05$). In contrast, no significant differences were identified in the context of combined stimulation with neurofeedback.

These results, illustrated in Figure 6.11, underscore the effectiveness of adaptive stimulation specifically in the alpha band in improving reaction time,

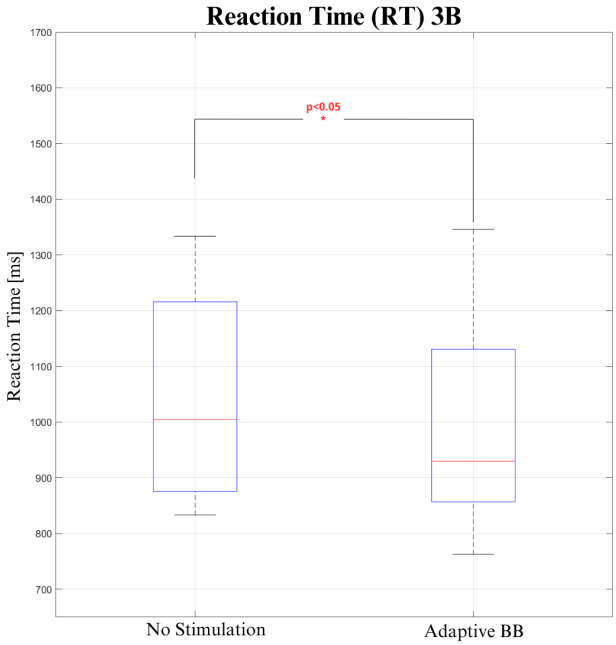

Figure 6.9. Boxplot comparing significative results for PC in 3-back: no stimuli condition vs neurofeedback bar.

in contrast to configurations involving a combined approach with neurofeedback. These findings suggest the need for further investigation to fully understand the potential and limitations of different brain stimulation modalities, particularly with regard to their ability to influence cognitive response speed.

Wilcoxon tests were applied in order to determine whether the integration of adaptive stimulation with neurofeedback led to improvements over the exclusive use of neurofeedback. The results, detailed in Figure 6.12, showed no significant improvements attributable to this combined approach. This outcome suggests that, under the experimental conditions adopted, adaptive stimulation, when combined with neurofeedback, does not outperform neurofeedback used in isolation.

This finding invites critical reflection on the synergistic potential between different neurostimulation technologies and underscores the importance of further research aimed at exploring the dynamics underlying the interaction between adaptive stimulation and neurofeedback in order to optimize interventions for cognitive enhancement. The analyses conducted provide evidence in favor of the effectiveness of adaptive stimulation in improving cognitive abilities, with a particular focus on working memory. However, contrary to initial expectations, the results did not demonstrate significant differences between

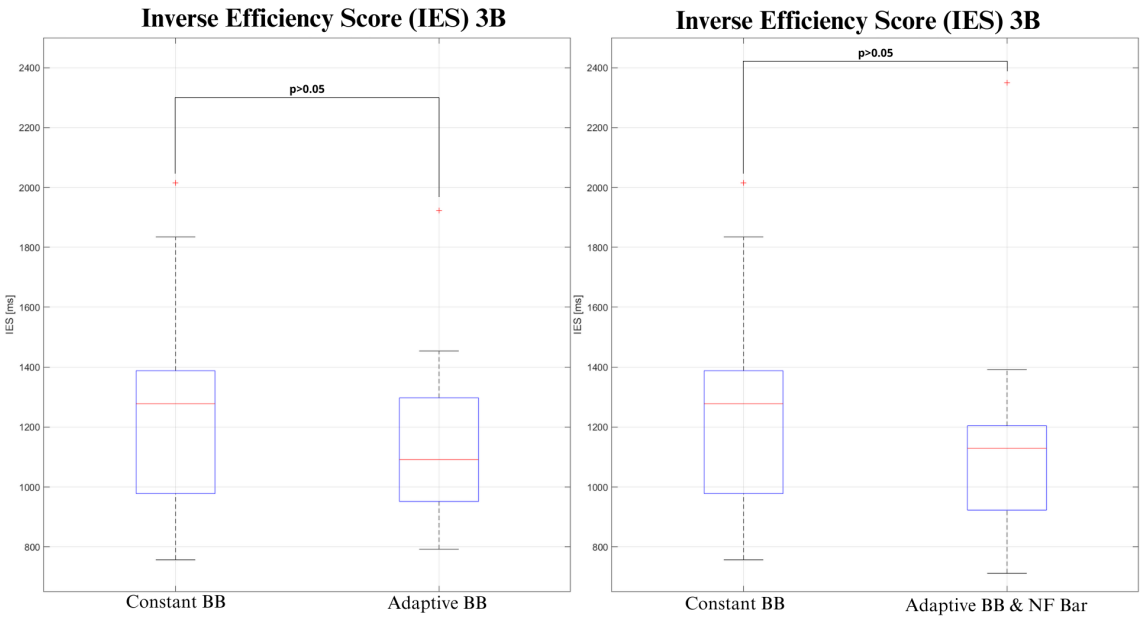

Figure 6.10. Boxplots comparing significative results for IES in 3-back: constant BB vs adaptive BB on the left; constant BB vs adaptive BB & neurofeedback bar on the right.

adaptive and constant stimulation modalities except for reaction time alone, raising the need for further investigation to better understand the underlying dynamics of these effects. Furthermore, the absence of significant improvements in the integration of neurofeedback with adaptive stimulation compared with the isolated use of neurofeedback raises questions about the synergy between these techniques, inviting a critical review of current strategies and suggesting fertile ground for future research.

Significantly, it points out that further investigation of the effectiveness of different stimulation modalities could benefit from the inclusion of a larger sample of subjects and the adoption of cognitive tasks of greater complexity. This approach could not only further emphasize the observed trends but also help establish the normality of the data, thus providing a more solid basis for interpreting the results. Therefore, we stress the importance of designing future studies that take these aspects into consideration in order to enrich the understanding of the impacts of neurostimulation and neurofeedback on cognitive function.

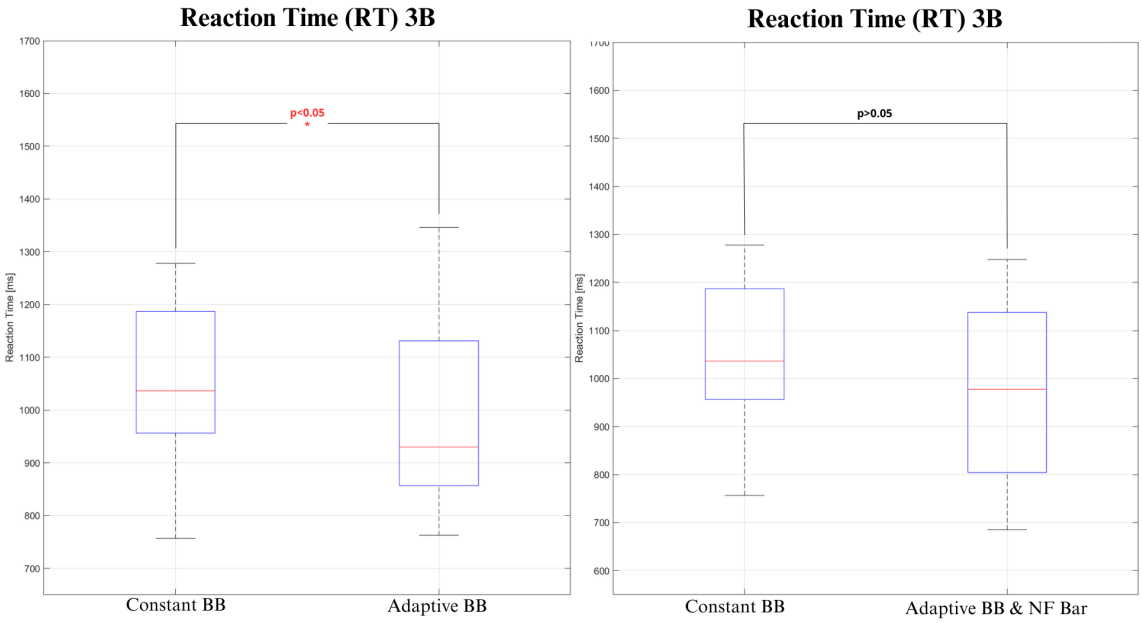

Figure 6.11. Boxplots comparing significative results for RT in 3-back: constant BB vs adaptive BB on the left; constant BB vs adaptive BB & neurofeedback bar on the right.

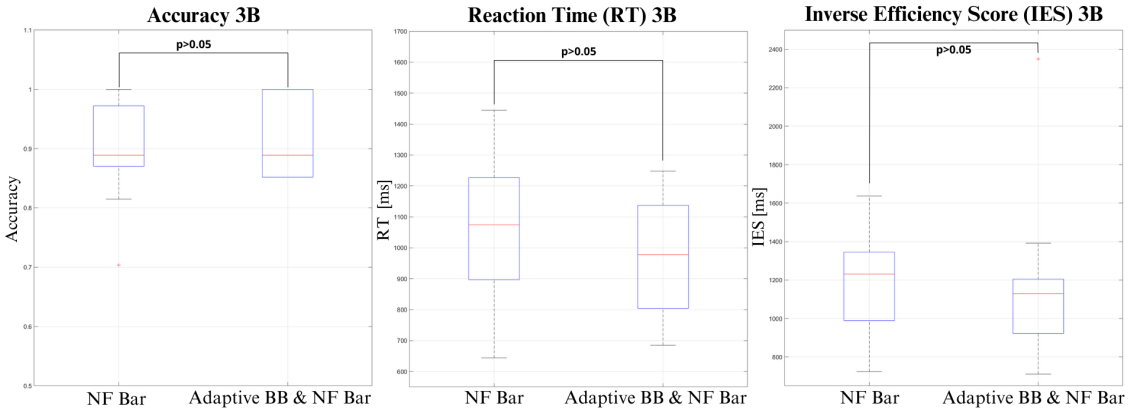

Figure 6.12. Boxplots comparing significative results in 3-back for PC on the left, RT in the centre, IES on the right. The compared stimuli are neurofeedback bar vs adaptive BB & neurofeedback bar.

Chapter 7

Conclusions and Future Developments

In the following sections, the various steps taken throughout this thesis will be meticulously examined, providing a thorough analysis of the associated pros and cons, as well as potential perspectives for future developments.

7.1 Conclusions

During this pilot study, various stimulation approaches were explored with the aim of enhancing users' working memory capacities. To achieve this, a Support Vector Regression was employed to dynamically modulate stimulation parameters based on the working memory level calculated every 500 ms. Among the different modalities tested, neurostimulation with alpha-band binaural beats, dynamically adapted according to the user's WML, exhibited the most significant improvement in overall performance. It is noteworthy that, currently, there are no real-time-adaptive neurostimulations specifically designed for working memory enhancement, positioning this research as an innovative contribution in this direction.

In the context of this study, various feature selection methods were evaluated to determine the most effective approach. Specifically, three filter methods, MRMR, PCA and Chi-square, along with a wrapper method, Backward Elimination, were tested. Initial trials with available data quickly led to the exclusion of MRMR and PCA due to their lower performance in conjunction with our chosen regression method. Both Chi-square and Backward Elimination showed comparable results; however, Backward Elimination was ultimately deemed impractical due to its excessive computational time. This

factor was particularly critical as it would prolong the duration subjects were required to remain equipped with experimental apparatus, making it unsuitable for the experimentation phase. Consequently, the final decision favored the Chi-square method, which offered a balance of efficiency and effectiveness suitable for our research needs. In the process of selecting machine learning algorithms, multiclass classifiers such as Random Forest, Decision Tree, and SVM were initially explored. However, since these approaches did not provide a continuous output, essential for the precise modulation of stimulation parameters in virtual reality, the focus shifted towards the use of regressors. During this phase, thorough experiments were conducted on various models, including LASSO (known for its feature selection capability), Random Forest Regression, Linear Regression, and Neural Networks. Hyperparameter optimization was crucial in this process, with significant time and effort dedicated to maximizing the performance of each regressor. Comparative analysis of the results then guided the selection of the most suitable model. This decision was driven by the need to maximize the accuracy and robustness of the model while maintaining good latency to enable real-time usage.

The distinctiveness of this work is primarily manifested through the use of a regressor tailored for each individual, ensuring a high level of precision due to customization for each user. This characteristic not only imparts remarkable accuracy to the regressor but also makes it a highly adaptable tool to the specific cognitive features of each subject. Additionally, the regressor demonstrates a remarkable ability to adapt neurofeedback and neurostimulations in real-time, maintaining minimal latency thanks to the nearly instantaneous calculation of the WML. However, it was observed that the initial relaxation phase poses a challenge, possibly due to variations in the user's concentration. This variability may be influenced by fleeting thoughts or other distractions, aspects that are clearly reflected in the EEG signal. It is in this phase that the regressor might encounter greater difficulties in predictions.

The use of virtual reality allowed the creation of an immersive environment, minimizing external distractions during task execution and stimulation reception. This feature contributed to maintaining a high level of efficiency in the neurostimulation process.

Among the various stimulations tested, the bar occasionally caused slight discomfort due to its up-and-down movement, perceived as a distraction at certain moments. Pulsed light, although often perceived, was generally considered non-annoying or distracting by participants. In contrast, binaural sounds never proved bothersome to subjects, who were often unaware of them,

proving advantageous even for non-aware individuals or in situations with limited conscious interaction. This "unconscious brain entrainment" underscores the power of neurostimulation in positively influencing cognitive processes without requiring conscious participation.

In conclusion, the results of this study provide a solid foundation for further exploration and future developments in the field of personalized neurostimulation for working memory enhancement. The combination of virtual reality, real-time adaptation, and binaural sounds has proven to be a promising methodology, paving the way for additional research to fully exploit this innovative approach.

7.2 Future Developments

This section outlines potential directions for the research conducted in the thesis, covering both technical aspects, such as regression performance, and considerations related to the experimental protocol.

Exploring more significant features related to working memory represents a crucial area for further investigation. Further exploration of the details of the EEG signal could lead to the identification of new relevant features, allowing for greater precision in evaluating the WML.

Simultaneously, examining more advanced approaches for feature selection in regression contexts could further optimize the model. The choice of more suitable feature selection methods could help refine the process of extracting crucial information from the EEG signal, thereby improving the robustness of the regressor.

Additionally, exploring more effective optimizations of the hyperparameters used for regression is a critical aspect of the improvement path. The adjustment of these parameters could undergo a more in-depth analysis to maximize the accuracy of the regression model during the training phase.

Further exploration of the most significant EEG channels for working memory is a promising research area. A more in-depth analysis of the spatial localization of brain activities involved in working memory could provide valuable insights to enhance the selection of EEG channels during feature extraction. This approach aims to optimize the sensitivity of the regression model to ensure a more accurate assessment of the WML.

Regarding neurostimulation frequencies, considering finer modulations, such as decimal-level adjustments, could be a fundamental optimization. This

modification might mitigate oscillations between whole frequencies, promoting a more stable convergence towards the optimal frequency during stimulation.

Expanding the variety of working memory tasks, such as incorporating 4-back trials or focusing exclusively on 3-back, is crucial for gaining a more detailed perspective on the effects of neurostimulation. Delving deeper into this cognitive exploration aims to reveal substantial improvements that might be overlooked in simpler scenarios. This expansion is particularly necessary since the relative simplicity of 2-back has led to high performances, making it challenging to identify potential improvements resulting from stimulations. Including more complex tasks will highlight the impacts of neurostimulation on working memory more precisely in scenarios requiring increased cognitive effort.

Increasing the number of training sessions distributed over multiple days, preferably non-consecutive, could provide a more accurate view of the long-term effects of stimulation on working memory. This approach would help isolate the specific effects of stimulation from potential interferences or accumulations of effects over time.

Considering the need to broaden the participant sample is essential to ensure the statistical representativity of the results. Expanding the sample could contribute to consolidating the obtained conclusions, making the study more generalizable and reliable.

Furthermore, evaluating and implementing improvements in the relaxation phase is a crucial aspect for advancing the study. Focusing not only on performance during the task but also on recovery during the relaxation phase could contribute to optimizing the overall effectiveness of neurostimulation.

Finally, the potential use of neurostimulation to improve conditions in patients with cognitive disorders, like Alzheimer's, or prevent them in at-risk individuals, presents a promising avenue for future development. The innovative approach of adapting neurostimulation based on WML could be incorporated into a commercial prototype aiming to enhance cognitive functions across various cognitive disorders. This personalized prototype would dynamically adjust treatment to individual neurocognitive conditions, marking a significant advancement in managing and preventing neurodegenerative diseases. It offers an innovative and tailored solution to the challenges associated with these conditions.

Appendix A

Real-Time Regression Results

This appendix presents the real-time regression analysis results for all user trials conducted as part of this thesis, visible in the following Figure A.1.

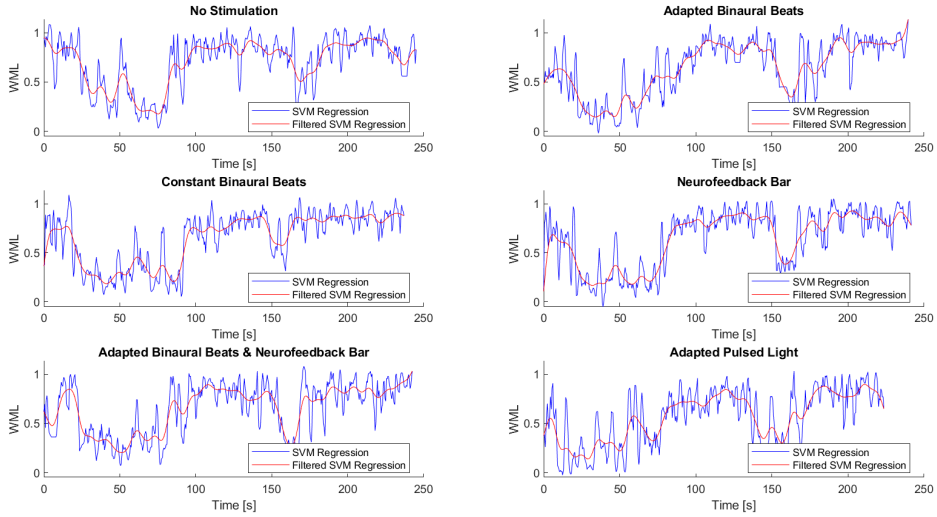

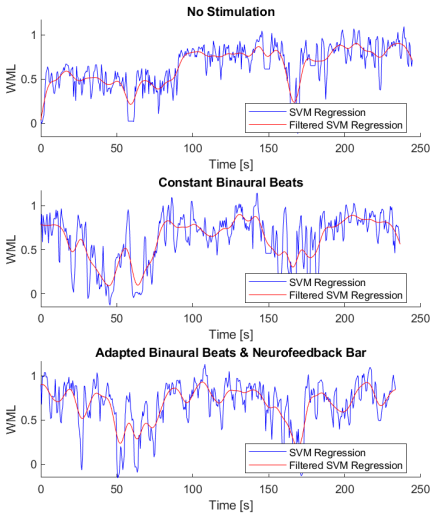
No Stimulation
WML
Time [s]
SVM Regression
Filtered SVM Regression

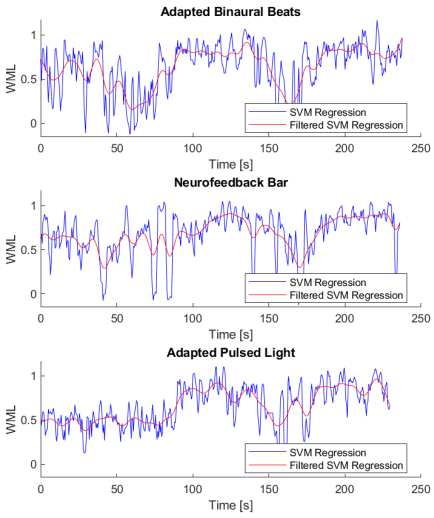
Adapted Binaural Beats
WML
Time [s]
SVM Regression
Filtered SVM Regression

Constant Binaural Beats
WML
Time [s]
SVM Regression
Filtered SVM Regression

Neurofeedback Bar
WML
Time [s]
SVM Regression
Filtered SVM Regression

Adapted Binaural Beats & Neurofeedback Bar
WML
Time [s]
SVM Regression
Filtered SVM Regression

Adapted Pulsed Light
WML
Time [s]
SVM Regression
Filtered SVM Regression

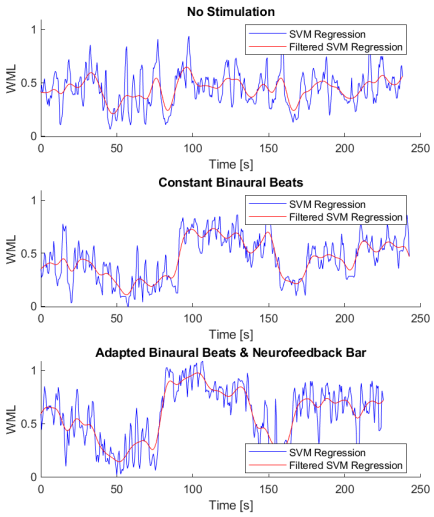
No Stimulation
WML
Time [s]
SVM Regression
Filtered SVM Regression

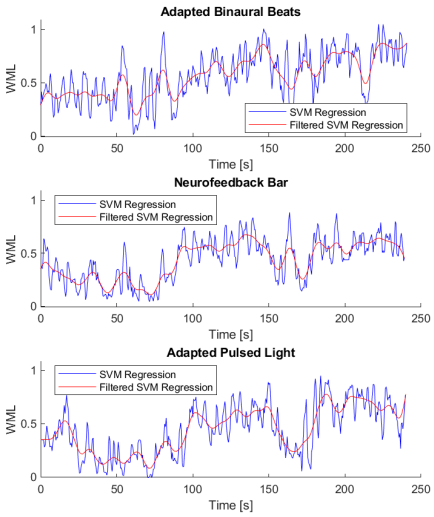
Adapted Binaural Beats
WML
Time [s]
SVM Regression
Filtered SVM Regression

Constant Binaural Beats
WML
Time [s]
SVM Regression
Filtered SVM Regression

Neurofeedback Bar
WML
Time [s]
SVM Regression
Filtered SVM Regression

Adapted Binaural Beats & Neurofeedback Bar
WML
Time [s]
SVM Regression
Filtered SVM Regression

Adapted Pulsed Light
WML
Time [s]
SVM Regression
Filtered SVM Regression

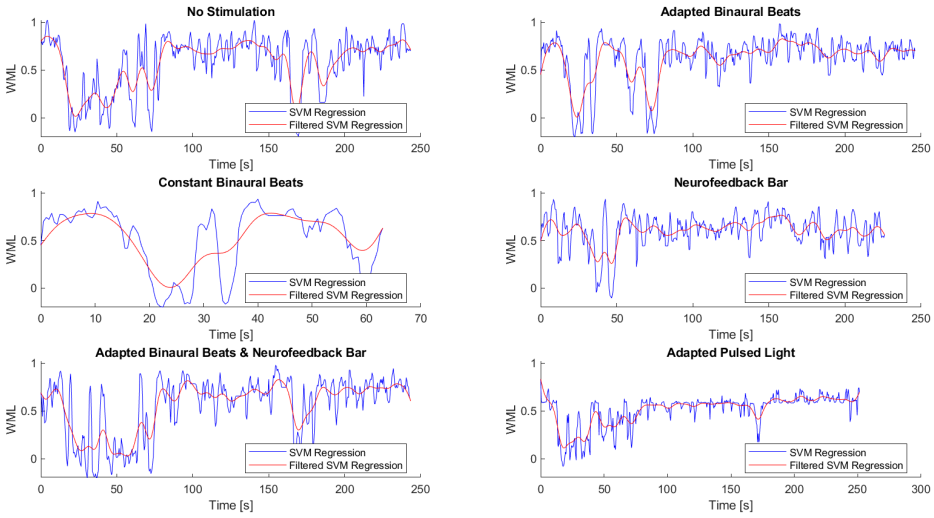
No Stimulation
Adapted Binaural Beats
Constant Binaural Beats
Neurofeedback Bar
Adapted Binaural Beats & Neurofeedback Bar
Adapted Pulsed Light
WML
Time [s]
SVM Regression
Filtered SVM Regression

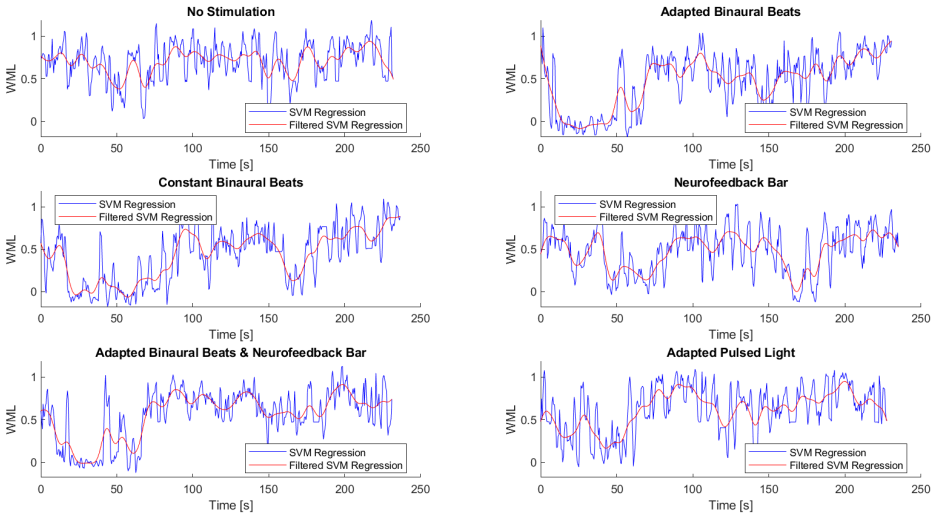
No Stimulation
Adapted Binaural Beats
Constant Binaural Beats
Neurofeedback Bar
Adapted Binaural Beats & Neurofeedback Bar
Adapted Pulsed Light
WML
Time [s]
SVM Regression
Filtered SVM Regression

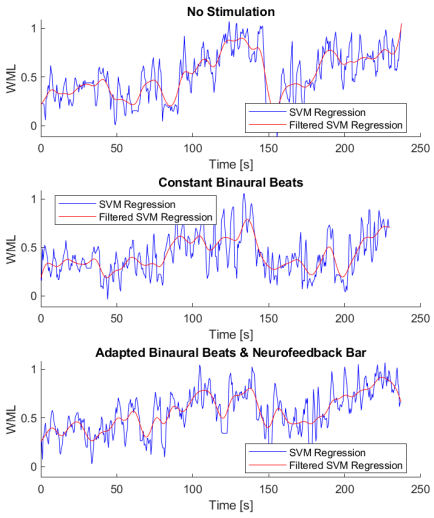
No Stimulation
WML
Time [s]
SVM Regression
Filtered SVM Regression

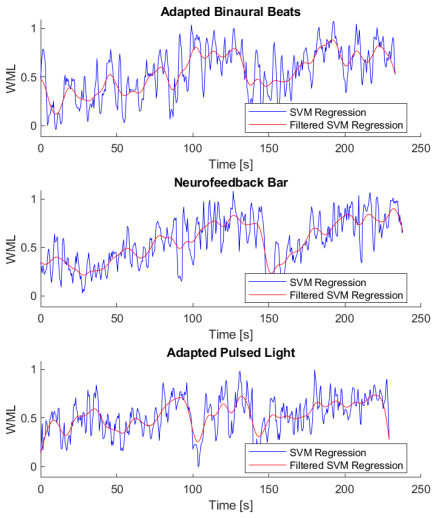
Adapted Binaural Beats
WML
Time [s]
SVM Regression
Filtered SVM Regression

Constant Binaural Beats
WML
Time [s]
SVM Regression
Filtered SVM Regression

Neurofeedback Bar
WML
Time [s]
SVM Regression
Filtered SVM Regression

Adapted Binaural Beats & Neurofeedback Bar
WML
Time [s]
SVM Regression
Filtered SVM Regression

Adapted Pulsed Light
WML
Time [s]
SVM Regression
Filtered SVM Regression

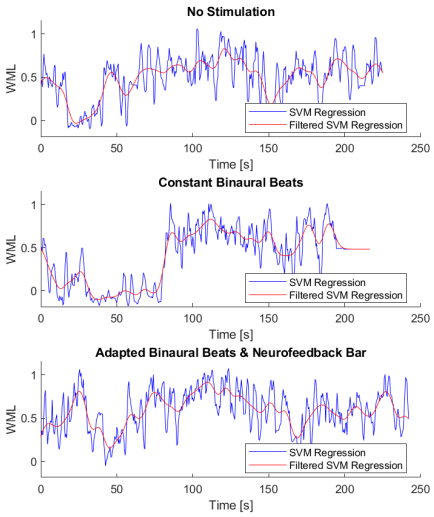
No Stimulation
WML
Time [s]
SVM Regression
Filtered SVM Regression

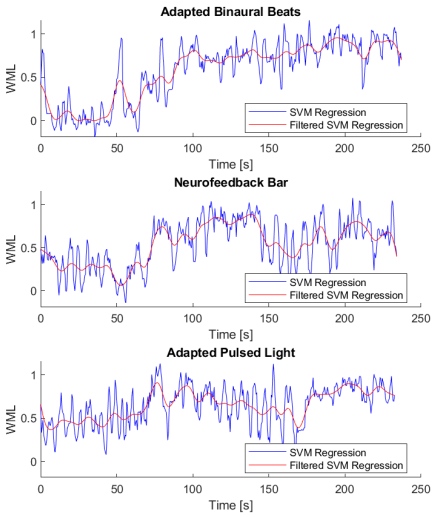
Adapted Binaural Beats
WML
Time [s]
SVM Regression
Filtered SVM Regression

Constant Binaural Beats
WML
Time [s]
SVM Regression
Filtered SVM Regression

Neurofeedback Bar
WML
Time [s]
SVM Regression
Filtered SVM Regression

Adapted Binaural Beats & Neurofeedback Bar
WML
Time [s]
SVM Regression
Filtered SVM Regression

Adapted Pulsed Light
WML
Time [s]
SVM Regression
Filtered SVM Regression

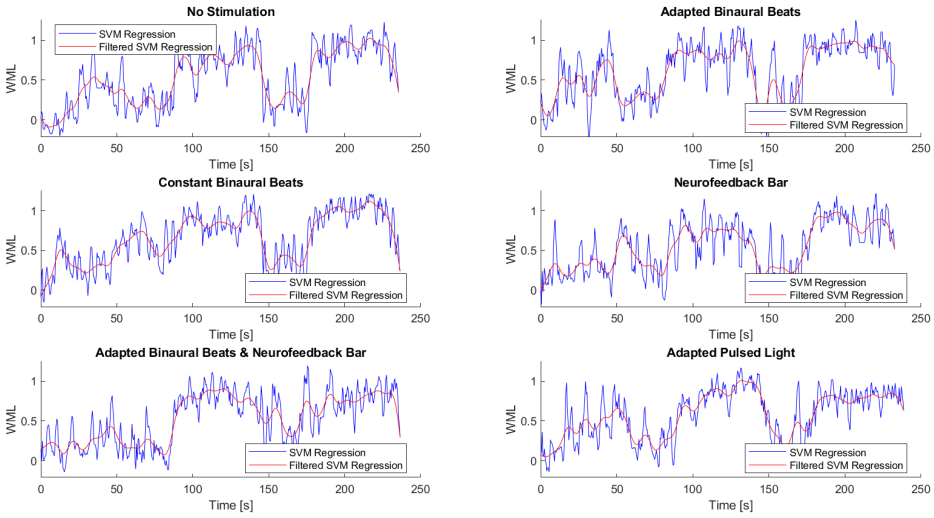
No Stimulation
Adapted Binaural Beats
Constant Binaural Beats
Neurofeedback Bar
Adapted Binaural Beats & Neurofeedback Bar
Adapted Pulsed Light
SVM Regression
Filtered SVM Regression
WML
Time [s]

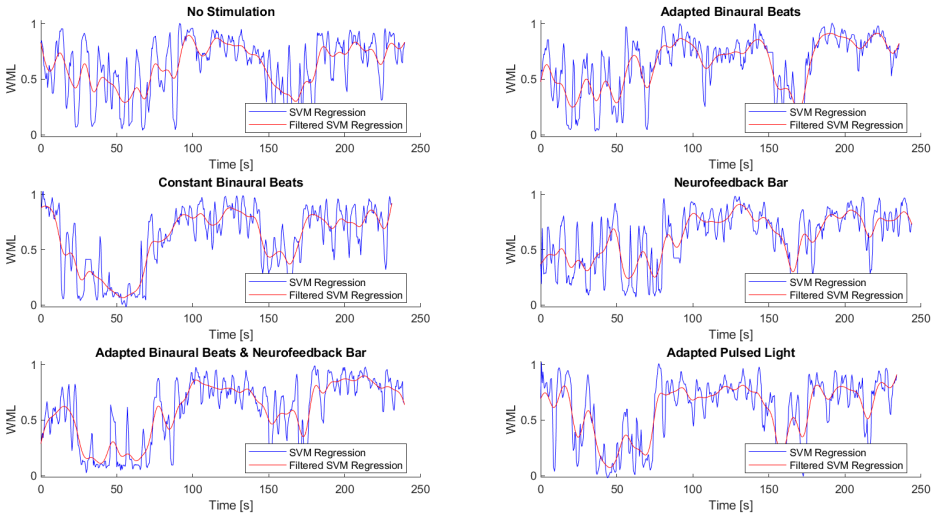
No Stimulation
Adapted Binaural Beats
Constant Binaural Beats
Neurofeedback Bar
Adapted Binaural Beats & Neurofeedback Bar
Adapted Pulsed Light
SVM Regression
Filtered SVM Regression
WML
Time [s]

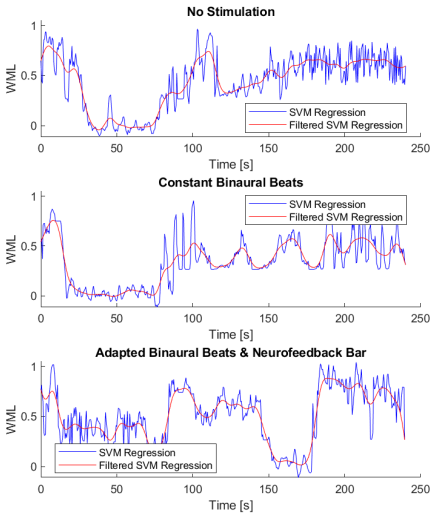
No Stimulation
WML
Time [s]
SVM Regression
Filtered SVM Regression

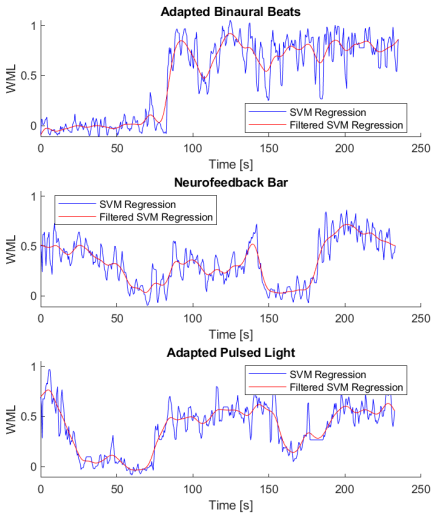
Adapted Binaural Beats
WML
Time [s]
SVM Regression
Filtered SVM Regression

Constant Binaural Beats
WML
Time [s]
SVM Regression
Filtered SVM Regression

Neurofeedback Bar
WML
Time [s]
SVM Regression
Filtered SVM Regression

Adapted Binaural Beats & Neurofeedback Bar
WML
Time [s]
SVM Regression
Filtered SVM Regression

Adapted Pulsed Light
WML
Time [s]
SVM Regression
Filtered SVM Regression

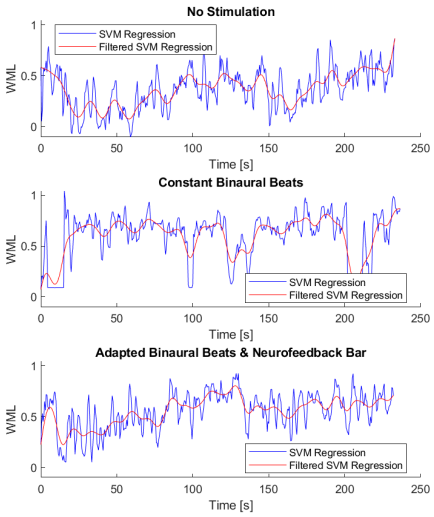
No Stimulation
WML
Time [s]
SVM Regression
Filtered SVM Regression

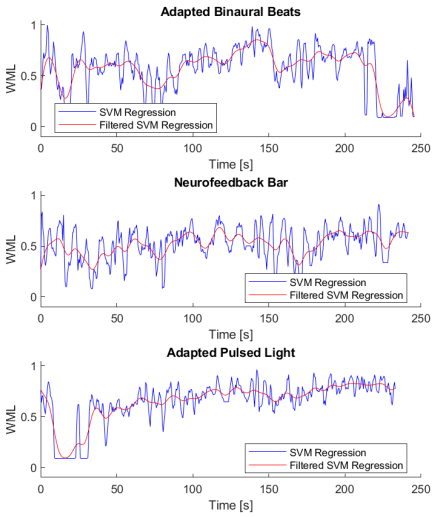
Adapted Binaural Beats
WML
Time [s]
SVM Regression
Filtered SVM Regression

Constant Binaural Beats
WML
Time [s]
SVM Regression
Filtered SVM Regression

Neurofeedback Bar
WML
Time [s]
SVM Regression
Filtered SVM Regression

Adapted Binaural Beats & Neurofeedback Bar
WML
Time [s]
SVM Regression
Filtered SVM Regression

Adapted Pulsed Light
WML
Time [s]
SVM Regression
Filtered SVM Regression

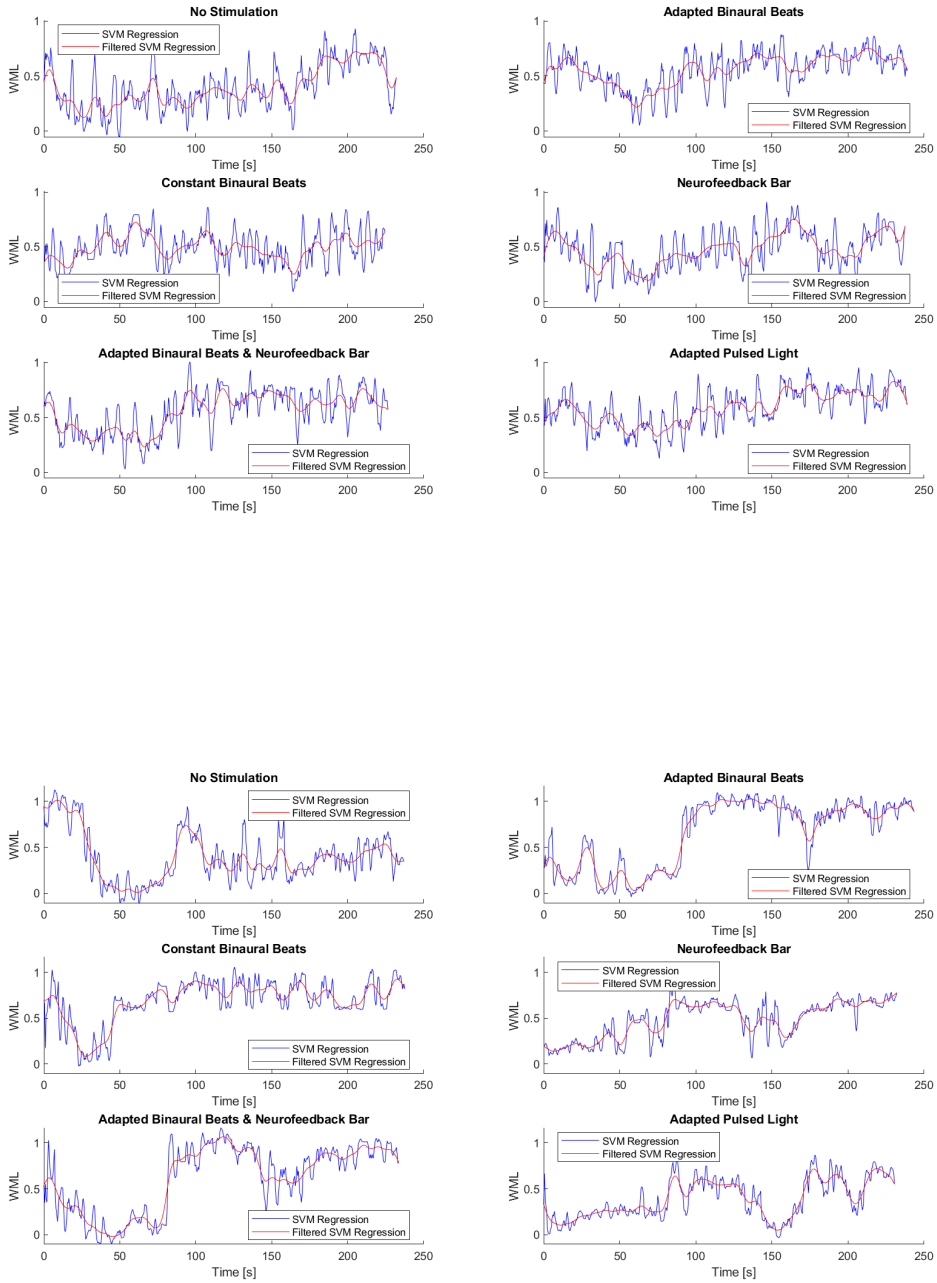

Figure A.1. Real-time regression analysis results for all user trials.

Bibliography

[1] Paradiso Bear Connors. *Neuroscience: Exploring the Brain*. Wolters Kluwer Health, 2016.

[2] Ernst Niedermeyer and Fernando Lopes da Silva. *Electroencephalography: Basic Principles, Clinical Applications, and Related Fields*. Lippincott Williams & Wilkins, 2005.

[3] M. Lazar. «Working Memory». In: *The Neuroscientist* (2017).

[4] MedlinePlus. *Gray and white matter of the brain*. Accessed: 2023-11-15. 2023. URL: https://medlineplus.gov/ency/imagepages/18117.htm.

[5] Nicole Baumann and Danielle Pham-Dinh. «Biology of Oligodendrocyte and Myelin in the Mammalian Central Nervous System». In: *Physiological Reviews* 81.2 (2001), pp. 871–927.

[6] R. Douglas Fields. «White Matter Matters». In: *Scientific American* 298.3 (2008), pp. 42–49.

[7] Cancer Research UK. *Diagram showing some of the main areas of the brain*. CC BY-SA 4.0 <https://creativecommons.org/licenses/by-sa/4.0>, via Wikimedia Commons. URL: https://commons.wikimedia.org/wiki/File:Diagram_showing_some_of_the_main_areas_of_the_brain_CRUK_188.svg.

[8] Priyanka A. Abhang, Bharti W. Gawali, and Suresh C. Mehrotra. «Chapter 1 - Introduction to Emotion, Electroencephalography, and Speech Processing». In: *Introduction to EEG- and Speech-Based Emotion Recognition*. Ed. by Priyanka A. Abhang, Bharti W. Gawali, and Suresh C. Mehrotra. Academic Press, 2016, pp. 1–17. ISBN: 978-0-12-804490-2. DOI: https://doi.org/10.1016/B978-0-12-804490-2.00001-4.

[9] Stephanie Willerth. «Chapter 2 - Introduction to the nervous system». In: *Engineering Neural Tissue from Stem Cells*. Ed. by Stephanie Willerth. Academic Press, 2017, pp. 17–38. ISBN: 978-0-12-811385-1. DOI: https://doi.org/10.1016/B978-0-12-811385-1.00002-9.

[10] Catherine J. Stoodley and J. Schmahmann. «Functional topography in the human cerebellum: A meta-analysis of neuroimaging studies». In: *NeuroImage* (2009).

[11] Jeffery P. Hogg Hayden Basinger. *Neuroanatomy, Brainstem*. Treasure Island (FL): StatPearls Publishing, 2023.

[12] John Rothwell. «Chapter 4 Meet the Brain: Neurophysiology». In: International Review of Neurobiology. Academic Press, 2009.

[13] R. Fields and Beth Stevens-Graham. «New insights into neuron-glia communication». In: *Science* (2002).

[14] Gasper Tkacik et al. «Searching for Collective Behavior in a Large Network of Sensory Neurons». In: *PLoS Computational Biology* 10 (2013). URL: https://api.semanticscholar.org/CorpusID:5722977.

[15] Nelson Spruston. «Spruston N. Pyramidal neurons: dendritic structure and synaptic integration. Nat Rev Neurosci 9: 206-221». In: *Nature reviews. Neuroscience* 9 (Apr. 2008), pp. 206–21. DOI: 10.1038/nrn2286.

[16] Wikimedia Commons. *Membrane Permeability of a Neuron During an Action Potential*. Accessed on 22-February-2024. 2023. URL: https://commons.wikimedia.org/w/index.php?title=File:Membrane_Permeability_of_a_Neuron_During_an_Action_Potential.svg&oldid=796575004.

[17] E. Ullian; S. Sapperstein; K. S. Christopherson; B. Barres. «Control of synapse number by glia». In: *Science* (2001).

[18] Wikimedia Commons. *Synapse Schematic*. 2023. URL: https://commons.wikimedia.org/w/index.php?title=File:SynapseSchematic_en.svg&oldid=724666137.

[19] Emily Finn, Russell Poldrack, and James Shine. «Functional neuroimaging as a catalyst for integrated neuroscience». In: *Nature* 623 (Nov. 2023), pp. 263–273. DOI: 10.1038/s41586-023-06670-9.

[20] Y F Tai and P Piccini. «Applications of positron emission tomography (PET) in neurology». In: *Journal of Neurology, Neurosurgery & Psychiatry* 75.5 (2004), pp. 669–676. ISSN: 0022-3050. DOI: 10.1136/jnnp.2003.028175. eprint: https://jnnp.bmj.com/content/75/5/669.full.pdf. URL: https://jnnp.bmj.com/content/75/5/669.

[21] Tatum WO 4th Hasan TF. «Ambulatory EEG Usefulness in Epilepsy Management.» In: *J Clin Neurophysiol.* (2021).

[22] F Lotte M Congedo A Lécuyer F Lamarche and B Arnaldi. «A review of classification algorithms for EEG-based brain–computer interfaces». In: *Journal of Neural Engineering* (2007).

[23] James Stone and John Hughes. «Early History of Electroencephalography and Establishment of the American Clinical Neurophysiology Society». In: *Journal of clinical neurophysiology : official publication of the American Electroencephalographic Society* 30 (Feb. 2013), pp. 28–44. DOI: 10.1097/WNP.0b013e31827edb2d.

[24] Min Suk Lee et al. «Characterization of Ag/AgCl Dry Electrodes for Wearable Electrophysiological Sensing». In: *Frontiers in Electronics* 2 (2022). ISSN: 2673-5857. DOI: 10.3389/felec.2021.700363. URL: https://www.frontiersin.org/articles/10.3389/felec.2021.700363.

[25] Bitbrain. *The Wet-EEG Cap: Semi-Dry, Saline & Gel EEG caps.* https://www.bitbrain eeg-cap. Aug. 2023.

[26] M.Knaflitz G.L. Cerone M. Gazzoni. *Strumentazione Biomedica.* Levrotto & Bella, 2022. ISBN: 8882182134.

[27] George H. Klem et al. «The ten-twenty electrode system of the International Federation. The International Federation of Clinical Neurophysiology.» In: *Electroencephalography and clinical neurophysiology. Supplement* 52 (1999), pp. 3–6. URL: https://api.semanticscholar.org/CorpusID:27778550.

[28] Robert Oostenveld and Peter Praamstra. «The five percent electrode system for high-resolution EEG and ERP measurements». In: *Clinical Neurophysiology* 112.4 (2001), pp. 713–719. ISSN: 1388-2457. DOI: https://doi.org/10.1016/S1388-2457(00)00527-7. URL: https://www.sciencedirect.com/science/article/pii/S1388245700005277.

[29] Brylie Christopher Oxley. *International 10-20 system for EEG-MCN.* https://commons.wikimedia.org/wiki/File:International_10-20_system_for_EEG-MCN.svg. 2017.

[30] M. Steriade et al. «Basic mechanisms of cerebral rhythmic activities». In: *Electroencephalography and Clinical Neurophysiology* 76.6 (1990), pp. 481–508. ISSN: 0013-4694. DOI: https://doi.org/10.1016/0013-4694(90)90001-Z. URL: https://www.sciencedirect.com/science/article/pii/001346949090001Z.

[31] Luca Mesin. *Introduction to biomedical signal processing*. ilmiolibro, 2017.

[32] Smita Tiwari, Shivani Goel, and Arpit Bhardwaj. «MIDNN- a classification approach for the EEG based motor imagery tasks using deep neural network». In: *Applied Intelligence* 52 (Mar. 2022). DOI: 10.1007/s10489-021-02622-w.

[33] Md Kafiul Islam, Amir Rastegarnia, and Zhi Yang. «Methods for artifact detection and removal from scalp EEG: A review». In: *Neurophysiologie Clinique/Clinical Neurophysiology* 46.4 (2016), pp. 287–305. ISSN: 0987-7053. DOI: https://doi.org/10.1016/j.neucli.2016.07.002. URL: https://www.sciencedirect.com/science/article/pii/S098770531630199X.

[34] İbrahim Kaya. «A Brief Summary of EEG Artifact Handling». In: *Brain-Computer Interface*. Ed. by Vahid Asadpour. Rijeka: IntechOpen, 2021. Chap. 2. DOI: 10.5772/intechopen.99127. URL: https://doi.org/10.5772/intechopen.99127.

[35] Lu Shen et al. «Successful alpha neurofeedback training enhances working memory updating and event-related potential activity». In: *Neurobiology of Learning and Memory* 205 (2023), p. 107834. ISSN: 1074-7427. DOI: https://doi.org/10.1016/j.nlm.2023.107834. URL: https://www.sciencedirect.com/science/article/pii/S1074742723001156.

[36] Aini Ismafairus Abd Hamid Wen Jia Chai and Jafri Malin Abdullah. «Working Memory From the Psychological and Neurosciences Perspectives: A Review». In: *Frontiers in Psychology* 9 (2018), p. 401. DOI: 10.3389/fpsyg.2018.00401.

[37] T. Klingberg et al. «Computerized Training of Working Memory in Children With ADHD - A Randomized, Controlled Trial». In: *Journal of the American Academy of Child & Adolescent Psychiatry* 41.3 (2002), pp. 375–383.

[38] M. Buschkuehl et al. «Working Memory Training in Young and Older Adults». In: *Psychology and Aging* 23.4 (2008), pp. 743–753.

[39] Sandhya Basu and Bidisha Banerjee. «Potential of binaural beats intervention for improving memory and attention: insights from meta-analysis and systematic review». In: *Psychological Research* 87 (July 2022). DOI: 10.1007/s00426-022-01706-7.

[40] J. Lubar. «Discourse on the development of EEG diagnostics and biofeedback for attention-deficit/hyperactivity disorders». In: *Biofeedback and Self-Regulation* (1991).

[41] Joshua E. Curtiss Vera C. Goessl and S. Hofmann. «The effect of heart rate variability biofeedback training on stress and anxiety: a meta-analysis». In: *Psychological Medicine* (2017).

[42] Michael Thompson and Lynda M. Thompson. «The Neurofeedback Book: An Introduction to Basic Concepts in Applied Psychophysiology». In: 2003. URL: https://api.semanticscholar.org/CorpusID:141828720.

[43] Hengameh Marzbani, Hamid Marateb, and Marjan Mansourian. «Methodological Note: Neurofeedback: A Comprehensive Review on System Design, Methodology and Clinical Applications». In: *Basic and Clinical Neuroscience Journal* 7 (Mar. 2016), pp. 143–158. DOI: 10.15412/J.BCN.03070208.

[44] George Papagiannakis et al. «A virtual reality brainwave entrainment method for human augmentation applications». In: 2015. URL: https://api.semanticscholar.org/CorpusID:17472401.

[45] Sao-Ee Goh Susan A. Yoon and Zhitong Yang. «Toward a Learning Progression of Complex Systems Understanding». In: *Complicity : An International Journal of Complexity and Education* (2019).

[46] D.C.W. Klooster et al. «Technical aspects of neurostimulation: Focus on equipment, electric field modeling, and stimulation protocols». In: *Neuroscience & Biobehavioral Reviews* 65 (2016), pp. 113–141. ISSN: 0149-7634. DOI: https://doi.org/10.1016/j.neubiorev.2016.02.016. URL: https://www.sciencedirect.com/science/article/pii/S0149763415301482.

[47] Johannes Vosskuhl, Daniel Strüber, and Christoph Herrmann. «Non-invasive Brain Stimulation: A Paradigm Shift in Understanding Brain Oscillations». In: *Frontiers in Human Neuroscience* 12 (May 2018). DOI: 10.3389/fnhum.2018.00211.

[48] Tobias Kaufmann, Elisa Holz, and Andrea Kübler. «Comparison of tactile, auditory, and visual modality for brain-computer interface use: A case study with a patient in the locked-in state». In: *Frontiers in neuroscience* 7 (July 2013), p. 129. DOI: 10.3389/fnins.2013.00129.

[49] Yoshihiro Noda et al. «Single-Pulse Transcranial Magnetic Stimulation-Evoked Potential Amplitudes and Latencies in the Motor and Dorsolateral Prefrontal Cortex among Young, Older Healthy Participants, and Schizophrenia Patients». In: *Journal of Personalized Medicine* 11 (Jan. 2021), p. 54. DOI: 10.3390/jpm11010054.

[50] Christine A. Edwards et al. «Neurostimulation Devices for the Treatment of Neurologic Disorders». In: *Mayo Clinic Proceedings* 92.9 (2017), pp. 1427–1444. ISSN: 0025-6196. DOI: https://doi.org/10.1016/j.mayocp.2017.05.005. URL: https://www.sciencedirect.com/science/article/pii/S0025619617303257.

[51] Stavros Zanos. «Closed-Loop Neuromodulation in Physiological and Translational Research». In: *Cold Spring Harbor Perspectives in Medicine* 9 (Dec. 2018), a034314. DOI: 10.1101/cshperspect.a034314.

[52] Alexander Fedotchev et al. «Human Body Rhythms in the Development of Non-Invasive Methods of Closed-Loop Adaptive Neurostimulation». In: *Journal of Personalized Medicine* 11 (May 2021), p. 437. DOI: 10.3390/jpm11050437.

[53] N SALANSKY, A FEDOTCHEV, and A BONDAR. «Responses of the Nervous System to Low Frequency Stimulation and EEG Rhythms: Clinical Implications». In: *Neuroscience & Biobehavioral Reviews* 22.3 (1998), pp. 395–409. ISSN: 0149-7634. DOI: https://doi.org/10.1016/S0149-7634(97)00029-8. URL: https://www.sciencedirect.com/science/article/pii/S0149763497000298.

[54] Pramila P. Shinde and Seema Shah. «A Review of Machine Learning and Deep Learning Applications». In: *2018 Fourth International Conference on Computing Communication Control and Automation (ICCUBEA)*. 2018, pp. 1–6. DOI: 10.1109/ICCUBEA.2018.8697857.

[55] Batta Mahesh. «Machine learning algorithms-a review». In: *International Journal of Science and Research (IJSR).[Internet]* 9.1 (2020), pp. 381–386.

[56] Wikipedia Contributors. *Backpropagation — Wikipedia, The Free Encyclopedia*. Accessed on 22-January-2024. 2024. URL: https://en.wikipedia.org/w/index.php?title=Backpropagation&oldid=1193114407.

[57] Yann LeCun, Yoshua Bengio, and Geoffrey Hinton. «Deep learning». In: *Nature* 521.7553 (May 2015), pp. 436–444. ISSN: 1476-4687. DOI: 10.1038/nature14539. URL: https://doi.org/10.1038/nature14539.

[58] Xing Hao, Guigang Zhang, and Shang Ma. «Deep Learning». In: *International Journal of Semantic Computing* 10.03 (2016), pp. 417–439. DOI: 10.1142/S1793351X16500045. URL: https://doi.org/10.1142/S1793351X16500045.

[59] Neuroelectrics. *Enobio 8 - Neuroelectrics*. URL: https://www.neuroelectrics.com/solutions/enobio/8.

[60] Neuroelectrics. *Neuroelectrics Wiki - NIC 2.0*. URL: https://www.neuroelectrics.com/wiki/index.php/NIC2.0.

[61] *Unity Technologies*. Accessed: 2024-01-13. URL: https://unity.com.

[62] *Unity Documentation - Creating and Using Scripts*. Accessed: 2024-01-13. URL: https://docs.unity3d.com/2021.3/Documentation/Manual/CreatingAndUsingScripts.html.

[63] Microsoft. *Visual Studio*. Accessed: 2024-01-13. URL: https://visualstudio.microsoft.com/.

[64] *Unity Industry*. Accessed: 2024-01-13. URL: https://unity.com/industry.

[65] Andrew E. Budson. *Can mindfulness change your brain?* May 2021. URL: https://www.health.harvard.edu/blog/can-mindfulness-change-your-brain-202105132455.

[66] *Meta Quest 2 official webpage*. Accessed: 2024-01-13. URL: https://www.meta.com/it/quest/products/quest-2/.

[67] *Meta Quest 2 technical specification*. Accessed: 2024-01-13. URL: https://www.meta.com/it/quest/products/quest-2/tech-specs/.

[68] *Meta Quest 2 official specification page*. URL: https://www.meta.com/it/quest/products/quest-2/#overview.

[69] *Snapdragon XR2 5G Platform*. Accessed: 2024-01-13. URL: https://www.qualcomm.com/products/mobile/snapdragon/xr-vr-ar/snapdragon-xr2-5g-platform.

[70] *Snapdragon XR2 Gen 2 Platform*. Accessed: 2024-01-13. URL: https://www.qualcomm.com/products/mobile/snapdragon/xr-vr-ar/snapdragon-xr2-gen-2-platform.

[71] Soraya J LeMarshall et al. «Virtual reality-based interventions for the rehabilitation of vestibular and balance impairments post-concussion: a scoping review». In: *Journal of Neuroengineering and Rehabilitation* 20.1 (Mar. 2023). DOI: 10.1186/s12984-023-01145-4. URL: https://doi.org/10.1186/s12984-023-01145-4.

[72] Soledad Ballesteros, Claudia Voelcker-Rehage, and Louis Bherer. «Editorial: Cognitive and Brain Plasticity Induced by Physical Exercise, Cognitive Training, Video Games, and Combined Interventions». In: *Frontiers in Human Neuroscience* 12 (May 2018). DOI: 10.3389/fnhum.2018.00169. URL: http://dx.doi.org/10.3389/fnhum.2018.00169.

[73] Luisa Cacciante et al. «Cognitive telerehabilitation in neurological patients: systematic review and meta-analysis». In: *Neurological Sciences* 43.2 (Nov. 2021), pp. 847–862. DOI: 10.1007/s10072-021-05770-6. URL: http://dx.doi.org/10.1007/s10072-021-05770-6.

[74] Neuroelectrics. *Neuroelectrics Wiki - MatNIC Matlab Toolkit*. URL: https://www.neuroelectrics.com/wiki/index.php/MatNIC_Matlab_Toolkit.

[75] P. Almquist. «Type of Service in the Internet Protocol Suite». In: *Request for Comments* (1992).

[76] Mary E. Shacklett, Amy Novotny, and Kate Gerwig. *TCP/IP*. July 2021. URL: https://www.techtarget.com/searchnetworking/definition/TCP-IP.

[77] LabStreamingLayer. *LabStreamingLayer Documentation*. URL: https://labstreaminglayer.readthedocs.io/info/intro.html.

[78] Santiago Pelegrina et al. «Normative data on the n-back task for children and young adolescents». In: *Frontiers in Psychology* 6 (Oct. 2015). DOI: 10.3389/fpsyg.2015.01544. URL: http://dx.doi.org/10.3389/fpsyg.2015.01544.

[79] Patrick D. Gajewski et al. «What Does the n-Back Task Measure as We Get Older? Relations Between Working-Memory Measures and Other Cognitive Functions Across the Lifespan». In: *Frontiers in Psychology* 9 (Nov. 2018). DOI: 10.3389/fpsyg.2018.02208. URL: http://dx.doi.org/10.3389/fpsyg.2018.02208.

[80] Anna Miró-Padilla, Elisenda Bueichekú, and César Ávila. «Locating neural transfer effects of n-back training on the central executive: a longitudinal fMRI study». In: *Scientific Reports* 10.1 (Mar. 2020). DOI: 10.1038/s41598-020-62067-y. URL: http://dx.doi.org/10.1038/s41598-020-62067-y.

[81] Zainab Mohamed et al. «Characterizing Focused Attention and Working Memory Using EEG». In: *Sensors* 18.11 (Nov. 2018), p. 3743. DOI: 10.3390/s18113743. URL: http://dx.doi.org/10.3390/s18113743.

[82] Wolfgang Klimesch. «EEG alpha and theta oscillations reflect cognitive and memory performance: a review and analysis». In: *Brain Research Reviews* 29.2 (1999), pp. 169–195. ISSN: 0165-0173. DOI: https://doi.org/10.1016/S0165-0173(98)00056-3. URL: https://www.sciencedirect.com/science/article/pii/S0165017398000563.

[83] Jinn-Rong Wang and Shulan Hsieh. «Neurofeedback training improves attention and working memory performance». In: *Clinical Neurophysiology* 124.12 (2013), pp. 2406–2420. ISSN: 1388-2457. DOI: https://doi.org/10.1016/j.clinph.2013.05.020. URL: https://www.sciencedirect.com/science/article/pii/S1388245713006949.

[84] Muhammad Danish Mujib et al. «Understanding the neurological mechanism involved in enhanced memory recall task following binaural beat: a pilot study». In: *Experimental Brain Research* 239.9 (July 2021), pp. 2741–2754. DOI: 10.1007/s00221-021-06132-6. URL: http://dx.doi.org/10.1007/s00221-021-06132-6.

[85] MathWorks. *Spectral entropy of signal - MATLAB pentropy*. URL: https://www.mathworks.com/help/signal/ref/pentropy.html.

[86] T. Higuchi. «Approach to an irregular time series on the basis of the fractal theory». In: *Physica D: Nonlinear Phenomena* 31.2 (June 1988), pp. 277–283. DOI: 10.1016/0167-2789(88)90081-4. URL: http://dx.doi.org/10.1016/0167-2789(88)90081-4.

[87] Michael J. Katz. «Fractals and the analysis of waveforms». In: *Computers in Biology and Medicine* 18.3 (Jan. 1988), pp. 145–156. DOI: 10.1016/0010-4825(88)90041-8. URL: http://dx.doi.org/10.1016/0010-4825(88)90041-8.

[88] Luca Mesin. «Estimation of Complexity of Sampled Biomedical Continuous Time Signals Using Approximate Entropy». In: *Frontiers in Physiology* 9 (2018). ISSN: 1664-042X. DOI: 10.3389/fphys.2018.00710. URL: https://www.frontiersin.org/articles/10.3389/fphys.2018.00710.

[89] MathWorks Italia. *Find outliers in data - MATLAB isoutlier*. URL: https://it.mathworks.com/help/matlab/ref/isoutlier.html.

[90] Max Kuhn and Kjell Johnson. *Applied Predictive Modeling*. Springer Science & Business Media, May 2013.

[91] *Univariate feature ranking for classification using chi-square tests - MATLAB fscchi2*. URL: https://www.mathworks.com/help/stats/fscchi2.html#mw_fb8352a0-b1a4-4af3-ba58-21c63ba7e3b2.

[92] MathWorks. *Understanding Support Vector Machine Regression*. URL: https://it.mathworks.com/help/stats/understanding-support-vector-machine-regression.html#buzow2a.

[93] Vladimir Vapnik. *The Nature of Statistical Learning Theory*. Springer: New York, 2000.

[94] XKCD-style ROC curve. *ROC curve - XKCD style*. June 2018. URL: https://commons.wikimedia.org/wiki/File:Roc-draft-xkcd-style.svg#filelinks.

[95] Hessel Engelbregt et al. «Effects of binaural and monaural beat stimulation on attention and EEG». In: *Experimental Brain Research* 239 (Sept. 2021), p. 3. DOI: 10.1007/s00221-021-06155-z.

[96] Miguel Garcia-Argibay, Miguel Angel Santed, and José Manuel Reales. «Efficacy of binaural auditory beats in cognition, anxiety, and pain perception: a meta-analysis». In: *Psychological Research* 83 (2018), pp. 357–372. URL: https://api.semanticscholar.org/CorpusID:51907173.

[97] Lorenza Colzato et al. «More attentional focusing through binaural beats: evidence from the global–local task». In: *Psychological Research* 81 (Jan. 2017). DOI: 10.1007/s00426-015-0727-0.

[98] Annika Notbohm, Jürgen Kurths, and Christoph Siegfried Herrmann. «Modification of Brain Oscillations via Rhythmic Light Stimulation Provides Evidence for Entrainment but Not for Superposition of Event-Related Responses». In: *Frontiers in Human Neuroscience* 10 (2016). URL: https://api.semanticscholar.org/CorpusID:12508863.

[99] Michael Terman and Jiuan Terman. «Controlled Trial of Naturalistic Dawn Simulation and Negative Air Ionization for Seasonal Affective Disorder». In: *The American journal of psychiatry* 163 (Jan. 2007), pp. 2126–33. DOI: 10.1176/appi.ajp.163.12.2126.

[100] Kian Ng, Andrew Bradley, and Ross Cunnington. «Stimulus specificity of a steady-state visual-evoked potential-based brain-computer interface». In: *Journal of neural engineering* 9 (May 2012), p. 036008. DOI: 10.1088/1741-2560/9/3/036008.

[101] Christoph Herrmann. «Human EEG responses to 1–100 Hz flicker: Resonance phenomena in visual cortex and their potential correlation to cognitive phenomena». In: *Experimental brain research. Experimentelle Hirnforschung. Expérimentation cérébrale* 137 (May 2001), pp. 346–53. DOI: 10.1007/s0022101.

[102] Christopher A. Brown K. Ecsy and Anthony K. P. Jones. «Cortical nociceptive processes are reduced by visual alpha-band entrainment in the human brain». In: *European Journal of Pain* (2018).

[103] François-Benoît Vialatte et al. «Steady-state visually evoked potentials: Focus on essential paradigms and future perspectives». In: *Progress in Neurobiology* 90.4 (2010), pp. 418–438. ISSN: 0301-0082. DOI: https://doi.org/10.1016/j.pneurobio.2009.11.005. URL: https://www.sciencedirect.com/science/article/pii/S0301008209001853.

[104] James Townsend and F. Ashby. «Methods of modeling capacity in simple processing systems». In: vol. 3. Jan. 1978, pp. 199–239.

[105] S. S. Shapiro and M. B. Wilk. «An Analysis of Variance Test for Normality (Complete Samples)». In: *Biometrika* 52.3/4 (1965), pp. 591–611. ISSN: 00063444. URL: http://www.jstor.org/stable/2333709 (visited on 02/03/2024).

[106] Frank Wilcoxon. «Individual Comparisons by Ranking Methods». In: *Biometrics Bulletin* 1.6 (1945), pp. 80–83.

[107] Marian Berryhill and Ingrid Olson. «The right parietal lobe is critical for working memory». In: *Neuropsychologia* 46 (Feb. 2008), pp. 1767–74. DOI: 10.1016/j.neuropsychologia.2008.01.009.